A thermodynamic investigation into the bistability of climates around the habitable zone

Dissertation with the aim of achieving a doctoral degree
at the Faculty of Mathematics, Informatics and Natural Sciences
Department of Theoretical Meteorology
Universität Hamburg

Submitted by Robert Boschi
in Hamburg, 2016

Day of oral defense: 09.06.2016

The following evaluators recommend the admission of the dissertation:

1. Prof. Dr. Valerio Lucarini

2. Prof. Dr. Maarten Ambaum

Eidesstattliche Versicherung
Declaration on oath

Hiermit erkläre ich an Eides statt, dass ich die vorliegende Dissertationsschrift selbst verfasst und keine anderen als die angegebenen Quellen und Hilfsmittel benutzt habe.

I hereby declare, on oath, that I have written the present dissertation by my own and have not used other than the acknowledged resources and aids.

Hamburg, 28.01.2016 Unterschrift *signature*:

_____

"A theory is the more impressive the greater the simplicity of its premises, the more different kinds of things it relates, and the more extended its area of applicability. Therefore the deep impression that classical thermodynamics made upon me. It is the only physical theory of universal content which I am convinced will never be overthrown, within the framework of applicability of its basic concepts."

Albert Einstein, Autobiographical Notes (1949)

Abstract

The goal of this thesis is to explore the potential multistability of the climate for a planet around the habitable zone. The methodology used here has been applied to the Earth system, but this investigation has more general relevance. A thorough investigation of the thermodynamics of the climate system is performed for very diverse conditions of energy input and infra-red atmosphere opacity.

Using PlaSim, an Earth-like general circulation model, the solar constant, S^*, is modulated between 1160 Wm^{-2} and 1510 Wm^{-2} and the CO_2 concentration, $[CO_2]$, between 90 ppm and 2880 ppm. It is observed that in such a parameter range the climate is bistable, i.e. there are two coexisting attractors, one characterised by warm, moist climates (W) and one by a completely frozen sea surface (Snowball Earth, SB). The tipping points of both the transitions (W$\rightarrow$SB and SB $\rightarrow$W) are located along straight lines in the (S^*,log$[CO_2]$) space. The dynamical and thermodynamical properties – energy fluxes, Lorenz energy cycle, Carnot efficiency, material entropy production – of the W and SB states are very different: W states are dominated by the hydrological cycle and latent heat is prominent in the material entropy production; the SB states are eminently dry climates where heat transport is realized through sensible heat fluxes and entropy mostly generated by dissipation of kinetic energy. It is also shown that the Carnot efficiency regularly increases towards each transition between W and SB, with a large decrease in each transition.

In the final part of the thesis, well-defined empirical functions are proposed which allow for expressing the global non-equilibrium thermodynamical properties of the system in terms of either the mean surface temperature or the mean planetary emission temperature. As a preliminary result, it is found that when reducing the rotation rate of the planet by a factor of two, the multistability properties, the quantitative estimators of the thermodynamics of the system, and the approximate parameterisations in terms of the surface of emission temperature are weakly affected. While the specific results presented in this thesis depend on some characteristics of the Earth system (e.g. rotation rate, position of the continents), this paves the way for the possibility of proposing efficient parameterisations of complex non-equilibrium properties and of practically deducing fundamental properties of a planetary system from a relatively simple observable.

Zusammenfassung

Das Ziel dieser Arbeit ist es die mögliche Multistabilität des Klimas von Planeten im Bereich der bewohnbaren Zone zu untersuchen. Die Methodik, die dazu verwendet wird, wurde bereits auf das Erdsystem angewendet, aber die vorliegende Untersuchung hat einen breiteren Anwendungsbereich. Eine gründliche Untersuchung der Thermodynamik des Klimasystems bei sich stark ändernden Energiezuflüssen und variierender infraroter Opazität der Atmosphäre wird durchgeführt.

Mit der Hilfe von PlaSim, einem erdähnlichen globalen Klimamodell, wird die solare Konstante S zwischen 1160 und 1510 $Wm^{-}2$ und die CO_2 Konzentration zwischen 90 und 2880 ppm moduliert. Es wird eine Bistabilität des Klimas in diesen Parameterbereichen detektiert, d.h. es gibt zwei nebeneinanderher existierende Attraktoren, einer zeichnet sich durch warmes, feuchtes Klima (W) aus, der Andere verfügt über eine komplett gefrorene Meeresoberfläche (Schneeballerde, SB). Die Umkipppunkte beider Übergänge (W→SB und SB→W) befinden sich entlang gerader Linien in (S^*,log[CO_2]) Koordinaten. Die dynamischen und thermodynamischen Eigenschaften – Energieflüsse, Lorenzenergiezyklus, Carnoteffizienz, materielle Entropieproduktion – der W und SB Zustände sind sehr unterschiedlich: W Zustände sind dominiert durch den Wasserkreislauf und die latente Wärme ist wichtig für die materielle Entropieproduktion; die SB Zustände haben vorwiegend ein trockenes Klima, welches Wärmetransport vorwiegend durch sensible Wärmeflüsse erreicht und Entropie hauptsächlich durch Dissipation von kinetischer Energie entsteht. Es wird auch gezeigt, dass die Carnoteffizienz sich normalerweise erhöht nahe der Umkipppunkte zwischen W und SB und sich stark vermindert während des Übergangs.

Im letzten Teil der Arbeit, definieren wir wohl definierte empirische Funktionen, die es erlauben die globalen thermodynamischen Nichtgleichgewichtseigenschaften des Systems in Abhängigkeit von entweder der durchschnittlichen Oberflächentemperatur oder der durchschnittlichen planetaren Emissionstemperatur. Ein vorläufiges Resultat dieser Arbeit ist, dass, wenn die Rotationsrate des Planeten halbiert wird, sich die Multistabilitätseigenschaften, die quantitativen Schätzer der Thermodynamik des Systems und die ungefähre Parametrisierung in Abhängigkeit von der Emissionstemperatur an der Oberfläche nur schwach beeinflusst werden. Obwohl die spezifischen Ergebnisse, die hier präsentiert wurden, von den Charakteristiken des Erdsystems abhängen (zum Bsp. Rotationsrate, Lage der Kontinente) zeigt diese Arbeit doch Wege auf möglicherweise eine Parametrisierung von komplexen Nichtgleichgewichtseigenschaften zu finden und damit defacto fundamentale Eigenschaften eines planetaren Systems von relativ simplen Observablen abzuleiten.

Contents

Chapter 1

Introduction

1.1 Motivation

The space and atmospheric science communities are entering a new era thanks to the Kepler mission which has shown that there are in fact a large number of exoplanets of Earth and super Earth size, though little more than this can be said at this point due to the low resolution of such data and indirect methods used. For some, the motivation for studying and searching for exoplanets is purely a fascination of discovering the full range and types of atmospheres there may be and how they behave. However, for many the driving question is habitability which at present is limited to a definition related to the water belt. This is defined between a minimum and maximum distance away from a star with a given mass where a planet must be for it to receive the required solar irradiance to maintain H_2O in a liquid state. This is however a rather incomplete view as planets containing water may in fact not meet the necessary conditions for supporting life due to unfavourable orbital parameters: Questions such as: is a slowly rotating planet with little or no magnetic field a viable candidate? Are planets with large obliquities, eccentricity or very slow diurnal cycles viable due to the highly transient nature of there planetary atmospheres? The result is these effects may make a clear stable climatology impossible and hinder the evolution of life (or at least as we know it). This is potentially never more true than for binary and multi-star systems which make up nearly half of the more than 4,000 exoplanet candidates detected by Kepler so far. In fact, at present only 31 exoplanets are considered to be potentially habitable though many require a closer look. A recent example where this has occurred was from a study by Cartier [14]. They reviewed some of the "most interesting" Kepler planet candidates using the Hubble space telescope to perform high-resolution imaging to spatially resolve the stellar multiplicity of Kepler-296, KOI-2626 and KOI-3049. As

a result, it was found that Kepler-296 was not a single object but a binary system comprising of two red dwarf stars. A recalculation of the stellar flux based on this new information has meant that the habitable zone of Kepler-296 is further out than previously thought. Consequently, the exoplanet Kepler-296 d which was previously thought to be within the habitable zone is now believed to be interior to it. By contrast, the more far out exoplanets Kepler-296 e and Kepler-296 f are now expected to be sitting within habitable zone. An up to date list of habitable exoplanet candidates is available from http://phl.upr.edu/projects/habitable-exoplanets-catalog.

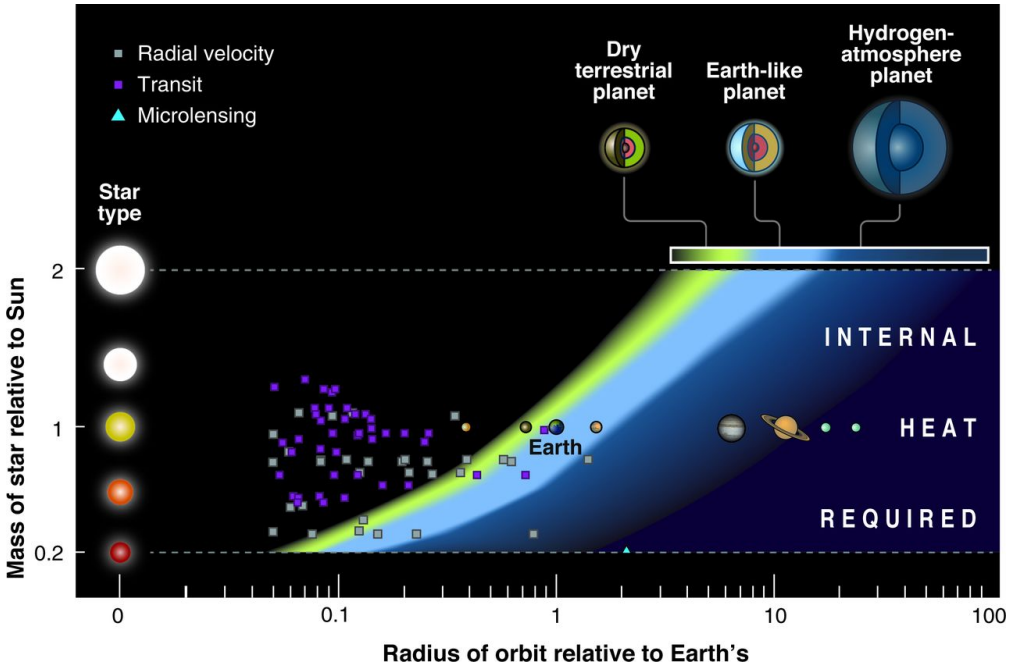

FIGURE 1.1: Average surface temperature in 3D baseline model (solid) and temperature in the 1D cloud-free model (dashed). Adopted from

One need look no further than the history of Earth to discover how conditions in our distant past were less than favourable for sustaining life. A bottleneck on cellular development during the Neoprotozoic era have led many to believe that the Earth has existed in the so called snowball (SB) state, a term first coined by Geobiologist Joseph Kirschvink, where the surface was either completely or nearly completely frozen over by ice. The importance of Snowball Earth theory is not simply that geologists wish to satisfy their curiosity about a distant and little known era of the planet's history but is also expected to have been of profound importance for Earth's burgeoning biosphere, and may have been the catalyst which led to the eventual appearance of photosynthesis and diversification of life in the run-up to the evolutionary explosion of the Cambrian Period where a wide variety of complex organisms formed. While the SB state may have threatened to wipe out single cell organisms, the photochemical reactions involving water vapour coupled with an extremely weak hydrological cycle, may have produced a vast amount of hydrogen peroxide which was then stored in the ice Liang et al. [64].

The end of the SB state would have then led to the release of oxygen to the atmosphere, so that the post SB Earth atmosphere contained about 21% compared to 1% prior to the SB Earth catastrophe.

Thermodynamics provides a means by which to describe the state of the climate of planetary systems and how they respond to perturbations. First conceived nearly 200 years ago, thermodynamics describes a specific aspect of all macroscopic systems in terms of certain fundamental bulk properties, namely the temperature, entropy, efficiency and work (Fermi [27]). Since then, more developed practical formulations of the equations governing thermodynamics have been derived and extended to the description of systems in a non-equilibrium state (Ambaum [3], DeGroot and Mazur [19], Kondepudi and Prigogine [53]). Indeed, thermodynamics provides key tools for studying non-equilibrium systems like the climate (Johnson [44, 45], Lucarini [75], Lucarini et al. [76, 77]), both for the Earth and for other planetary bodies. In relation to its bulk properties, thermodynamics make fundamentally universal statements which are beyond reproach, thus providing the best means by which to assess the physical consistency of a system being modelled. However, general circulation models (GCM's) suffer from an imperfect closure of the energy cycle as a result of artificial sources and sinks of energy due to limitations in numerical schemes. This is likely to explain the observed model cold bias and represents a violation in the laws of thermodynamics.

Relatively little work relating to the large scale thermodynamic properties of the climate has been done. The full benefit and range of applications where this approach may be applied is not yet well understood but could prove to be an invaluable tool for analysing Earth's atmosphere and that of the vast number of planetary systems being discovered. This may be especially useful in analysing the climate response of planetary atmospheres like Earth with a condensing phase, which are likely to support multistability due to the positive albedo feedback (Lucarini et al. [77]). In such cases, more than one distinct climatic regime may exist, one where the climate is mostly warm and moist and the other being dry with an ice covered surface. In order for a planetary system to support two such distinct climatic regimes without a stable intermediary state, the response of the system to perturbations must be to some extent non-linear to allow for the transition between both regimes to occur abruptly. It therefore follows, that planetary systems with a condensing phase are intrinsically more unpredictable and require more extensive investigation. To this end, the motivation of this thesis is to make a small step towards understanding the extent to which the thermodynamic properties can have in improving our understanding of climate response to different types of forcings. This will be done by using one of the most thermodynamically consistent GCM's, PlaSim, to perform a hysteresis experiment where the climate is forced by modulating the solar constant for

a wide range of CO_2 concentrations. The change in the thermodynamic quantities will then be analysed with respect to these perturbations and one another.

1.1.1 Planetary Systems, processes of the Atmosphere and Modelling Climate Sensitivity

Opik [87] first discussed the possibility of a global glaciation of Earth but concluded that a considerable decrease in the solar constant (S^*) was necessary. However, during the cold war era, motivated by the possibility of a nuclear winter - the result of a large dust injection into the atmosphere due to nuclear explosions - Budyko [12], Sellers [106] showed using simple thermodynamic energy balance models (EBM) that a decrease of only $2\% - 5\%$ in the absorbed solar radiation may potentially bring about the Snowball Earth state. They argued that a global catastrophe where global glaciation of Earth is made possible with such a relatively small decrease in the absorbed radiation via a positive sea-ice albedo feedback - specifically, Budyko [12], Sellers [106] results suggested that if the glacial extent encroached beyond 30° away from the poles, the increased global reflectivity, associated with the high albedo ($0.6-0.85$) of the expanding ice coupled with the low albedo ($0.1-0.3$) of the ocean it replaces, would mean the Earth surface and atmosphere may no longer be able to absorb sufficient energy from the sun to stop the sea-ice development from continuing all the way to the equator. This essentially means that there exists no stable climate states where the sea-ice extent is greater than $0°-30°$ and less than $0°-90°$. This implies that there will be a bifurcation in the global temperature thus increasing the real possibility that there may have existed a real snowball climate on Earth.

However, in EBM models a detailed representation of the atmosphere is missing, thus the effect of the climate dynamics is neglected, so that the response of properties such as the meridional enthalpy transport (MET), crucial for accurately calculating temperature change, both globally and regionally, is instead prescribed or calculated via an over simplified parametrisation. As urged by both Budyko [12], Sellers [106], such experiments must be built on using more general models which take into account the non-linear characteristics of the climate. The importance of considering the orbital properties of a planet on its fluid dynamics - and in turn global climate variability and sensitivity - can be clearly witnessed in both the laboratory and in outer space. For example, by altering the differential heating and rotation of an annulus one may analysis the different possible flow patterns corresponding to a variety of dynamical regimes which provides a surprisingly good analogue for studying the underlying processes which occur in the atmosphere, as well as pointing to the possibility of planetary atmospheres with rather different dynamics to those of Earth. Fig. 1.2 gives examples of such experiments where

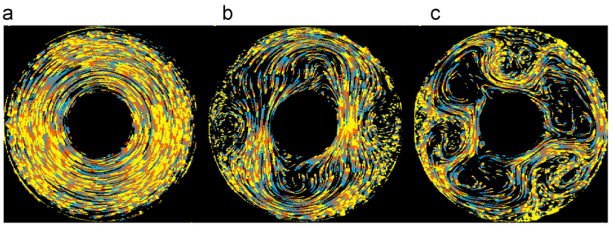

FIGURE 1.2: Showing 3 cases of the upper level fluid flow pattern in a differentially heated rotating annulus where the rotation rate, Ω is (a) 0.3 rads^{-1} (b) 1.0 rads^{-1} (c) 3.0 rads^{-1}. The flow of (a) steady and axisymmetric while (b) and (c) show equilibrated baroclinic waves and eddies which have a steady amplitude in (b) but unsteady and chaotic in (c). Adopted from Read [102]

.

the rotation rate is varied under fixed differential heating, leading to three distinct fluid regimes from steady, axisymmetric to unsteady, chaotic flow from a slow to fast rotating annulus, respectively. From a climate perspective, the reason why this is so important is that these different flow regimes lead to different heat transports which have an impact on the global but in particular local differences in temperature both in space and time.

Within our Solar System, Venus, Mars and Titan are the most similarly sized planetary bodies to Earth which have significant atmospheres. Venus has been referred to as Earth's twin due to it's comparative size and mass. Additionally, they are of the most comparable in distance from the Sun relative to the other planets in the Solar System. Yet, due to the difference between their orbital parameters and atmospheric composition they are observed to have surprisingly different temperatures, temperature distributions and climate dynamic features. The atmosphere of Venus is mostly composed of CO_2, and is about 100 times thicker than that of the Earth, which results in a larger green house forcing and means that the fluid also has a far greater thermal inertia. The surface temperature of Venus is approximately 750K as a result of the high IR opacity and despite the high planetary albedo (0.7 comparable to ice covered planet). The consequence of this means that despite the slow retrograde planetary rotation rate (240 days and a diurnal cycle of 116 days), the day-night contrast (and the horizontal temperature distribution in general) is small.

By contrast to Venus, at first sight Saturn's moon Titan would appear to have little in common with Earth as the solar insolation is smaller by two orders of magnitude, surface temperature is about 95K and has a diameter only 50% larger and is only 80% more massive than Earth's natural satellite, the Moon. However, thanks largely to evidence provided by the Cassini (and Voyager) spacecraft, comparisons are also being drawn between Titan and Earth, though rather than mostly for its bulk characteristics as is the case with Venus, instead for the similarity of the weather features and processes believed to occur within its atmosphere and at the surface. Observations suggest that methane

behaves as an analogue to water on Titan (Coustenis [16], Flasar et al. [28], Niemann et al. [85], Tobie et al. [115]) existing at the surface in solid and liquid form leading to river canals, while also as a gas (and clouds) in the atmosphere performing an analogous role to the hydrological cycle, transferring latent heat energy vertically and from warmer to colder regions, via evaporation at the surface and eventually condensing to form clouds which rainout in the atmosphere. Additionally, changes in the surface height on Titan of about 10m between flybys as well as data pertaining to the density of the moon suggest that a global wide liquid water ocean may exist below its surface.

When comparing Titan to Venus many of the differences in composition, vertical and horizontal profiles[1] and the amount of total atmospheric mass are even larger than they are relative to Earth. Nevertheless, unlike Earth the atmospheric circulations of both Venus and Titan are well known to exhibit a variety of similar enigmatic features such as strong super-rotation[2](Lebonnois et al. [60], Tokano et al. [116], Yamamoto and Takahashi [123]) by virtue of the fact that both bodies rotate slowly and strongly absorb IR radiation in the atmosphere leading to the pressure gradients in the atmospheric fluid being balanced by the centrifugal force (Cyclostrophic balance, Leovy [62], Limaye [67]) rather than the Coriolis force (geostrophic balance) which dominates large scale flow on Earth due to the fast planetary rotation rate.

For all the telluric bodies[3] in the solar system, the solar irradiance over a long time average peaks along the equatorial band. The net heating therefore occurs at the equator and net cooling over the polar regions. The resulting differential heating drives the convective atmospheric circulations, transferring heat vertically from the equatorial region upwards and horizontally towards the poles. Such thermally direct atmospheric circulations are commonly refereed to as a Hadley cell (Huang and McElroy [42]), normally in reference to the Earth's atmosphere though is now more generally used in the description of atmospheres from other planetary bodies which display similar properties (Edson et al. [24]) as those discussed here . The Hadley cell is characterised by a rising branch, located in the region of net heating, though the exact position is perturbed by any asymmetry of the surface boundary conditions about the equator, due to the differences in specific heat capacity, albedo and orographic height of the sea, land and ice. The extent of the Hadley cell for a given atmosphere is to a first order controlled by the planetary rotation rate: the larger the planetary rotation rate, the smaller the extent of the Hadley cell. The result is that when planets rotate rapidly heat is transferred less

[1] On Venus and titan, the dominant variations in space and time are due to the diurnal and season cycles, respectively

[2] Super-rotation is characterised by a faster rotation of the atmosphere compared to the rotation rate of the solid body, and is most likely found in slowly rotating planetary bodies.

[3] Planetary bodies which are Earth-like in terms of composition, primarily containing silicate rocks and metals.

effectively polewards allowing the resulting atmospheric state to support a larger meridional temperature gradient than in the case of slowly rotating planetary bodies. This then also dictates the prevalent regions of large scale cloud cover which are intrinsically related to the positioning of the rising and falling branches of the meridional overturning circulation. The cloud cover in turn modifies the local energy imbalance by changing the planetary albedo (Donohoe and Battisti [20, 21]) as well as the absorption spectrum of the atmosphere to incoming and outgoing radiation which in turn reorganises the climate state until the net global energy imbalance over a long time mean is approximately zero. In this sense it is clear that along with the solar distribution, the rotation rate and the resulting circulation regime of the atmospheric fluid directly impact the temperature distributions and climatology.[4]

The EBM experiments illustrate that even just by considering the global energy balance and albedo change, it is possible to get a non-linear response when changing a single climate parameter (Bódai et al. [6], Budyko [12], Ghil [34], Sellers [106]). However, as briefly described above their are many feedbacks between many interacting processes which may produce a non-linear response and it is only by their explicit consideration in conjunction with one another, can the true response of the climate be deduced. The procedure by which this occurs is further complicated by the fact that these processes interact within and across a wide range of spatial and time scales covering many orders of magnitude. Therefore, the most important difficulty of climate theory is that there does not exist a simple way to define the closure of the system Lucarini and Ragone [78]. Convection which results in the vertical and horizontal mass transport of the Hadley circulation leads to the large synoptic scale eddy motions which provide kinetic energy (K) to the zonal flow Lorenz [71, 72]. These continually transfer energy down to progressively smaller eddy structures, where molecular diffusion of K becomes important and viscous dissipation of energy acts as a sink of K on Kolmogorov length scales (Kolmogorov [52]). Leconte et al. [61] shows using the LMD model to simulate the climate, that under a 1D radiative-convective configuration, temperature increase to an increase in solar flux is far higher than in the case of the full 3D planetary representation as shown in Fig. 1.3. Furthermore, though both cases show a non-linear monotonic increase in temperature, the functional form i.e. climate sensitivity, differers. One of the main focus' of this thesis will be to investigate how dependent climate sensitivity is on two types of processes which provides a forcing to the climate - one which controls

[4]Note also, that unlike the other telluric bodies in the solar system, Titan's general circulation exhibits the strongest seasonal changes. In and around the time of the equinox a convective Hadley cell forms centred around the equator extending towards the poles, while, during the solstice the patten changes, with a single cell forming which extends from the South to the North pole, efficiently transporting energy from one pole to the other. Seasonality does also have an effect on the Hadley cells structure and may cause a single though far narrower singular structured form of the Hadley cell to occur on Earth and more clearly on Mars due to its thinner atmosphere and lower thermal inertia.

the incoming and the second which does so for the outgoing radiation. The net effect in both cases is to change the internal energy of the climate system.

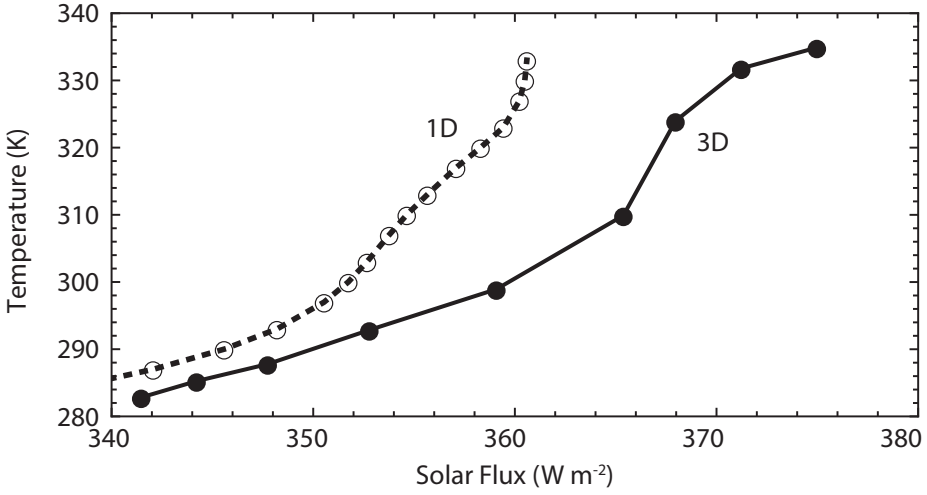

FIGURE 1.3: Average surface temperature in 3D baseline model (solid) and temperature in the 1D cloud-free model (dashed). Adopted from Leconte et al. [61]

Clouds also serve as an excellent example of a feature of the climate system which act on large spacial scales but depend on its small scale properties. The nucleation of gaseous molecules (i.e water on Earth and methane on Titan) are often found to develop into synoptic or even planetary scale cloud structures, as in the case of Venus. As mentioned above, though there formation is largely instigated by the thermally driven vertical motions of the atmosphere, their molecular properties and thus the radiation absorption spectrum has a complex response to the conditions of the surrounding state of the atmospheric fluid, in terms of the temperature, pressure, humidity and aerosol contents. The interaction of clouds with incoming SW or outgoing LW radiation is therefore able to provide either a net warming or cooling effect on the overall climate state due to the way they modify the local climate energy imbalance. For Earth's present climate state, the net effect of clouds on the TOA fluxes has been established and confirmed through various satellite scanning instruments on board the Earth Radiation Budget Experiment (ERBE), Clouds and the Earth's Radiant Energy System (CERES) and most recently the French Scanner for Radiation, that globally, they reflect more incoming SW radiation than they absorb outgoing LW radiation and therefore have a cooling effect on the climate by decreasing the surface temperature by about 5 degrees Celsius. However, this sum is composed from a mixture of cloud types, where those which tend to form in the upper atmosphere have a net warming effect. A major question at present is how the changing atmospheric conditions due to the continuing situation of anthropogenic climate warming will impact the type of cloud formation in the future. If the overall contribution of clouds with a net warming effect was to increase (decrease),

their role would provide a positive (negative) feedback and thus increase (decrease) climate sensitivity and would add to (mitigate) any future run away greenhouse effect.

Ideally, an explicit mathematical description of all processes on all time and spacial scales would be included, however doing so would of course be computationally impossible. It is instead necessary to choose the correct model which best suits the requirements of the experiment - a model resolution which is sufficiently high and can run the experiment within the allotted time which accurately resolves the most relevant processes. Realistically what is potentially achievable is a suit of models which allows the user to access the full model hierarchy including: radiative convective models, EBM's, Simplified forcing GCM's and state of the art full global climate models based around a universal set of equations, capable of recreating virtual representations of any planetary body based on known information. As a result, the atmosphere is rich with processes which are not explicitly represented in models such as shallow and deep convection key to the motion of the fluid and the formation of clouds that transfer sensible and latent heat energy between the planet surface, atmospheric boundary layer and through to the upper atmosphere. Despite their importance, convective clouds pose a great challenge for atmospheric modelling at all scales. As they are too small to be explicitly resolved so need to be parameterised in climate and weather models. Even in convective-scale numerical weather prediction models that try to explicitly represent deep convective motions (Holloway et al. [40]), the shallow boundary layer clouds and the sub-cloud layer still need to be parameterised. Such parameterizations are at the source of large uncertainties; their limited skill both reflects the complexity of the system and our poor knowledge of the involved processes and scale interactions.

Regardless, it is necessary to parametrise the important sub-grid scale processes ultimately meaning that there applicability is limited within a range of conditions for-which it is possible to confirm their validity via observations or experimental data. It is therefore possible to recreate current climate conditions with appropriate tuning of the parameterisations with a fair degree of accuracy (though still many phenomena are not well or at all represented) but how accurately results under climate conditions which stray significantly far from that of the Earth in models is debatable without a good proxy available for comparison. Nevertheless, with the large number of degrees of freedom available in such models, a great number of processes may be explored and with greater accuracy when compared with EBM's. As it could be the case that the climate may change dramatically with only a 2°C change in the solar forcing, the range of applicable stable states may be rather narrow indeed. However, in general whether large changes to the climate state are realised is dependant on the initial conditions along the climatic attractor on which it exists . It has however been possible to recreate the general features of the atmospheric dynamics of the telluric bodies of the solar system

based on current observation however, of course many features remain far from being well understood.

There is a clear overlap developing between the space and atmospheric science communities where previously the focus has been on an accurate representation of radiation and atmospheric dynamics, respectively. The indirect measurement of many Earth- like exoplanets has accelerated curiosity in sharing expertise for developing more versatile climate models, particularly as resolving such planets from observation with more than a couple of pixel accuracy at best is probably decades away. However, limited knowledge of the bulk, orbital and spectral properties of exo-planetary bodies should be sufficient to learn within some reasonably well defined bounds, about the nature of circulations and the possibility for habitability, perhaps even on a regional level for these newly discovered worlds.

As a result of the physical design difficulties and huge costs involved in developing the next generation of telescopes to properly view extra solar planetary bodies, much of the insights over the following decades should come from the modelling community. It is therefore the responsibility of modellers to continue developing more flexible GCM's which allow for the comparison of the limited information of the spatially integrated spectral properties of available exoplanet observations with GCM's, in order to attempt to develop realistic climates of the known exoplantary systems. Flexible models should have the ability to accept an exhaustive range and variety of parameters and processes connected to the planets radiative, bulk and orbital properties, photo chemistry, atmospheric composition (including aerosols). It will then be possible to decide on which specific exoplanet candidates to focus on in order to ask more specific research questions i.e. which candidates are most suited to supporting life due to favourable fluid dynamic properties to instigate the chemical development of proteins, be it carbon based or otherwise. The continuing developments of such models through collaborations should bring about more rapid development and provide the ability to turn on and off modules at will to provide the the range of conductible experiments. Models also provide a great testing ground for analysing the effectiveness of new observational techniques for indirectly identifying properties of exoplanets. Furthermore, GCM's can play a prominent role in developing new and improved techniques of how better to observe various orbital properties. Coupled with improved understanding of the climate system, one may develop a taxonomy of exoplanets with a hierarchical structure that allows for a better understanding of which questions suit which problems, thus allowing for the various scientific communities involved, be it observers, theoreticians, modellers etc, to understand how to tackle the problem better with the correct overview in mind. Furthermore, the work of simpler models for understanding the fundamental physical mechanisms behind climate is still critical, and while we exist in the era of big data, the fundamentals must

not be left behind and we must ensure that the physical principals are better focused on so that models are consistent.

1.1.2 Thesis Overview

The importance of the thermodynamic climate properties has been somewhat neglected by the climate science community, this being most evident in the large/notable imbalance in the global energy budget intrinsic to all IPCC GCM's Lucarini and Ragone [78]. The climate system is an excellent example of a forced dissipative system maintained far from thermodynamic equilibrium and as such it shall be these properties which are focused on in the analysis of this thesis, in particular, surface temperature (T_S), material entropy production (S_{mat}), Carnot efficiency (η), work (done by the atmospheric motions) (W) and meridional enthalpy transport (MET). As such, this thesis will show/demonstrate by consideration of a wide array of climate states how these properties change relative to differing climate conditions and compared to one another, through clear visual representation of the climatic manifolds and functional dependences, with respect to the climate forcings. The results of these experiments hopes to provide a better understanding of the relevance and meaning of these properties in terms of the study of climate and in doing so provide an alternative way of viewing the general state of the climate from a thermodynamic perspective. Furthermore, it will also show how changes to the rotation rate modify the shape of the manifold and in doing so, the climate sensitivity and bistable properties.

This is done by modulating in combination both the the CO_2 concentration and the solar constant (S^*) which provides two distinct methods by which to modify the total energy contained within the climate system. The former does so indirectly through the infra-red opacity which controls the energy leaving the climate system in the form of the outgoing LW radiation while the latter directly alters the energy entering the system from incoming solar radiation. Furthermore, the effect of modifying the baroclinic properties of the fluid dynamics on climate sensitivity is also examined via changes to the planetary rotation rate, respectively.

As outlined in this chapter, my thesis re-examines for the case of an Earth-like planet, whether being in the habitable zone is a sufficient condition for ensuring the presence of liquid water at the surface and provides insights pertaining to climate sensitivity and bistability from a thermodynamic perspective. This has been done by performing an extensive parametric study exploring the effect of changing the solar irradiance and the atmospheric opacity (the latter modulated by the CO_2 concentration) for an Earth-like planet. Additionally, the robustness of the functional dependence of the examined

thermodynamic quantities with the surface and emission temperatures are tested for changes to the planetary rotation rate and the diurnal cycles independently.

The structure of this thesis is as follows:

Chapter 2 - Physical Concepts for Climate Dynamics: The underlining concepts relevant to this thesis are discussed and summarised. Firstly the energetics of the climate system are described. The concept of considering the Earth system analogous to a heat engine is introduced, the properties of which are then defined in terms of the systems thermodynamic properties.

Chapter 3 - Snowball Earth, Bistability and feedbacks in the Climate System: The problem of critical transitions is considered in the context of the climates response to perturbations. Climate model evidence for the multistable properties of the Earth due to the albedo feedback is reviewed along with a description of the climate features which act as feedbacks in aid of or to hinder the abrupt transitions when moving between warm and snowball climate regimes. Finally, research on in to climate bistability which utilises the ideas discussed in chapter 2 is discussed.

Chapter 4 - Thermodynamic Insights into the role of Solar Forcing and Opacity: The goal of this chapter is to diagnose the previously defined thermodynamic properties using the PlaSim GCM in order to gain a better understanding of what they represent from within a climatological context and what this teaches us about non-equilibrium nature of the climate system. The chapter begins with a comparative study between the warm (W) and snowball (SB) climate states. This provides a setting to the subsequent analysis in the remainder of the chapter which first focuses on the bi-stability properties of the Earth system in the context of the change in the T_S and S_{mat} within the S^*-[CO_2] phase space. Building on this, a relative comparison of how differently the thermodynamic properties vary across the S^*-[CO_2] phase space, depending on the attractor, W or SB, being traversed. Conclusions are drawn between the dynamic and thermodynamic climate properties.

Chapter 5 - Parametrisations: Using the same data as before the S^* and [CO_2] dependence is removed and the thermodynamic properties of the system are analysed as a function of T_S and T_E. The same experiment is then repeated but for the case of an Earth like planet rotating at half the normal rate of the contemporary Earth. By doing so, there is a significant change to the climate dynamics. A comparison is then made between the thermodynamic properties of both sets of data is made.

Chapter 6 - Conclusion: The results of this thesis are summarized and their interpretation are discussed. An outlook for possible future work to expand the scope of the findings made here is then given.

The appendices contains supplementary information. Appendix A has two addition figures and B provides description of the model set up and description of PlaSim, the GCM used for this thesis work.

Chapter 2

Concepts and Methods

The purpose of chapter 2 will be to provide the conceptual background and methodology which shall be used to investigate the problem of critical transitions of the global climate system in chapters 4 and 5. In particular, chapter 2, will describe the relevant theory pertaining to the energetics of the climate system. Firstly, the processes which contribute to the overall energy budget of the climate are discussed, followed by a description of the energy exchange between the warm equatorial and cold polar regions of the planet. This leads on to the final part of this section which describes the thermodynamic tools that shall be used in the remaining chapters. Too this end, the concept of treating the atmosphere as a heat engine is introduced which then provides a frame work in which to describe the climate system in terms of its fundamental thermodynamic properties.

2.1 Physical Concepts for Climate Dynamics

2.1.1 The Energy Budget of optically thin Planetary Atmospheres

Earth may be considered an open thermodynamic system, partly absorbing radiation from the Sun (Ambaum [3], Lucarini [75], Lucarini et al. [76, 77], Peixoto et al. [93], Peixoto and Oort [94]). This energy is exchanged with the atmosphere and ultimately re-irradiated back out to space in the form of long wave radiation (LW), while the rest is reflected without interaction as short wave radiation (SW). Considering the Earth system as a single object acting under constant forcing, over long time periods, steady state will ultimately be achieved with the first law of thermodynamics (Fermi [27]) dictating that the globally absorbed incoming solar radiation (ASR) is balanced by the outgoing LW fluxes (OLR) as measured at the top of the atmosphere (TOA), provided

the parameters of the system remain fixed. The resulting global energy budget ($\dot{E}$) of the planet will then be zero,

$$\overline{\{ASR - OLR\}} = \overline{\left\{F_R^{TOA}\right\}} = \overline{\{\dot{E}\}} = 0 \tag{2.1}$$

where $\overline{F_R^{TOA}}$ is the net radiative fluxes at the TOA. The over line, dot and curly brackets denote long time means, time derivatives and global integration, respectively. In order for the incoming solar fluxes to degrade into outgoing LW fluxes, they must be absorbed by the atmosphere and/or surface, thus increasing the internal (I) and potential energy (P) of the Earth system. The type and extent of the interaction is dependent on the material properties of the system where the relatively high transparency of the atmosphere to incoming SW solar radiation on Earth means the majority is absorbed at the surface before re-emission as LW radiation (Trenberth and Fasullo [118]). By contrast to the SW fluxes, the atmosphere is strongly absorbent to LW radiation which is then consequently and continuously re-emitted, scattered and re-absorbed, by the surface and in the atmosphere, before escaping into space. The resulting energy budget at the surface, E_S is,

$$\overline{\left\{F_{LW,S}^{\uparrow} - F_{LW,A}^{\downarrow} - F_{SW,S}^{\downarrow} + +F_{SH} + F_{LH}\right\}} =$$

$$\overline{\{F_{R,S} + F_{SH} + F_{LH}\}} = \overline{\{\dot{E}_S\}} = 0 \tag{2.2}$$

Where $F_{LW,S}^{\uparrow}$ is the thermal emission released from the surface in the LW region of the spectrum as $T_S << T_{sun}$ and may be computed as σT_S^4. The LW and SW radiation absorbed at the surface from the atmosphere and Sun are given by $F_{LW,A}^{\downarrow}$ and $F_{SW,S}^{\downarrow}$, respectively. Additionally, turbulent fluxes acting on molecular scales are generated at the surface: sensible heat fluxes (F_{SH}) drive the convection of the atmospheric fluid on large scales, while the evaporation of water in the oceans, biosphere and lithosphere indirectly warm the atmosphere via latent heat fluxes (F_{LH}).

Under present Earth conditions, latent heat energy provides the largest net contribution of energy lost by the surface to the atmosphere (Fasullo and Trenberth [26]), however, under climate conditions such as the snowball (SB) state where the atmosphere is intrinsically dryer, the relative contributions between the latent and sensible heat fluxes are rather different with the latter dominating(Abbot et al. [1], Abbot [2], Lucarini et al. [77]). Through the Clausius-Clapeyron relation the magnitude of the evaporation increases exponentially with temperature, thus, the latent heat transfer to the atmosphere becomes a progressively more efficient process with increasing temperature. A more

detailed description of the difference in the energy transport processes of the SB and warm (W) climate states shall be discussed in the following chapters.

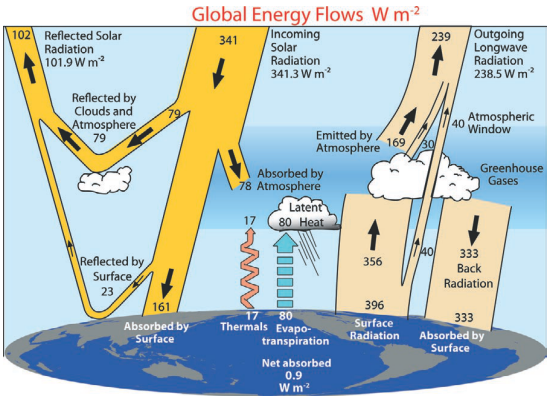

FIGURE 2.1: The global annual mean Earth's energy budget for the Mar 2000 to May 2004 period (Wm^{-2}). The broad arrows indicate the schematic flow of energy in proportion to their importance. Adopted from Trenberth and Fasullo [118].

2.1.2 The Meridional Heat Transport

The energetics of the climate system will now be discussed. As a first step, the specific energy is introduced. The addition of the energies associated with the process which occur within the atmosphere give the total specific energy per unit mass (e) of the atmospheric fluid as,

$$e = c_v T + gz + Lq_l + \frac{1}{2}\mathbf{c}^2; \tag{2.3}$$

while the corresponding equivalent expressions for the lithosphere and ocean are, $e_{lith} = c_{lith}T + gz$ and $e_{oc} = c_{oc}T + gz + \mathbf{c}^2/2$, respectively, where terms 1, 2 and 3 on the RHS of Eq. 2.3 are the internal, potential and latent energies, which together give the moist static energy. c_v, T, g, z, L, q_l are the specific heat capacity at constant volume, temperature, acceleration due to gravity, the height above the surface, latent heat of vaporisation and specific humidity, respectively. The final term is the K per unit mass which is a direct representation of the convection generated by the sensible heat fluxes in terms of the velocity ($\mathbf{c}^2 = u^2 + v^2 + w^2$) of the wind field.

When observing the internal workings of the climate system up close, the short period of the diurnal cycle (24h) with respect to the thermal inertia keeps the zonal structure roughly symmetric. The focus of the solar irradiance resides over the tropics due to the spheroidal form of Earth which receives roughly 5 times as much as the poles so that there

exists a latitudinal dependency of the ASR. If one imagines the hypothetical scenario where the latitudes bands are decoupled so no horizontal transport could occur, each vertical column would eventually reach its own steady state where $OLR(\varphi) = ASR(\varphi)$ and the equator to pole temperature gradient would be much larger than in the present Earth climate. In the real atmosphere, the large difference in the density of adjacent latitude bands means this scenario is unstable, giving rise to baroclinic eddies which work in response to these differences by redistributing energy from the low to high latitudes via what is commonly referred to as the meridional heat transport or more specifically, the meridional enthalpy transport (MET), as the process also involves the exchange of mass. The atmospheric component of the MET can be calculated directly from the components of the total specific energy as summarised by Eq. 2.3. It is then possible to estimate the MET of the climate system indirectly from the radiative fluxes as described by Lucarini and Ragone [78], which shall be summarized below. Beginning by first considering the instantaneous change in time (t) for the local balance of the total energy density for an atmospheric fluid which contains the kinetic and moist static energy components as follows Peixoto and Oort [94],

$$\frac{\partial \rho e}{\partial t} = -\nabla.(\rho e \mathbf{c}) - \nabla.\mathbf{F}_R - \nabla.\mathbf{F}_S - \nabla.\mathbf{F}_L - \nabla.(p\mathbf{c} + \tau.\mathbf{c}), \tag{2.4}$$

and is expressed as the sum of the divergence of the vectors: the total energy transport, radiative ($\mathbf{F}_R$), sensible ($\mathbf{F}_S$), and latent ($\mathbf{F}_L$) fluxes, where ρ is the density; τ is the stress tensor; and $\mathbf{c}$ is the velocity vector. The final term represents the work at the boundary by the pressure (p) and stresses (τ). It is however convenient to rearrange Eq. 2.4 by combining p and e so as to explicitly represent the enthalpy of the system, $h = e + p/\rho$ as,

$$\frac{\partial \rho e}{\partial t} = -\nabla.\mathbf{J}_h - \nabla.\mathbf{F}_R - \nabla.\mathbf{F}_S - \nabla.\mathbf{F}_L - \nabla.(\tau.\mathbf{c}), \tag{2.5}$$

Where the first term represents the total enthalpy transport ($\nabla.\mathbf{J}_h = (\rho e + p)c = \rho h v$). All terms on the RHS contain processes which involve the conversion and/or transfer of energy within the climate system. In addition, terms 2 and 5 also contain those processes which connect the Earth system with the surrounding universe. In particular, the influx of solar radiation and outgoing fluxes are contained within the second term on the RHS, while the final term provides an often neglected source of mechanical work performed on the system through the gravitational interaction between celestial bodies which is most evident from the ocean tides. While from the context of the Earth system this represents a relatively small component of energy, other planetary bodies such as Europa undergo far more extreme gravitational interactions due to the ellipticity and

close proximity to the relatively massive Saturn. The resulting stresses generate massive frictional heating which liquefies the interior and releases energy at the surface[1].

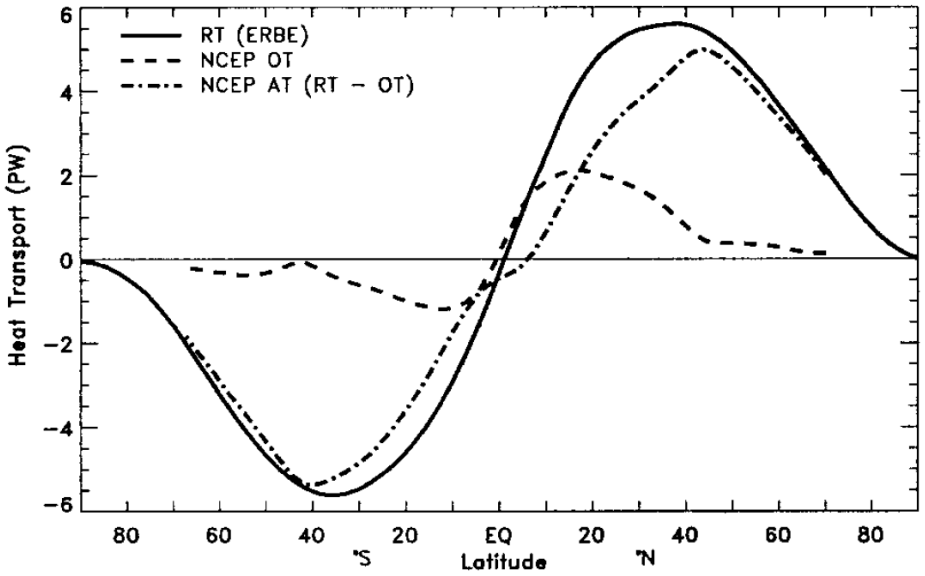

FIGURE 2.2: Annual meridional enthalpy transports estimated from satellite and reanalysis data (PW), for the atmosphere (dash-dotted), Ocean (dashed) and total (solid). Adopted from Trenberth and Caron [117].

To all intents and purposes, the ocean should be considered a mechanically driven system Kuhlbrodt et al. [54] rather than a heat engine as the amount of K responsible for maintaining the observed ocean circulation against dissipation via wind stresses, far out weights the generation of P via heating at the surface. The ocean contribution to the global entropy budget is therefore assumed to be negligible. The MET is obtained by integrating over x and z as,

$$\int\int \rho v h(\varphi')dxdz = \int_{Z_s}^{TOA}\int_0^{2\pi} \rho v(I + gz + Lq_l + \frac{1}{2}\mathbf{c}^2 + p/\rho)dxdz; \tag{2.6}$$

and for the ocean as,

$$\int\int \rho v_{oc} h_{oc}(\varphi')dxdz = \int_{z_b}^{Z_s}\int_0^{2\pi} \rho v(I_{oc} + gz + \frac{1}{2}\mathbf{c}_{oc}^2 + p/\rho_{oc})dxdz; \tag{2.7}$$

Where the final term on the RHS is the word done by the pressure at the surface but are represented here as a property transport and has been additionally included to accurately represent that this is indeed the energy transport which includes the enthalpy defined as $I + p/\rho$ (Fermi [27]). Thus, $h = e + p/\rho$ is used rather than e on the LHS, where ρ and p

[1] note, not included in the description are terms pertaining to the geothermal, electrical and nuclear forms of energy, which while negligible to the state of the Earth's atmosphere may well provide significant external energy contributions in the case of other exoplanetary atmosphere's.

are the specific volume and pressure, respectively. The subscript oc denotes quantities pertaining to the ocean.

The ASR to a first order, is largely fixed for atmospheres which are optically thin to incoming solar radiation (Donohoe and Battisti [20, 21]), however energy conservation dictates that a consequence of the MET is that the magnitude of the OLR is decreased in the low latitudes and increased at the poles, thus there exists a net energy surplus in the Tropics and deficit in the Polar region. As the equilibrium temperature of a given latitude band is related to the OLR as, $T_{eq}(\varphi) = \sqrt[4]{OLR(\varphi)/\sigma}$, the energy transport acts to decrease the meridional temperature gradient.

Expressing Eq. 2.5 in terms of spherical coordinates and applying the thin shell approximation where the height of the atmosphere (z) is assumed to be negligible compared to the radius of Earth, (R) so that $R \approx R + z$, as follows,

$$\frac{\partial \rho e}{\partial t} = \frac{1}{Rcos\varphi}\frac{\partial J_{h\lambda}}{\partial \lambda} - \frac{1}{Rcos\varphi}\frac{\partial J_{h\varphi}cos\varphi}{\partial \varphi} - \frac{\partial J_{hz}}{\partial z} - \frac{\partial}{\partial z}[F_{Rz} + F_{Sz} + F_{Lz} + (\tau.\mathbf{c})_z] \quad (2.8)$$

where φ is the latitude and λ is the longitude. The horizontal components for the final term on the RHS have been neglected as the vertical component is at least an order of magnitude larger (Peixoto and Oort [94]). To examine the meridional structure, Eq. 2.8 must be vertically and zonally integrated as,

$$[\dot{E}_T] = -\frac{1}{R}\frac{\partial T_T}{\partial \varphi} + [F_R^{TOA}], \quad (2.9)$$

where $\dot{E}_T$ is the net energy balance of the entire planet as a function of time and space, F_R^{TOA} are the net radiative fluxes at the TOA. The square brackets indicate that the relevant quantities are expressed as zonal averages, which for an arbitrary variable X is calculated as, $[X(t,\varphi)] = \int_0^{2\pi} X(t,\lambda',\varphi)Rcos\varphi d\lambda'$, so that,

$$T_T(t,\varphi) = \int_0^{2\pi}\int_{z_b}^{TOA} J_{h\varphi}(t,\lambda',\varphi,z')Rcos\varphi dz' d\lambda', \quad (2.10)$$

Fig. 2.3 illustrates how the variation in the zonally integrated OLR is more homogeneous than the ASR thus giving rise to an energy surplus in the Tropics and deficit at the poles, the magnitude of which is given by the areas between both lines. The surplus and deficit regions may therefore be considered as the latitudes which act as the main source and sinks, respectively, of energy moving to and from Earth system, averaged over one complete solar cycle. In quasi-steady state, where the energy budget is assumed to

be zero, the energy deficit is equal to the energy surplus which consequently is equal to the total energy which can be transfer from low to high latitudes, the latitudinal dependence of which is shown in Fig. 2.2. The MET is therefore constrained by the relative differences between the meridional OLR and ASR flux profiles. Furthermore, the latitude of maximum MET is intrinsically linked to the point where the profile of the ASR and OLR intercept one another. By association, the properties of the climate which modify the OLR and ASR profiles (including the MET itself) influence the magnitude and latitudinal distribution of MET. Though making predictions about the response of the MET is never trivial, making certain assertions as to its behaviour under transient conditions is more intuitive as one may assume the system tends to-forwards steady state. However, once the system stabilises after a transient period due to a given change to the climate forcing, the final value of the MET in steady state is far less predictable due to the interdependence of the feedbacks between all processes. For instance, the initial transient response to an increase in the solar forcing will be to increase the MET. One of the main responses to this initial increase in MET will be to decrease the polar surface albedo as a consequence of increased sea-ice melt which in turn will increase the polar OLR. It is therefore not possible to assume that in the final state of the system, the MET will have increased or decreased. In fact, it shall be shown later that within the limit of a range of differently forced climate steady states supporting a partially ice covered surface, the MET is a rather robust quantity and remains largely unchanged.

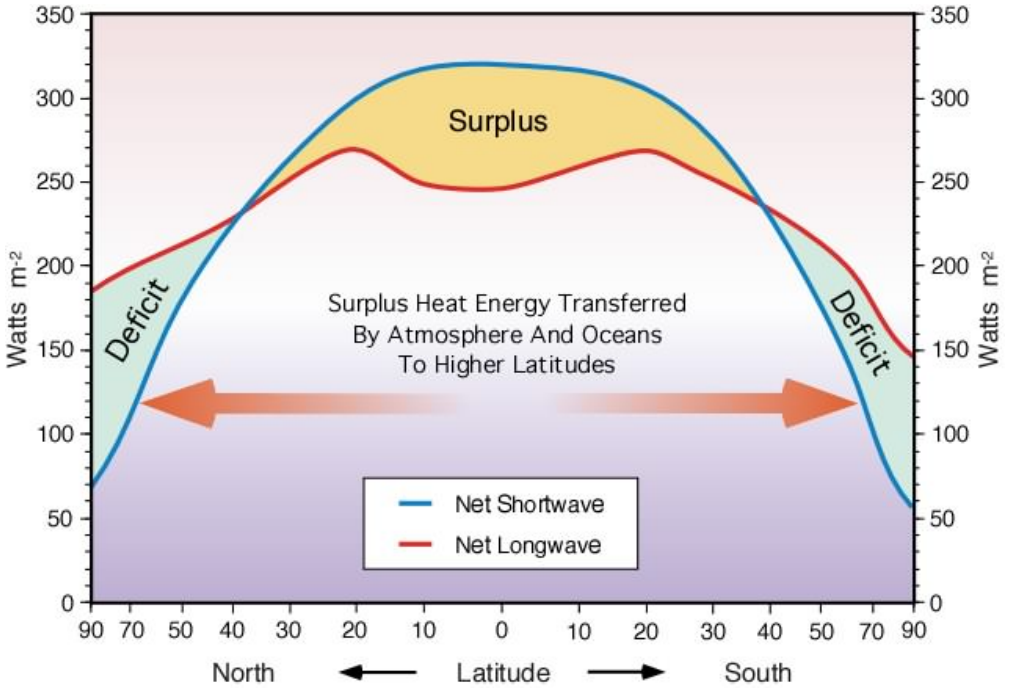

FIGURE 2.3: The average annual absorbed incoming solar (blue line) and emitted outgoing infra-red (red line) radiation by the Earth and the atmosphere. Taken from Pidwirny [96].

In order to illustrate the importance of the MET, consider for a moment its possible implication on climate sensitivity and bistability as viewed from the simple frame work of a 1-D EBM. For instance, if one considers a hypothetical climate with a sufficiently strong MET , the equator to pole gradient will be small as a result of lower equatorial and higher polar temperatures. Such a climate will therefore also see a more even change in climate sensitivity across all latitudes with a decrease in solar insolation, S^*, where the poles will be warmer and the tropics colder. Conversely, at the other extreme, where the MET in very weak , the temperature gradient will be large and the transition to the snowball state will occur at relatively high values of S^*. As discussed earlier, from Eq. 2.1, the climate system may be considered in steady state if the incoming and outgoing fluxes at the TOA cancel out. A prerequisite for this to occur is that the system remains under constant forcing for a sufficiently long period of time that allows for all internal processes to reach steady state. The multitude of time scales involved are typically of the order of 1 year in the atmosphere and up to thousands of years in the case of the ocean circulation, plus the variability of both the internal forcings such as volcanic eruptions, as well as external forcing of the Sun's radiation as it ages, mean that the climate system has never truly existed in steady state. However, during periods where the change in such forcings have been minimal, the system maybe regarded as being in a quasi-steady state.

Applying the steady state assumption of Eq. 2.1 to Eq. 2.10 means that the LHS goes to zero. The total average MET through a given latitude boundary may therefore be calculated indirectly from the radiative fluxes at the TOA as,

$$\overline{T_T}(\varphi) = -\int_{\varphi}^{\pi/2} \overline{[F_R^{TOA}](\varphi')} R \partial \varphi', \tag{2.11}$$

Where the upper integration limit is chosen to be at either one of the poles (+ or - $\pi/2$) where the convergence of the fluxes across all longitudes means the transport is approximately zero.

$$\overline{T_T}(\varphi) = -\int_{\varphi}^{\pi/2} \overline{[F_R^{TOA}]^{corr}(\varphi')} R \partial \varphi', \tag{2.12}$$

where

$$\overline{[F_R^{TOA}]^{corr}(\varphi')} = \overline{[F_R^{TOA}](\varphi')} - \overline{[F_R^{TOA}]} \tag{2.13}$$

Similar analysis maybe performed to separately deduce the components of the transport below the surface ($\overline{T_{surf}(\varphi)}$) and of the atmosphere ($\overline{T_{atm}(\varphi)}$) as,

$$\overline{T_{surf}(\varphi)} = \overline{T_{oc}(\varphi)} = -\int_{\varphi}^{\pi/2} \overline{[F_R]_{surf}(\varphi')} R\partial\varphi', \tag{2.14}$$

$$\overline{T_{atm}(\varphi)} = -\int_{\varphi}^{\pi/2} \overline{[F_R]_{atm}(\varphi')} R\partial\varphi', \tag{2.15}$$

The land component of the surface is solid and thus may only transfer energy horizontally via the highly inefficient method of conduction so that over long time averages the net fluxes at the solid surface boundary can be assumed to be zero locally. The fluid motion of the oceans mean locally an imbalance may exist and is assumed to be the sole source of the MET component at and below the surface, which is evaluated from the net surface fluxes which locally is non-zero. Similarly, the motions of the atmosphere mean that the local energy imbalance of the atmosphere is also non-zero for a given vertical column, however in both cases the global imbalance reduces to zero. Furthermore, the energy fluxes associated with the atmospheric component of the MET can be deduced from the difference between the fluxes at the TOA and at the surface as, $\overline{[F_R]_{TOA} - [F_R]_{surf}} = \overline{[F_R]_{atm}}$.

There have been numerous attempts to produce empirical estimates for the MET however such a task is thwart with difficulty and thus far all contain significant errors. Trenberth and Caron [117], Fasullo and Trenberth [26] and Trenberth and Fasullo [118] use measurements of the TOA fluxes from satellite data to calculate MET. The limitations of such methods relate to the inhomogeneous satellite coverage. For this reason Mayer and Haimberger [83] suggest that employing European Centre for Medium-Range Weather Forecasts (ECMWF) Re- Analysis Interim (ERA-Interim) data is better suited for investigation of the global energy budget. Nonetheless, though these results may improve matters, there still exists a significant margin for error.

An accurate estimate for MET would be useful in helping to determine the performance of state-of-the-art models though as a caveat, one must always be aware of false positives - right results for wrong reasons - and must be considered together with further information pertaining to the thermodynamic and dynamical properties of the climate system for which non physical sources and sinks of energy may occur due to nonconserving numerical schemes Gassmann [33] as well as explicitly missing physical processes such as the reintroduction of heat from dissipated kinetic energy Becker [5] back in to the system and a non conserving hydrological cycle (Liepert and Previdi [65], Liepert and Lo [66]).

Lucarini et al. [79] provide estimates for the MET based on CMIP3 and CMIP5 model data for the pre-industrial and SRESA1B scenario's shown in Fig. 2.4. The peak value of the MET over all models tested, ranged between 4.3-6.2PW and 4.9-6.1PW for southern and northern hemispheres, respectively, in the pre-industrial scenario.

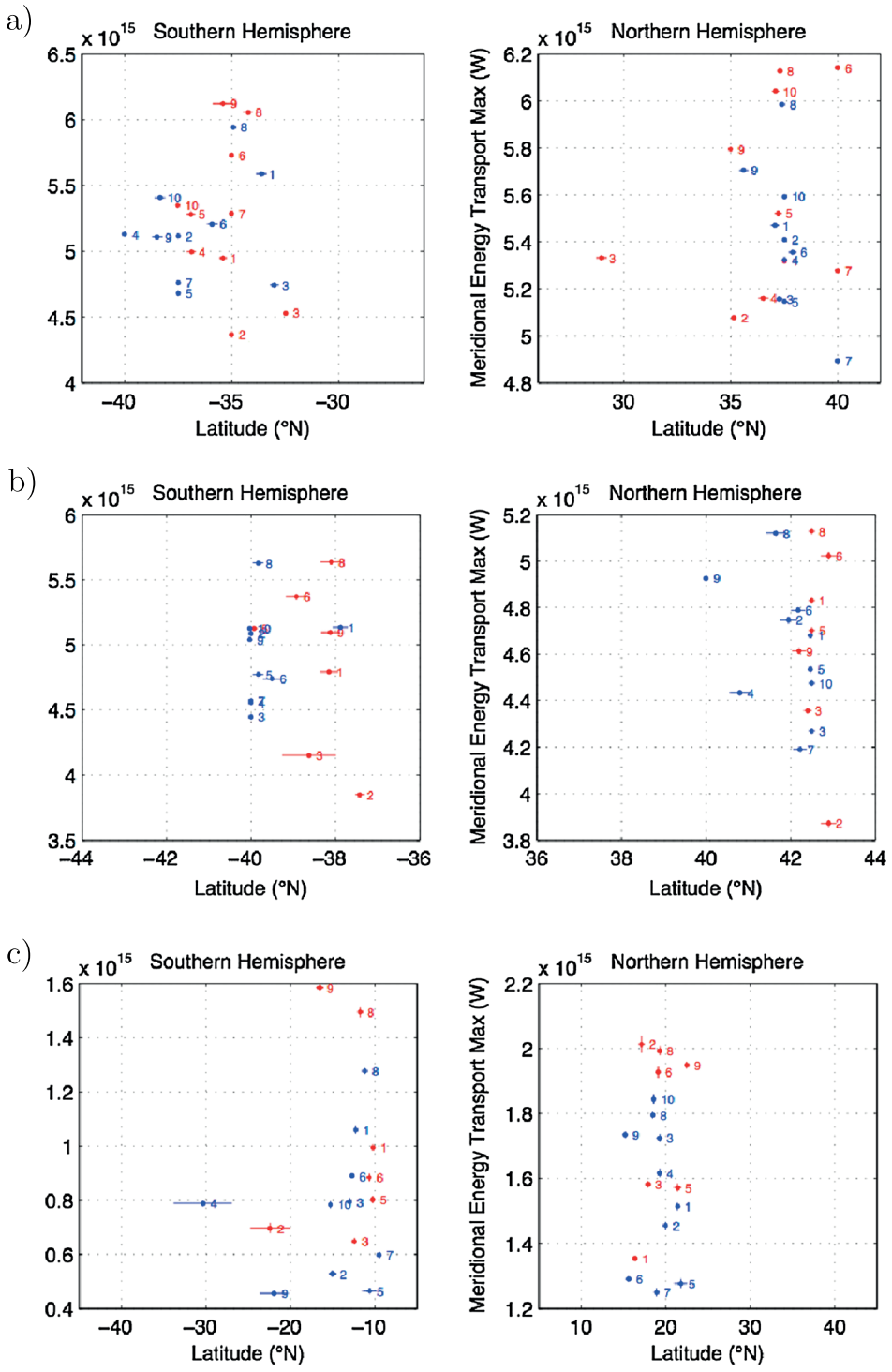

FIGURE 2.4: Value and position of the peak of the poleward MET in the pre-industrial scenario for (a) the whole climate, (b) atmosphere, and (c) ocean for the some of the CMIP3 (red) and CMIP5 (blue) general circulation models. Adopted from Lucarini and Ragone [78]. See Lucarini and Ragone [78] for model codes in Table 1.

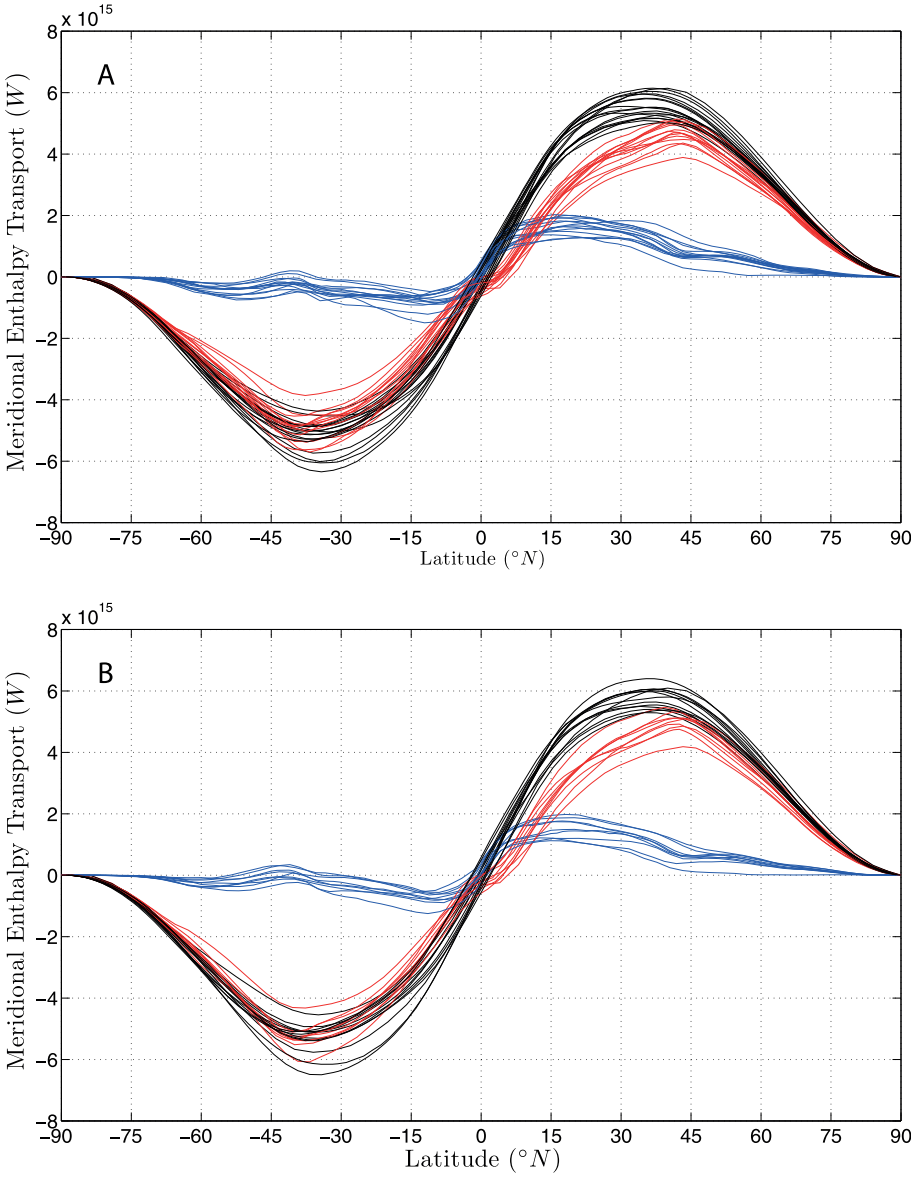

FIGURE 2.5: Mean total MET by the climate system (black lines), the atmosphere (red lines), and the ocean (blue lines) in (a) the pre-industrial scenario and (b) the SRESA1B scenario for the 22nd century for all models where suitable data are available. Adopted from Lucarini and Ragone [78].

2.1.3 The Atmospheric Heat Engine

Neglecting the relatively weak contribution from tidal forces, the complex motions of the atmosphere occur without any injection of mechanical energy external to the Earth system. Instead, differential solar heating causes the development of weather disturbances which act to address the resulting imbalance in the energy distribution via a series of energy transformations. In the following session the energy transformation processes and weather disturbances which occur within the atmosphere are discussed.

It was Margules [81] who first discussed the concept of available potential energy in relation to the development of storms however its first formal treatment on the general circulation of the atmosphere was described by Lorenz [71]. Take a barotropic atmosphere where the pressure gradient is exactly compensated for by the force of gravity and no horizontal pressure gradient exist in any region. Such an atmosphere may contain a large reserve of potential energy though none is available to perform work. If this state was either heated or cooled in a uniform manner so all regions remained in radiative equilibrium, the total potential energy (which contains both the potential energy and internal energy) for the state would increase or decrease accordingly however still no energy would be made available to do work. Conversely, if strong gradients exist but the system is in thermal equilibrium so no energy is exchanged, again no energy would be made available to do work.

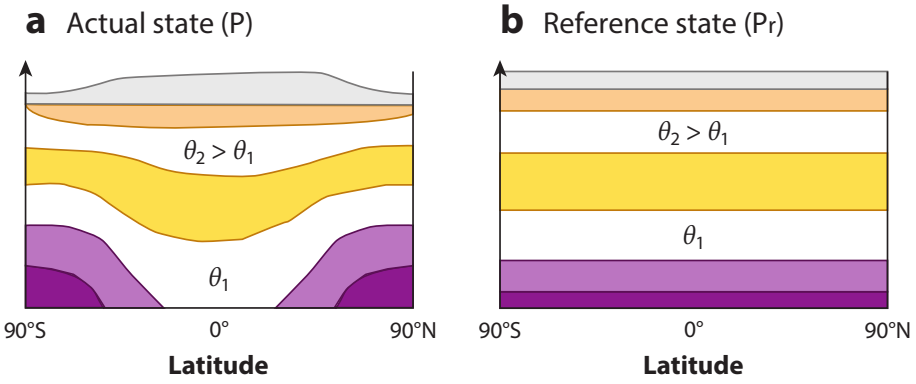

FIGURE 2.6: Figure shows the isentropic rearrangement of mass from the (a) the actual atmospheric state with a total potential energy, P, which after the conversion ($C(A, K) = W$) of the available potential energy to kinetic energy (K), is ultimately dissipated via irreversible viscous processes, which without any further generation of potential energy, G, from external forcings results in the (b) Lorenz-Margules reference state, P_r. Adopted from Tailleux [114].

Heating of the Earth's surface by the Sun means that there exists a non-uniform distribution of temperature along isobars in many regions thus implying that the atmosphere exists in a state where work is done transforming potential into kinetic energy. The kinetic energy (K) which is then continuously dissipated through fictional processes which

act to restore the system to its minimum potential energy (P_r) state where it is both horizontally and statically stable. If this state were to occur, the total potential energy would reach its minimum value and therefore the gain in kinetic energy, its maximum. The difference between the potential energy/kinetic energy, before and after the adiabatic rearrangement of all fluid particles, is therefore equal to the maximum amount of potential energy available to be converted to kinetic energy and is thus referred to as the available potential energy, A and is defined as,

$$A = P - P_r \tag{2.16}$$

where $P_r = \int (I + \Phi)_r dm$, is the reference state for the minimum total potential energy. $P = \int (I + \Phi) dm$ is the total potential energy of the present climatic state and $\Phi = gz$.

Normally, A will be applied for cases where there is a positive flux into the system due to the nature of the Earth-Sun system however it is important to note that in general A is positive definite, even when there is a net removal of energy fluxes from a system. Furthermore, it is only necessary that the flux to be applied differentially for A to be non zero. If two fluid systems begin from a given reference state, P_r but one is differentially cooled and the other warmed by the same amount at an arbitrary point A, the system now has potential energy, $P_c < P_r$, and $P_w > P_r$, respectively. In both cases the generated $A > 0$. Therefore, it is observed that regardless of the sign of the flux $A > 0$. As in the case of hydrostatic equilibrium,

$$\int_0^\infty (I + \Phi) dz = \int_0^\infty c_p T dz = \int_0^{p_0} c_p T \frac{dp}{g}, \tag{2.17}$$

an expression for A may be obtained in terms of the temperature for the current (T) and reference states (T_r),

$$A = \int_V c_p (T - T_r) dm = \int_V c_p T \left(1 - \frac{T_r}{T}\right) dm \tag{2.18}$$

and in terms of the pressure for the current (P) and reference states (P_r) by substitution of the relationship of the potential temperature, $\theta = T(p_0/p)^\kappa$ as,

$$A = \int_V c_p \theta \frac{(p^\kappa - p_r^\kappa)}{p_0^\kappa} dm = \int_V c_p T \left(1 - \left(\frac{p_r}{p}\right)^\kappa\right) dm \tag{2.19}$$

where $\kappa = R/c_p$.

Lorenz [71] goes on to derive a simplified expression for A, by approximating P_r and P as the two-dimensional variance of temperature on a constant pressure surface, as follows,

$$A = (c_p/2) \int \Gamma(T^2 - \tilde{T}^2) dm \tag{2.20}$$

where $\tilde{T}$ is the average temperature and Γ is an inverse measure of the gross global mean static stability Peixoto and Oort [94],

$$\Gamma = -(\kappa\theta/pT)(\partial\tilde{\theta}/\partial p)^{-1} = (\gamma_d/\tilde{T})(\gamma_d - \tilde{\gamma})^{-1} \tag{2.21}$$

In the real atmosphere the external forcing from differential solar heating and other external sources is provided continuously, thus it is the balance between the rate at which the available potential energy is generated, G, and the subsequent conversion to other energy forms which dictate the rate at which the available potential energy changes, $\frac{\partial A}{\partial t} = \dot{A}$ as,

$$\dot{A} = G - C(A, K). \tag{2.22}$$

The subsequent, conversion ($C(A, K)$) from $\dot{A}$ to Kinetic energy ($\frac{\partial K}{\partial t} = \dot{K}$) before ultimately being dissipated (D) means,

$$\dot{K} = C(A, K) - D, \tag{2.23}$$

The Lorenz energy cycle for the atmosphere is illustrated by Fig. 2.7. Over long time averages where the energy budget, $\dot{E} = 0$, the rate of generation of available potential energy and dissipation of kinetic energy converge toward the same magnitude until they balance,

$$\overline{G} = \overline{C(A, K)} = \overline{D} > 0, \tag{2.24}$$

where the greater than sign indicates that D must be positive and,

$$G = \int_V \left(\frac{T - T_R}{T} \right) \dot{Q} dm \tag{2.25}$$

Consequently, over a long time average of the climate state, the strength of the complete Lorenz energy cycle, may be deduced independently by directly measuring any of the components of Eqs. 2.25. Within climate models, it is easiest to diagnose D, which will be the method used in subsequent chapters to directly ascertain the strength of the Lorenz energy cycle and thus $C(A, K)$ which may be considered the work done by the climate system, $\dot{W}$.

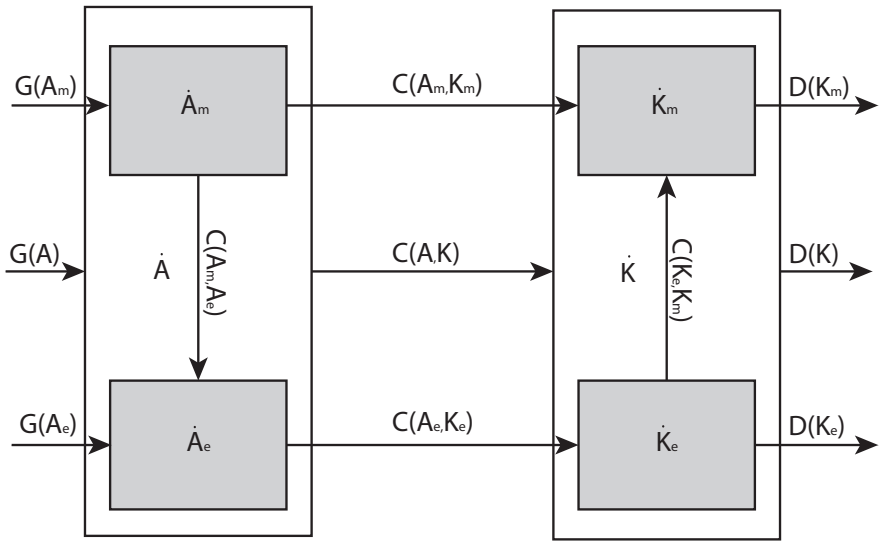

FIGURE 2.7: Figure shows the Lorenz energy cycle represented in two and four component form by the clear rectangular and gray square boxes, respectively. The two-component energy cycle shows the available potential energy ($\dot{A}$) is generated ($G(A)$), converted ($C(A, K)$) to kinetic energy ($\dot{K}$), and subsequently dissipated (D). The Four-box model of the energy cycle decomposes $\dot{A}$ and $\dot{K}$ into their mean ($\dot{A}_m$,$\dot{K}_m$) and eddy ($\dot{A}_e$,$\dot{K}_e$) components and illustrates the conversions of energy ($C(A_m, A_e), C(A_e, K_e), C(A_m, K_m), C(K_e, K_m)$) which occur between them.

In order to differentiate between the long and short term components of the atmospheric energy budget, Lorenz [71] goes on to also decomposes the mean and eddy components of the kinetic and potential energy. The Lorenz energy cycle then contains the exchange between kinetic (K_m) and available potential (A_m) energy of the mean circulation and the kinetic (K_e) and available potential (A_e) energy of the eddy exchanges which is illustrated in Fig. 2.7. The processes that can be associated with these exchanges are: barotropic instability for an exchange between K_m and K_e, baroclinic instability for an exchange between A_m and A_e and between A_e and K_e, which is associated with cyclone activity in the mid-latitudes Li et al. [68]. Peixoto and Oort [94] apply values to the

Lorenz energy cycle, though some of which are not directly measured but instead are inferred, concluding that the energy exchange occurs by the sequence $A_m \rightarrow A_e \rightarrow K_e \rightarrow K_m$.

2.1.4 Carnot efficiency of the climate

[2]

The idea of considering the atmosphere as an engine analogous to that of a heat engine is conceptually subtle though not incomprehensible. A thermodynamic heat engine performs work on it's surroundings, W, operating between two thermal reservoirs where the energy flux from the warm reservoir, Q_{in} with a temperature, T_w flows to the engine. The remaining energy leaving from the engine, Q_{out}, must therefore be the difference between Q_{in} and W so that, $Q_{out} = Q_{in} - W$. The fraction of Q_{in} which results in W is therefore the Carnot efficiency, $\eta = W/Q_{in} = 1 - Q_{out}/Q_{in}$, where it may subsequently be shown that $\eta = 1 - T_c/T_w$.

Conceptually, the simplest way to interpret the climate system in the context of a heat engine is by considering the warmer low latitudes which receive a net surplus of energy as the warm reservoir and the colder high latitudes where a net deficit of energy represents the cold reservoir, between which the MET acts to equilibrate the system, in part, directly through the motions of the atmosphere. The action of converting A to K requires work to be done which is ultimately dissipated and returned to the system in the form of heat. Peixoto and Oort [94] suggests that the efficiency of the Earth heat engine to be low as the temperature difference between warm (T_W) and cold (T_C) regions is relatively small. He provides an estimate for the Carnot efficiency given by:

$$\eta_h = (T_W - T_C)/T_W \leq 10\%, \tag{2.26}$$

where the subscript h denotes that 2.26 is the horizontal component of η, as derived by [79].

The Carnot efficiency is an idealised engine which works under the assumption that the expansion and compression stages of a heat engine are adiabatic so that the change in entropy for the entire cycle, $\delta S_{cycle} = 0$, thus 2.26 represents an upper bound to η_h.

From synoptic down to infinitesimal small scales, the instantaneous differences within the climate state over a volume, V, that encompasses the climate system mean that the

[2]Extracts from **Boschi R.**, V. Lucarini, S. Pascale, 2013. *"Bistability of the climate around the habitable zone: a thermodynamic investigation"*, Icarus 226, 1724-1742.

Earth and it's atmosphere exist in an out of thermodynamic equilibrium state, thus, the assumptions applied to classical thermodynamics are invalid here as the climate system is open to external forcings and evolves with time. It is instead necessary to describe the thermodynamic properties of the system in terms of time derivatives where it is useful to summarise the instantaneous total energy budget ($\dot{E}(V)$) here simply in terms of the total potential energy which includes the moist static potential energy, $\dot{P} = \dot{\Psi} + D - W$ and $\dot{K} = W - D$ as,

$$\dot{E}(V) = \dot{P}(V) + \dot{K}(V). \tag{2.27}$$

The penultimate equation reiterates Eq. 2.23 where the notation for the conversion term $C(A, K)$ has been replaced with W as the conversion of $\dot{A}$ to $\dot{K}$ shall be discussed interms of the work being done by the system. It can be assumed that locally, at each moment in time, the system exists in thermodynamic equilibrium where the heating rate is,

$$\dot{q} = \dot{s}T, \tag{2.28}$$

for each local region and is considered a thermal reservoir of size dV which exchange radiative F_{rad} and turbulent F_{turb} fluxes as,

$$\dot{q} = 1/\rho(\epsilon^2 - \nabla\dot{H}), \tag{2.29}$$

where $\epsilon^2 > 0$ is an additional heating term arising as a consequence of the viscous dissipation of kinetic energy and $H = F_{turb} + F_{rad}$. Integrating $\dot{q}$ over the entire climate gives,

$$\dot{Q} = \int_V \rho\dot{q}dV = \dot{\Psi} + D = \dot{P} + W = \int_V \epsilon^2 dV - \int_V \nabla\dot{H}dV, \tag{2.30}$$

where $\dot{\Psi}$ is the sum of the non-frictional diabatic heating from the convergence of turbulent sensible heat, moist and radiative fluxes, which equate to the total energy input to the climate system, so that $\dot{\Psi} = \dot{E}$. At each instant in time, to properly represent the warm and cool reservoirs for the entire climate system, inclusive of the horizontal and vertical components of $\dot{Q}$, V must be divided in to subdomains V^+ where $q = q^+ > 0$ and V^- where, $q = q^- < 0$, giving,

$$\dot{Q} = \dot{Q}^+ + \dot{Q}^- = \int_{V^+} \rho\dot{q}^+ dV + \int_{V^-} \rho\dot{q}^- dV, \tag{2.31}$$

as shown in Fig. 2.9

In the case of long time averages where steady state conditions are applicable, $\overline{\dot{\Psi}} = \overline{\dot{P}} = \overline{\dot{K}} = 0$, where from Eq. 2.30 and 2.31, the difference in $\overline{\dot{Q}}^-$ and $\overline{\dot{Q}}^-$ becomes,

$$\overline{D} = \overline{W} = \overline{\dot{Q}}^+ + \overline{\dot{Q}}^- = \overline{\dot{Q}} \geq 0. \tag{2.32}$$

As the dissipation is always positive, Eq. 2.32 implies that $\left|\overline{\dot{Q}}^+\right| \geq \left|\overline{\dot{Q}}^-\right|$, where the difference between both is due to the work done in maintaining the circulation against dissipation.

The first and second laws of thermodynamics dictate that $\overline{W}$ must be less than $\overline{\dot{Q}}^+$, the energy inputted to the system. The proportion of $\overline{\dot{Q}}^+$ from V^+ that results in work being done by the atmosphere therefore is the carnot efficiency, η_c which defines the ability of the atmosphere to perform work as,

$$\overline{W} = \eta_c \overline{\dot{Q}}^+ \tag{2.33}$$

where,

$$\eta_c = \frac{\overline{W}}{\overline{\dot{Q}^+}} = \frac{\overline{\dot{Q}^+} + \overline{\dot{Q}^-}}{\overline{\dot{Q}^+}} = 1 + \frac{\overline{\dot{Q}^-}}{\overline{\dot{Q}^+}} \tag{2.34}$$

As shown in [72] and clarified in [44, 45] the long term average of the work performed by the system is equal to the long-term average of the generation of available potential energy, as is typical of forced-dissipative steady states. The Earth exists in a steady state maintained far from equilibrium by net radiative heating in the warm region (low latitudes on Earth) and net cooling at the cold regions (high latitudes on Earth), which are compensated by large scale transports performed by the planetary atmosphere.

Assuming equilibrium on spatial scales far smaller than V [19] so that locally $\dot{Q} = \dot{s}T$ where $\dot{s}$ is the time derivative of the entropy density. The total rate of change of the entropy of the system is:

$$\dot{S} = \int_{V^+} dV \rho \dot{q}^+ / T + \int_{V^-} dV \rho \dot{q}^- / T = \int_{V^+} dV \rho |s^+| + \int_{V^-} dV \rho |\dot{s}^-| = \dot{S}^+ + \dot{S}^- \tag{2.35}$$

where $\dot{S}^+ > 0$ and $\dot{S}^- < 0$. Using Eq. 2.35 and assuming that the Earth system is in a steady state, over a long time average,

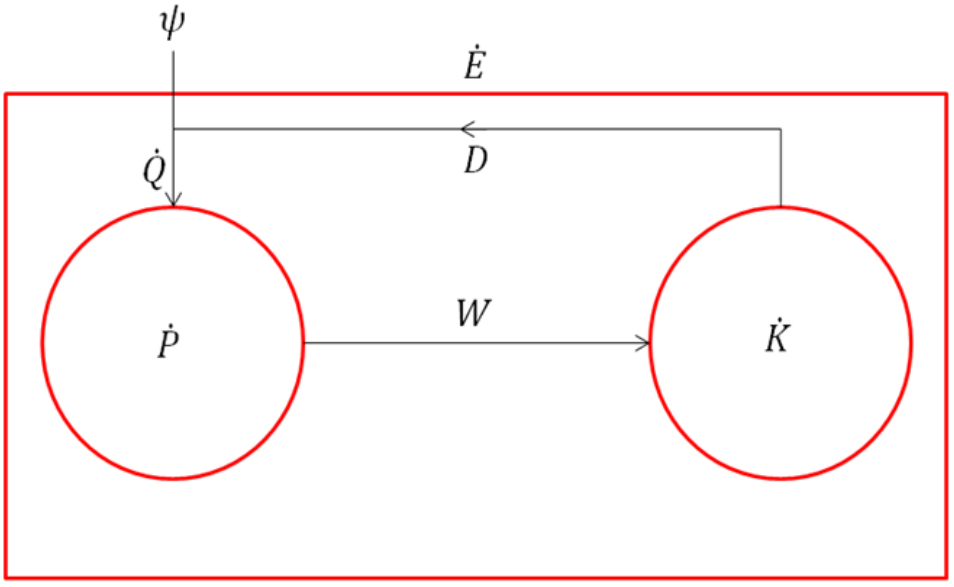

FIGURE 2.8: Schematic figure showing the two main classes of energy: Potential (P) and Kinetic (K); and the transfer processes (ψ, W, D) which exchange energy between them. $\dot{E}$ is the total energy within the system and $\dot{Q} = \psi + D$ is the total heating rate due to dissipation (D) and the convergence of heat fluxes (ψ) . W is the work done by the system. ψ includes the external radiative input to the climate system from the Sun, therefore $\dot{E} = \psi$.

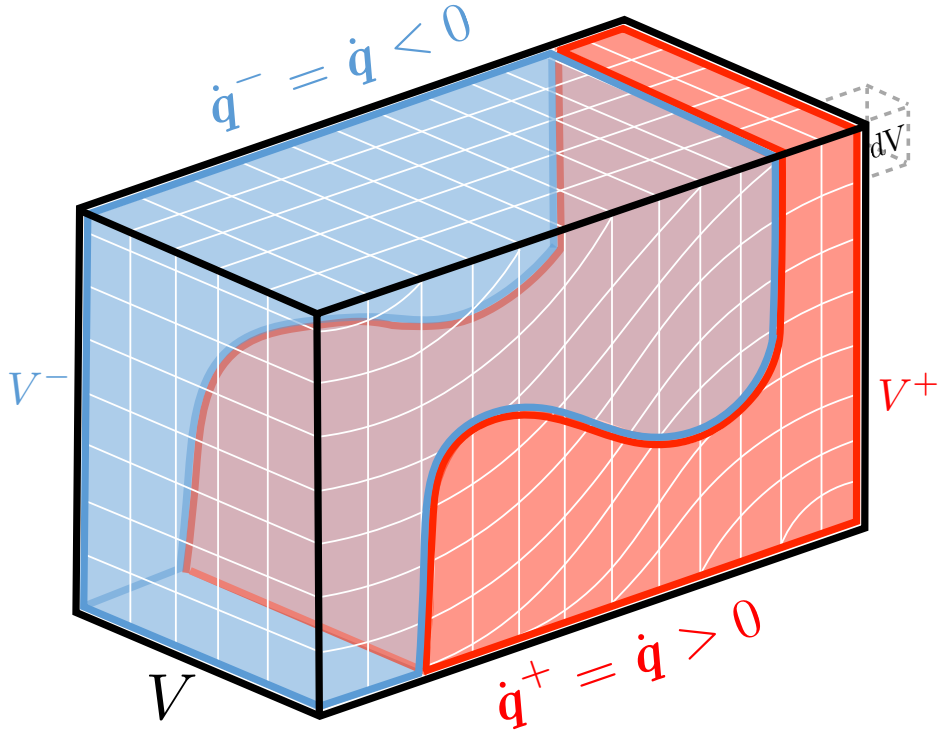

FIGURE 2.9: Schematic figure based on results from Lucarini et al. [76], showing the partitioning of the atmosphere in terms of positive $(\dot{q}^+)$ and negative $(\dot{q}^-)$ heating rates.

$$\overline{\dot{S}}^{+} + \overline{\dot{S}}^{-} = \overline{\dot{S}} = 0. \tag{2.36}$$

Therefore, $2\overline{\dot{S}}^{+} = \overline{\int_V dV\rho|\dot{s}|}$, so that $\overline{\dot{S}}^{+}$ measures the absolute value of the entropy fluctuations throughout the domain. When integrating over the whole domain and considering long time average, the following equivalent expressions for the thermodynamic quantities are obtained: $\overline{\dot{Q}}^{+} = \overline{\dot{S}}^{+}\Theta^{+}$ and $\overline{\dot{Q}}^{-} = \overline{\dot{S}}^{-}\Theta^{-}$, where Θ^{+} and Θ^{-} are the time and space averaged temperatures of the V^{+} and V^{-} domains, respectively. Since $|\overline{\dot{S}}^{+}| = |\overline{\dot{S}}^{-}|$ and $|\overline{\dot{Q}}^{+}| \geq |\overline{\dot{Q}}^{-}|$, it can be shown that $\Theta^{+} \geq \Theta^{-}$, i.e absorption typically occurs at higher temperature than release of heat ([44, 93]). The efficiency of the Carnot engine of the climate system can thus be defined in terms of the temperatures, Θ^{+} and Θ^{-} as,

$$\eta_c = \frac{\overline{\Theta}^{+} + \overline{\Theta}^{-}}{\overline{\Theta}^{+}} = 1 - \frac{\overline{\Theta}^{-}}{\overline{\Theta}^{+}}. \tag{2.37}$$

2.1.5 The Entropy Budget and the Material Entropy Production

The second Law of thermodynamics applies to isolated systems where the only exchange in energy occurs between internal processes and imposes that energy can only move toward a state of lower availability and tends toward homogeneous solutions where the entropy is maximised. This therefore implies that,

$$\overline{\dot{S}} \geq 0. \tag{2.38}$$

In order to apply the second law to an open system such as the Earth's climate a term must be introduced to represent the change in entropy due to the divergence of fluxes across the boundary between the internal system and its surroundings ($\dot{S}_e$) so that,

$$\overline{\dot{S}} = \overline{\dot{S}}_e + \overline{\dot{S}}_i, \tag{2.39}$$

where as stated in Eq. 2.36, $\overline{\dot{S}} = 0$ in steady state and gives the total entropy budget of the Earth system. The irreversible internal processes of the Earth system act to increase the internal entropy of the system ($\dot{S}_i$) through the dissipation of kinetic energy and the heat transport along the temperature gradient due to the net heating and cooling at low and high latitudes. The positive constraint on the internal irreversible processes thus implies that a negative entropy flux toward the Earth system balances $\dot{S}_i$, so that, $\overline{\dot{S}}_i = -\overline{\dot{S}}_e$. The entropy of the surrounding system (Sun and space) thus grows due to

its interaction with and degradation by the Earth. As the Earth receives a flux of solar radiation (F_{SW}) at an emission temperature, $T_{sun} \approx 5800K$, which is then released as LW radiation from the atmosphere (F_{LW}) back to space with an emission temperature, $T_E \approx 255K$, the external entropy, $\dot{S}_e$, increases by

$$\overline{\dot{S}}_e = -F_{SW,LW}(1/T_E - 1/T_{Sun}) \approx -900mWm^{-2}, \tag{2.40}$$

where it is assumed $F_{SW} = F_{LW} = F_{SW,LW} = 240Wm^{-2}$ under steady state.

The entropy production of the internal irreversible processes manifests itself in the degradation of SW solar energy to the eventual emittance of LW radiation at the TOA. Kleidon [51] provides a detailed analysis of the break down of contributions associated with processes involved in the entropy production in the Earth system which is summarised in Fig. 2.10. However, a simplified entropy budget (Fraedrich and Lunkeit [31], Lucarini [75], Ozawa [89]) containing the most significant processes can be written as,

$$\begin{aligned}\overline{\dot{S}_i} = F_{turb}(1/T_A - 1/T_S) + F_{SW,S}(1/T_S - 1/T_{Sun}) + ... \\ F_{SW,A}(1/T_A - 1/T_{Sun}) + F_{LW}(1/T_A - 1/T_S),\end{aligned} \tag{2.41}$$

Where the terms on the right-hand side are contributions by (1) turbulent fluxes, (2) the absorption of the solar radiation at the surface; (3) the absorption of the solar radiation in the atmosphere (4) the interaction between the atmosphere and the surface by long-wave radiation.

Goody, 2000 indicates that the radiative entropy production cancels out and have no net effect on the climate system, thus only the entropy production processes which occur within the fluid medium require consideration. In this way, $\dot{S}$ may be written in such a way that the respective radiative and internal irreversible contributions may be grouped separately as,

$$\dot{S} = -\int_V \frac{\nabla.\mathbf{F_R}}{T} dV + \dot{S}_{mat}, \tag{2.42}$$

where the sum of the contributions to the globally integrated turbulence entropy production is often referred to as the material entropy production ($\dot{S}_{mat}$). It is this convention which shall be adopted here where the main contributing processes associated with $\dot{S}_{mat}$ are the dissipation, sensible and latent heat fluxes, which provide a direct method for calculation of the average rate of the material entropy production as follows,

$$\overline{\dot{S}_{mat}} = \overline{\int_V \frac{\epsilon^2}{T} dV} + \overline{\int_V \vec{F}_{SH} \cdot \nabla \frac{1}{T} dV} + \overline{\int_V \vec{F}_{LH} \cdot \nabla \frac{1}{T} dV} \tag{2.43}$$

where, ϵ^2 is the dissipation of kinetic energy. $\vec{F}_{SH}$ refers to the sensible heat fluxes due to small-scale turbulence while $\vec{F}_{LH}$ to the latent heat fluxes from both small-scale and large scale processes. More precise formulations are discussed by Kleidon [51] with the reader once more referred to Fig. 2.10. .

From Eq. 2.42, it naturally follows that under steady state conditions,

$$\overline{\dot{S}_{mat}} = -\int_V \frac{\overline{\nabla . \mathbf{F_R}}}{T} dV \tag{2.44}$$

Similarly, it is also possible to calculate an estimate for $\overline{\dot{S}_{mat}}$ indirectly from the radiative fluxes via substitution of 2.42 and 2.40 into 2.39 and rearranging to give:

$$\overline{\dot{S}_{mat}} = F_{turb}(1/T_A - 1/T_S) = F_{SW,S}(1/T_S - 1/T_{Sun}) + ... \tag{2.45}$$
$$F_{SW,A}(1/T_A - 1/T_{Sun}) + F_{LW}(1/T_A - 1/T_S) + F_{SW,LW}(1/T_E - 1/T_{Sun}),$$

2.1.5.1 Estimating the vertical and horizontal components of the material entropy production

It is possible to formulate a useful alternative expression for indirectly calculating $\overline{\dot{S}}_{mat}$ which simply performs an area integral for the net radiative fluxes at the surface and at the TOA. One of the useful outcomes is that the expression will be divided into vertical and horizontal components, which gives rise to the 4 box model of the climate (Fig. 2.11). As discussed in previous sections, the low opacity of the atmosphere to incoming SW radiation, $F_{SW,S}$, means they are mainly absorbed at the surface on land and the first few metres of the ocean. Thus to a good approximation, it may be assumed that the temperature, $T_{SW,S}$, at which absorption occurs is equal to that of the subsequent LW radiative emissions, $F_{LW,S}$, away from the surface so that the indirect calculation for the material entropy budget of the surface may be given by:

$$\int_A \left(\frac{F_{SW,S}}{T_{SW,S}} + \frac{F_{LW,S}}{T_{LW,S}} \right) dA = \int_A \frac{F_{SW,S} + F_{LW,S}}{T_S} dA = \int_A \frac{\dot{q}_S}{T_S} dA, \tag{2.46}$$

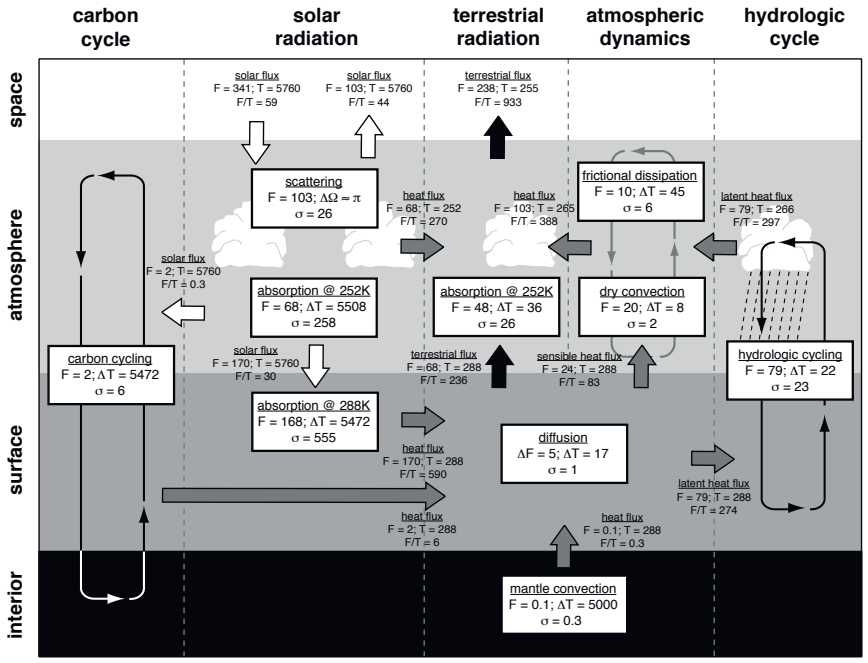

FIGURE 2.10: Estimated entropy budget of Earth. The white arrows denote fluxes of solar radiation; black arrows, terrestrial radiation; and grey arrows, heat fluxes. F states the magnitude of the flux, T the characteristic temperature, the solid angle, and F/T the associated entropy flux. The boxes denote dissipative processes with the associated magnitudes of the heat fluxes, temperature differences, and entropy production. Numbers do not necessarily balance due to uncertainties and rounding errors. Adopted from Kleidon [51].

Where $T_{SW,S} = T_{LW,S} = T_S$.

Similarly, the material entropy production associated with processes occurring within the bulk of the atmosphere may be given as:

$$\int_A \left(\frac{\overline{F}_{SW,A}}{T_{SW,A}} + \frac{\overline{F}_{LW,A}}{T_{LW,A}} \right) dA = \int_A \frac{\overline{F}_{SW,TOA} - \overline{F}_{SW,S}}{T_{SW,A}} dA + \int_A \left(\frac{\overline{F}_{LW,TOA} - \overline{F}_{LW,S}}{T_{LW,A}} \right) dA, \tag{2.47}$$

Where the fluxes from the atmosphere are calculated from the difference between the fluxes at the TOA and the surface, $\overline{F}_A = \overline{F}_{TOA} - \overline{F}_S$. In general it is not trival to assume that the absorption of F_{SW} and emission of F_{LW} will occur at the same temperature (T_A) in the atmosphere, which is strongly dependant on its chemical properties through out the fluid. However, as in the case of the Earth's troposphere the hydrological cycle plays a dominant role in the absorption of F_{SW} and latent heat release as F_{LW}, a notion supported by estimates presented by [31]. It has thus been suggested by Lucarini et al.

[79] from where the analysis in this section originates, that the approximation $T_{SW,A} \approx T_{LW,A} \approx T_E$ may be applied, with the average atmospheric temperature assumed to be approximately equal to the blackbody temperature (T_E) of a vertical column in the atmosphere. Such an assumption is useful as it simplifies the computation and ultimately means that the final expression will represent a constraint on the upper bound of the vertical component of the material entropy production as opposed to an actual estimate under present climate conditions as $T_S - T_E > T_S - T_A$. The sum of Eq. 2.47 and 2.46 thus gives an estimate for $\overline{\dot{S}_{mat}}$.

$$\begin{aligned}\overline{\dot{S}}_{mat} &\approx \int_A \left(\overline{F}_{SW,S} + \overline{F}_{LW,S}\right)\left(\frac{1}{T_S} - \frac{1}{T_E}\right) dA + \int_A \frac{\overline{F}_{SW,S} + \overline{F}_{LW,S}}{T_E} dA \\ &\approx \int_A \overline{\dot{q}}_{surf}\left(\frac{1}{T_{surf}} - \frac{1}{T_E}\right) dA - \int_A \frac{\nabla_{\mathbf{H}}.\overline{\mathbf{H}}}{T_E} dA \approx \overline{\dot{S}}^{vert}_{mat} + \overline{\dot{S}}^{hor}_{mat}\end{aligned} \tag{2.48}$$

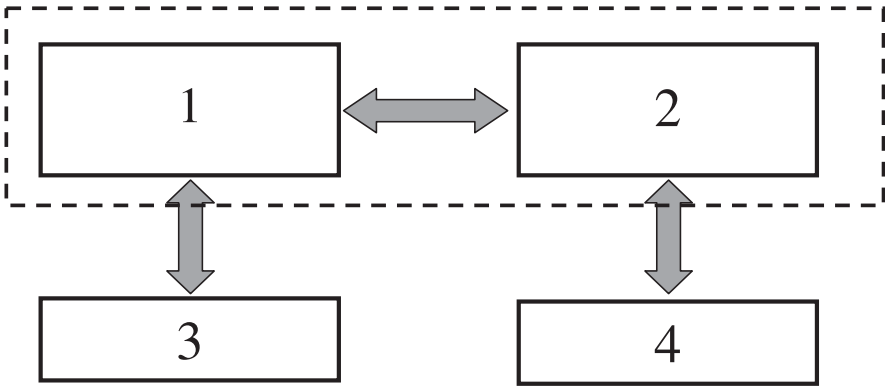

FIGURE 2.11: Minimal conceptual diagram for the material entropy production of a planetary system. Box 1 represents the warm (low latitudes) and box 2 the cold (high latitudes) fluid regions, coupled by enthalpy transport. Boxes 3 and 4 represent warm (low latitudes) and cold (high latitudes) surface domains, coupled vertically to boxes 1 and 2, respectively, but not to each other. The dashed rectangle encloses the reduced two-box model previously considered in the literature. Adopted from Lucarini et al. [79].

The resulting formulae is rearranged in a form where the first term gives the net energy flux passing between the surface and atmospheric reservoirs and is positive as $T_S > T_E$ and $\overline{F}_{SW,S} + \overline{F}_{LW,S} = \overline{F}_{LW,TOA} + \overline{F}_{SW,TOA} = 0$. The second term may be related indirectly to the horizontal entropy production where it is assumed that under steady state the net radiative fluxes at the TOA balance with the convergence of the horizontal transport, $\mathbf{H}$, integrated over the entire atmosphere. The approach provided here is consistent with the minimal conceptual model for the entire planet where it may be shown ([75]) the vertical component of $\overline{\dot{S}_{mat}}$ dominates as a result of the latent heat transport which provides a highly efficient equilibrating mechanism, thus acting to limit the generation of available potential energy which is realised through a decrease in both

the vertical and horizontal temperature gradients, firstly, by decreasing T_S through absorption of solar radiation and secondly increased warming of the atmosphere as a result of the subsequent release of energy in the upper troposphere.

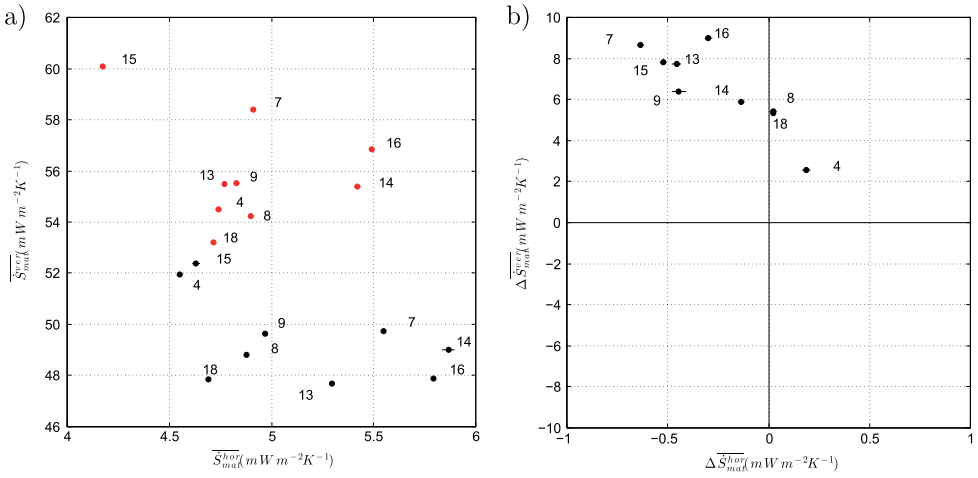

FIGURE 2.12: (a) Scatter plot of the contributions to the rate of material entropy production due to horizontal (x axis) and vertical (y axis) processes. Each point corresponds to a GCM from the CMIP3 data set in pre-industrial (black) and post-industrial (red) scenarios (updated from Lucarini et al (2011)). (b) Difference between the SRESA1B scenario run (average of the last 30 years of the 23rd century and the pre-industrial climatology). Model codes are in the reference. Adopted from Lucarini and Ragone [78].

As described above, Lucarini [75] shows how to indirectly estimate the horizontal and vertical fluxes from Eq. 2.48. Using the CMIP3 models, more than 90 percent of the global entropy production was estimated to be due to vertical processes such as convection, while the remainder is mainly due to the MET as shown in Figure 2.12. Furthermore, it implies that in most cases the warmer temperatures of the post industrial era increase this disparity relative to the colder preindustrial simulations, which mostly may be accounted for by increased convection and reduced horizonal temperature gradients as a result of reduced sea-ice in the polar regions and increased latent heat transport.

The terms of the entropy budget in Eq. (2.35) can be linked with those of the entropy production in eq. (2.43) . The second law of thermodynamics states that the entropy variation of a system at temperature T receiving an amount of heat δQ is larger than or of equal to $\delta Q/T$ (Landau and Lifshitz [58]). In this case:

$$\overline{\dot{S}_{mat}(V)} \geq \overline{\dot{S}_{min}(V)} = \overline{\left(\frac{\int_V dV\rho\dot{Q})}{\int_V dV\rho T}\right)} = \overline{\left(\frac{Q^+ + Q^-}{\langle\Theta\rangle}\right)} \approx$$

$$\approx \frac{\overline{Q^+} + \overline{Q^-}}{\overline{\langle\Theta\rangle}} = \frac{\overline{W}}{\overline{\langle\Theta\rangle}} \approx \frac{\overline{W}}{\frac{(\Theta^+ + \Theta^-)}{2}} \tag{2.49}$$

where $\overline{\dot{S}_{mat}(V)}$ is the long-term average of the material entropy production, $\overline{\dot{S}_{min}(V)}$ is its lower bound, i.e. the minimal value of the entropy production compatible with the presence of a Lorenz energy cycle with average intensity $\overline{W}$ and $\langle\Theta\rangle$ is the density averaged temperature of the system. The approximation holds as long as the impact of the cross-correlation between the fluctuations of the work and the fluctuations of the globally averaged temperature is neglected. This term is small because the fluctuation of the globally averaged temperature are determined by the fluctuations of the radiative balance, which are weakly correlated to those of the work.

Moreover, in the last approximation it is assumed that $\langle\Theta\rangle$ can be estimated as the mean of the two Carnot temperatures Θ^+ and Θ^-. This can be justified by assuming that the atmospheric volumes where net heating and net cooling occur are of comparable size. This is indeed true on Earth, where the regions of net atmospheric warming are well approximated to be centred around the Equator between about $[30^oS, 30^oN]$, with all other regions associated with net cooling (Donohoe and Battisti [21], Lucarini et al. [76]).

$\dot{S}_{min}(V)$ can be explicitly written as:

$$\begin{aligned}\overline{\dot{S}_{min}(V)} \approx \frac{\overline{W}}{(\Theta^+ + \Theta^-)/2} = \frac{\eta\overline{Q^+}}{(\Theta^+ + \Theta^-)/2} = \\ = \eta\frac{\Theta^+}{(\Theta^+ + \Theta^-)/2}\overline{\dot{S}^+} = \frac{\eta}{1-\eta/2}\overline{\dot{S}^+} \approx \eta\overline{\dot{S}^+}\end{aligned} \tag{2.50}$$

where the last approximation holds as long as $\eta \ll 1$, which is typically the case. Therefore, η sets also the proportionality factor relating the lower bound to the entropy production of the system $\overline{\dot{S}_{min}(V)}$ due to macroscopically irreversible processes to the absolute value of the entropy fluctuations inside the system due to macroscopically reversible heating or cooling processes. Note that if the system is close to equilibrium ($\eta \to 0$), the entropy production vanishes because there is no generation of K and there is no transport of heat. The lower bound to the material entropy production corresponds to the contribution coming from the dissipation of K through viscous processes. Therefore, the average material entropy production can be expressed as $\overline{\dot{S}_{mat}} = \overline{\dot{S}_{min}} + \overline{\dot{S}_{exc}}$, where $\dot{S}_{exc}$ is the excess of entropy production with respect to the minimum, which results from the heat transport down the temperature gradient (Lucarini [75]). The term α can be defined as:

$$\alpha \approx \frac{\overline{S_{exc}}}{\overline{S_{min}}} \approx \frac{\int_V dV\overline{(\vec{F}_{SH} + \vec{F}_{LH}) \cdot \nabla(\frac{1}{T})}}{(\overline{W}/\langle\Theta\rangle)} \geq 0 \tag{2.51}$$

which is a parameter of the irreversibility of the system and is zero if all the production of entropy is due to the unavoidable viscous dissipation of the mechanical energy. As $\overline{\dot{S}_{mat}} \approx \eta\overline{\dot{S}^{+}}(1+\alpha)$, the entropy production is maximized if there is a joint optimization of heat transport and the production of mechanical work. Note that, if heat transport down the temperature gradient is very strong, the efficiency η is small because the difference between the temperatures of the warm and cold reservoirs is greatly reduced (the system is almost isothermal), whereas, if the transport is very weak, the factor α is small. The parameter α introduced above is related to the Bejan number $\mathcal{B}e$ as $\mathcal{B}e = \alpha + 1$ (Paoletti et al. [90]).

Chapter 3

Snowball Earth, Bistability and feedbacks in the Climate System

In chapter 3, the problem of critical transitions is described specifically in the context of the climates response to perturbations. Firstly, using evidence provided by simulations from EBM's and GCM's, the importance of the sea-ice albedo feedback to climate sensitivity and the resulting bistability between warm moist (W) and Snowball (SB) climates, is introduced. This is followed by a discussion on other important feedbacks which may act to facilitate or hinder the transition to and from the SB state. The large scale climatic features of the SB and W climates are then also compared. To finish, I build on the conceptual understanding discussed in chapter 2 by providing examples of how this thermodynamic methodology has so far been applied to investigate bistability and climate response near and far from tipping points, using GCM's.

If one decreases the incoming solar radiation incident on the Earth's surface sufficiently, at some stage the surface temperature will inevitably decrease to a point where the climate system will no longer support ice free regions even at the equator which is commonly referred to as a hard snowball or simply a snowball state as is illustrated in Fig. 3.1. The word "hard"is often used in order to distinguish this state from the hypothesised soft snowball or water belt states where rather than a completely solid ocean, the climate supports an ocean which is frozen everywhere except along the equatorial band (Pollard and Kasting [98]).

The path taken in reaching such a state and thus the nature of these states are the subject of much debate. Knowledge of the snowball Earth state is of particular importance to climate science where understanding climate sensitivity, variability and tipping points are critical issues relevant not just to sea-ice development but also many other features such as the thermohaline circulation and mid-latitude blocking.

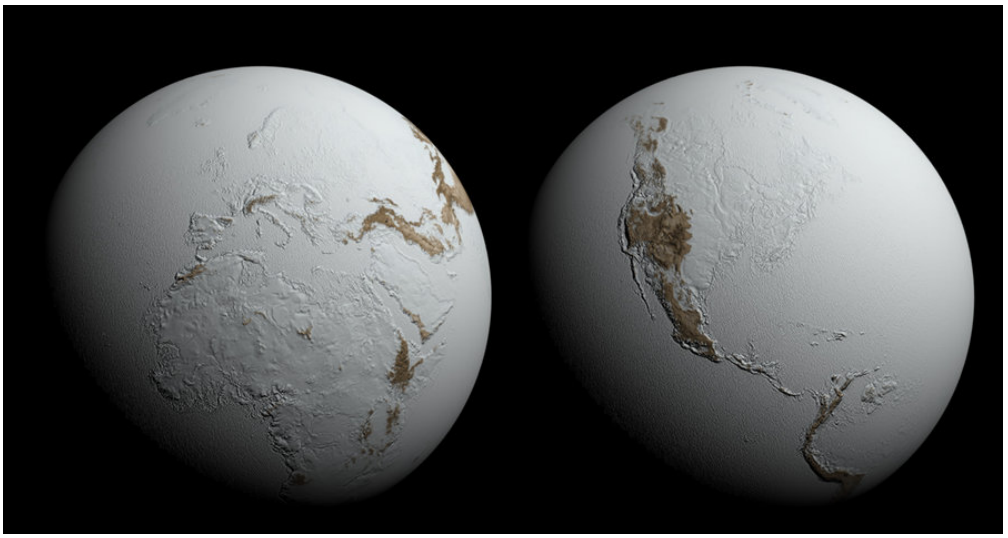

FIGURE 3.1: Illustration of how the Earth may have looked under hard snowball Earth conditions. Taken from http://pixgood.com/snowball-earth.html.

3.1 The Sea-Ice Albedo Feedback

The simplest way to represent the global climate system is as a single object where the surface temperature, T_S is dependant on the balance between the incoming absorbed (ASR) and outgoing (OLR) energy flux where the fraction of absorbed radiation from incoming solar radiation, S^*, is controlled by the albedo, α. The planet is assumed to behave as a blackbody at the TOA, defined by the Stefan–Boltzmann law (Ambaum [3], Peixoto and Oort [94]). To relate OLR to the T_S rather than the emission temperature, T_E, a gray body approximation is used in the form of a dimensionless coefficient, ϵ, which effectively represents the insulating properties of the atmosphere. Additionally, the heat capacity (C) of the surface's material properties may be included to take into account the energy storage and the resulting transience within the climate to give a time-dependant form of the 0-D EBM (Goosse [35], Pierrehumbert et al. [99]).

$$C\dot{T_S} = ASR - OLR = \pi R^2 S^*[1 - \alpha(T_S)] - 4\pi R^2 \epsilon \sigma T_S^4. \tag{3.1}$$

Where the subscript t indicates the time derivative, R is the planetary radius and $Q = S^*/4$, is the solar irradiance As discussed in section 2.1.1, over long time averages Eq. 3.1 goes to zero so that $ASR = OLR$.

Fig. 3.2 demonstrates the ice-albedo feedback in a 0D EBM model, where the albedo has been varied between 55° - 65°, which alters the entrance and in particular the exit from the snowball state. Higher albedo means the climate cools more quickly near the transition so that the SB state is entered at a higher value of $[CO_2]/S^*$.

The SB state will thus exist at a lower temperature and the transition from the SB state therefore occurs at a higher value of forcing by CO_2/S^*. Using a lower value for the ice albedo has two main consequences. Firstly, the extent of the isea-ice is greater before the transition to the snowball state is able to occur. Secondly, the CO_2 concentration maybe decreased further before the transition as more radiation is absorbed by the climate system. The resulting SB state will absorb more radiation at the surface and be warmer so the transition back to the warm state occurs with less additional forcing compared to when the albedo is set higher. The larger effect of the albedo on the temperature of the SB state compared to the warm state therefore means that the position of the $SB \rightarrow W$ transition is a stronger function of the albedo than the $W \rightarrow SB$ transition, so that the width of the bistable region will decrease with decreasing albedo difference between that of sea-ice and ocean (and land) surface.

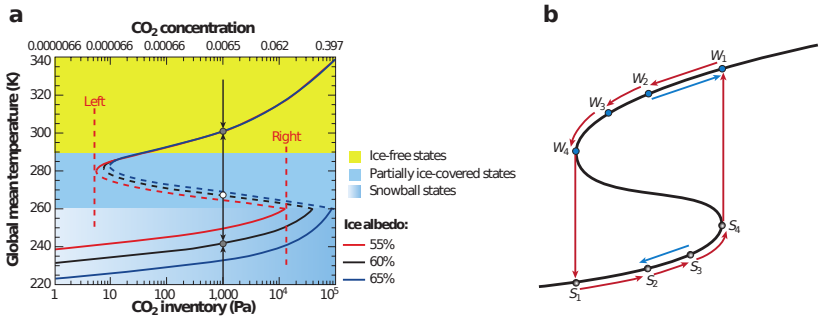

FIGURE 3.2: (a) Bifurcation diagram showing results from a 0-D EBM experiment, performed by modulating the CO_2 concentration under constant solar force where, $S^* = 1285 W m^{-2}$, albedo of ice free regions is 0.2, T_i=260K,T_o=290K. Adopted from Pierrehumbert et al. [99].

A rather useful extension of the 0-D EBM is the 1-D EBM of Sellers [106][1] which has been adopted by Ghil [34] and more recently Bódai et al. [6]. As noted by Bódai et al. [6], "this allows for more insightful thermodynamic non-equilibrium properties to be resolved and supports a higher-dimensional phase space where more complicated dynamical behaviour is possible". Here, only latitude bands are resolved and zonal symmetry is assumed so that the energy balance equation of the climate system becomes:

$$C(\phi)T_{S,t} = Q(\phi)[1 - \alpha(\phi, T_S)] - \epsilon(\phi, T_S)\sigma T_S^4 + \frac{1}{sin\phi}\frac{\partial}{\partial\phi}[sin\phi \cdot k(\phi, T_S)]T_{S,\phi}. \quad (3.2)$$

where ϕ denotes the latitudinal dependence An additional diffusion term (3) is required to account for the MET between latitude bands. To this end,

[1]Note, for computation simplicity, Sellers [106] implements the time-independant model neglects terms pertaining to heat storage and is thus .

$$k(\phi, T_S) = k_1(\phi) + k_2(\phi)g(T_S), g(T_S) = \frac{c_4}{T_S^2} exp(-C_5/T_S), \tag{3.3}$$

is included which appropriately parameterises the sensible and latent MET transports separately via the first and second terms on the RHS, respectively.

The most significant findings from both Sellers [106] and Budyko [12] were the extent to which the temperature dependence of the albedo from water fusion under ever cooling climate conditions could have on the climate sensitivity as illustrated in figure 3.3. When the albedo is assumed to be temperature independent, as might be expected in an atmosphere without a condensing phase, T_S decreases linearly with respect to S^*. Conversely, T_S demonstrates strong bifurcation with respect to S^* when temperature dependence is introduced. In all EBM's α is defined between maximum (α_i) and minimum (α_0) values which represent a completely ice covered and a completely ice free surface, respectively. Between, α is graduated as a function of temperature,

$$\alpha(\phi, T_S) = \begin{cases} \alpha_i & \text{for } T_S \leq T_{S,i} \\ \alpha & \text{for } T_{S,i} \leq T_S < T_{S,0} \\ \alpha_0 & \text{for } T_S \geq T_{S,0} \end{cases} \tag{3.4}$$

where Sellers [106] uses $\alpha = \alpha(\phi, T_S) = b(\phi) - ST_S$, where S is a constant for adjusting the sensitivity of α to changes in T_S and the coefficient b for each latitude was chosen as to best fit the observed data (See Sellers [106] for details).

Typically, the positive sea-ice albedo feedback means there exists no stable states where the sea-ice fraction, implied from α, is greater than 0.5 - 0.6 and less than 1, which results in a discontinuous change in T_S as a function of the change in climate forcing from either changes in incident solar fluxes or infra-red opacity such as CO_2 concentration.

In the case of the EBM's used in Ghil [34] and Bódai et al. [6] described in Eq. 3.3, $\alpha = \alpha(\phi, T_S) = b(\phi) - c_1[T_m + min(T_S - c_2 z(\phi) - T_m, 0)]_c$. Details of the various parameters c_1, T_m, c_2, z and more are explained in detail in Dwyer and Pettersen [23]. Such a setup, allows for the complete climate hysteresis to be realised including the return from the SB to the W climate state as shown below in 3.4.

Initiation of Snowball State with Dynamic Ocean Coupling

The change from a partial ice covered state thus occurs via an abrupt transition. While such ideas are nice in theory, it wasn't until Kirschivink [50], using the idea of the Snowball Earth hypothesis as a mechanism to explain various geophysical and biological

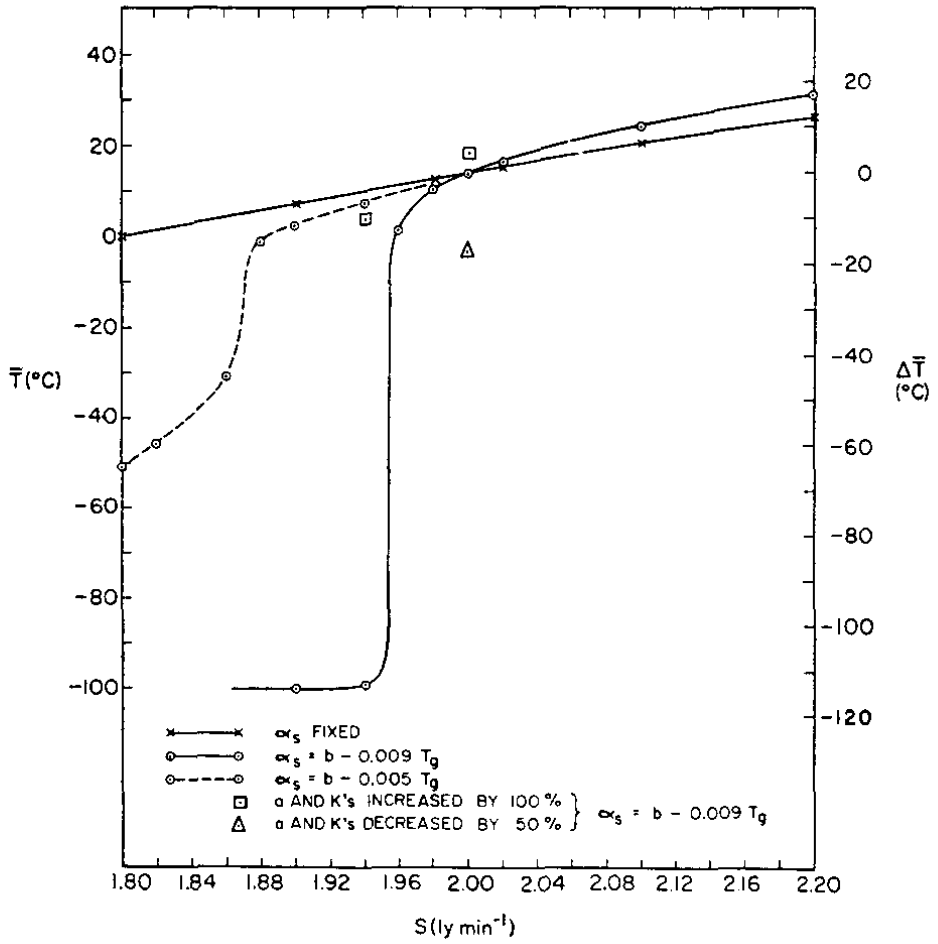

FIGURE 3.3: (a) Bifurcation diagram showing results from a 1-D EBM experiment, performed for a variety of solar forcings. Adopted from Sellers [106].

phenomena, was the possibility of such a state seriously considered not just as a plausible idea in a general sense but that it may have also occurred during the Neoprotozoic era on Earth.

A study by Yang et al. [124], using a fully coupled atmosphere–ocean–land–sea-ice model, the National Center of Atmospheric Research's (NCAR) CCSM3, shows that when dynamic ocean coupling is used, the warm climate state may initially transition to either a soft or hard SB configuration, depending on how much the CO_2, solar forcing are reduced in combination with one another and the value of the sea-ice albedo. With albedo (sea-ice = 50; snow = 78) and CO_2 (286ppm) kept constant, reducing the solar constant by 10.5% results in a "hard" snowball state. Repeating the same experiment with CO_2 decreased to between 1/2 and 1/8 of its original value, yields a soft snowball states in combination with decreasing solar forcing. Further cooling of these states inevitably leads to a hard SB state. When the CO_2 concentration was set to a 16th of pre-industrial level, decreasing solar flux again leads to a transition straight to a hard snowball state. This again highlights the potential importance of all major climatic

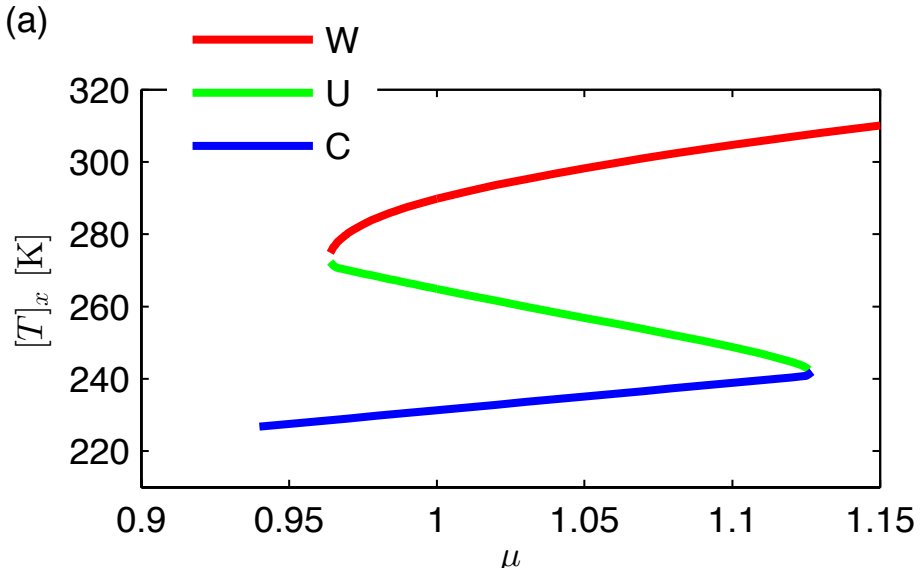

FIGURE 3.4: (a) Bifurcation diagrams. The dependence of the average temperature given as μ is shown for the three equilibrium solutions of the 1d EBM. Adopted from Bódai et al. [6].

variables in correctly diagnosing the type of Earth SB state to expect. The results are show in Fig. 3.5.

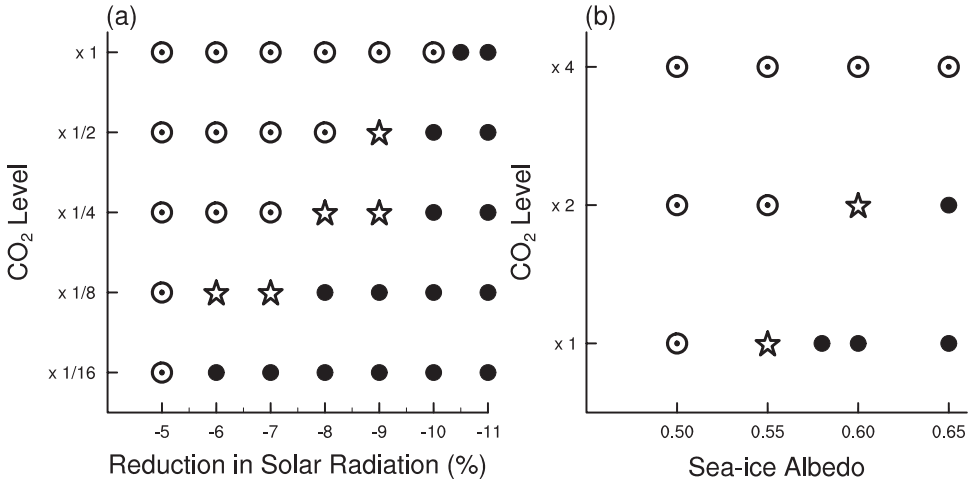

FIGURE 3.5: (a) Bifurcation diagram showing results from a 0-D EBM experiment, performed by modulating the CO_2 concentration under constant solar force where, $S^* = 1285 Wm{-}2$. Adopted from Yang et al. [124].

The response of the ocean dynamics to a cooling climate are a key aspect to the possible formation of a "soft" snowball state. As the sea-ice migrates towards the equator, the increase in the meridional temperature gradient leads to a strengthening of the Hadley circulation. In response, there is an intensification of the wind driven ocean

circulation which transports energy polewards and acts to mitigate sea-ice development in the tropics. Additionally, as more of the ocean freezes, salt is ejected and increases the salinity of the remaining unfrozen ocean, lowering the freezing temperature. The increased salinity strengthens the overall poleward circulation. Conversely, increased oceanic transport of energy results in melting at the sea-ice fronts which desalinates the water in that region and increases stratification, weakening the downwelling branch of the ocean circulation (Yang et al. [124]).

The intensification of the Hadley cell acts in response to the increase in the Equator to pole temperature gradient but does not lead to a large increase in the MET away from the tropics as there is a roughly corresponding decrease in the energy transport from latent heat (Yang et al. [125]).

Exit from Snowball State

As has been shown, the potential for forming a snowball Earth state does not require a huge change in the radiative forcing to occur, it does however require a large increase in solar forcing or infra-red opacity in order to exit back to a warm state. Thus the major stumbling block for snowball theory has been to explain the mechanism by which the Earth returned from a snowball to the present climate state.

EBM's suggest that under constant solar forcing (in this case $1285m^{-2}$), the concentration of CO_2 would need to be between 10000 ppm and 300000 ppm (e.g. see Fig. 3.2) for an average global ice albedo between 55 and 65, respectively. The difference in the range is indicative of the CO_2 greenhouse effect saturating when at high concentrations in the atmosphere.Thus, only a 10% difference in the albedo can potentially have an enormous impact on the CO_2 levels needed to leave the snowball state. However, there are significant differences in the albedo of solid water in its various forms, be it old or newly formed, snow or ice as well as the ratios in which they form. Making a prediction as to the likely average albedo within the 55 to 65 range is largely guess work. Typically, snow and bare ice has an albedo range of $65 \rightarrow 87$ and $57 \rightarrow 80$, under cloudy and clear sky conditions respectively, where the upper end of the range is due to snow and the lower from ice (Brandt et al. [9], Dadic et al. [18], Hudson et al. [43], Kindel et al. [49], Warren et al. [121]). The relative differences between the clear and cloudy sky albedo's relate to the fact that clouds are optically thin to sections of the EM spectrum, such as visible light, which are more strongly reflected by ice and snow. Blue ice, for which the number density and size distribution of the bubbles within it determine the albedo [Bohren, 1983; Warren et al., 1993], has been reported to have an albedo as low as 55 [Bintanja and van den Broeke, 1995; Bintanja, 1999; Liston et al., 1999; Reijmer et al., 2001]. The salinity of ice also decreases over time. Depending on the region, older

ice will tend to be suseptable to a variety of deposits such as dust, salt, frost and snow which increase or decrease the albedo correspondingly. Additionally, new and old melt ponds at the surface have a value of around 40 and 20, respectively.

Dadic et al. [18] does however suggest that equatorial ice greater than 0.3m thick should retain the albedo it had when newly formed. The migration rate of bubbles from cold to warm regions within the ice due to the vapour transport in the oppose direction can potentially lead to a decrease in the surface albedo via light scattering. Experimental results and heat-flow modelling suggest than the sublimation rate should be greater than the bubble migration rates so that the albedo of freshly formed ice should remain approximately constant over time. This is potentially a rather useful result as it allows for the possibility to assess the albedo of a SB state, (at least) in the Equatorial regions where deglaciation is crucial for the exit from the SB state, by using present icy conditions in specific regions, such as Allen Falls, as a proxy.

3.2 Cloud Feedback

Although extremely cold, the Arctic monthly mean cloud cover is extensive, ranging from 50% to 80% throughout the year. Though a SB state would be even colder and despite early thinking to the contrary, cloud feedbacks are likely to be equally important to the climatology of the SB state, especially for the equatorial deglaciation needed to exit the SB state. This is highlighted by the intermodel SB study of Abbot et al. [1] which shows that where similar albedo's to the bare ice were applied, differences in the cloud radiative forcing were mostly responsible for the differences in the climate states of the various models which were used.While in warm climate states it is not clear whether clouds have a net warming or cooling effect, their relative closeness in albedo to the surface albedo of a SB state mean globally they will have a net warming effect.

In EBM's, a CO_2 concentration of 0.2 bar is normally a sufficient criteria to transition from a SB to a warm climate, however Pierrehumbert [97] reports based on GCM simulations, that even with a 0.2 bar concentration of CO_2 and a conservatively low value of surface albedo, the T_S would be 30K below what is necessary to exit the SB state. This demonstrates the impact of explicitly including additional feedback mechanisms can have and shows that providing evidence supporting the snowball earth hypothesis is not trivial. It is however likely that cloud forcings were not adequately accounted for in the aforementioned experiment.

More recently Abbot [2] shows that the cloud radiative forcing is likely to be around a factor of two greater than in Pierrehumbert [97]. Here, the limited area (120km x 120km

x 17.5km) System for atmospheric modelling (SAM) model, which incorporates a cloud resolving scheme, demonstrated that provided the surface temperature is notably higher than the cloud top temperature, estimated to be 215K, convection will occur leading to sufficient cloud ice which is optically thick to infra-red radiation. The usefulness of this experiment is in understanding the nature of the kind of cloud formation and it's radiative effects rather than provide a description of the SB state as a whole. The transport from the region is prescribed here as 15Wm^{-2} based on transports diagnosed from GCM SB experiments. Even with a relatively small amount of cloud formation when compared to the modern climate, it was shown that this would provide a radiative forcing of 10-20Wm^{-2}. To put this into context, under snowball conditions and assuming an albedo of 0.6, this equates to a change in solar insolation of between 100-200 Wm^{-2}. Typically, EBM's and GCM's (Lucarini et al. [77], Pollard and Kasting [98]) have shown that the bistable region may have a width of about 20 Wm^{-2} interms of radiative forcing.

Furthermore, the cloud ice fraction vertically spans a similar temperature range as the modern Earth which thus translates to a lower cloud top height of approximately 9km compared to 15km. In prescribing the energy transfer, the cloud formation is biased and it would in addition be interesting to test the sensitivity of this experiment to a range of outputed energy transports. Donohoe and Battisti [20, 21] shows that in GCM simulations, clouds impact the magnitude of the MET produced as a result of the change to the planetary albedo. In the SB state where the surface albedo is similar to that of the clouds this maybe less significant though differences in the spectral albedo may none the less be crucial. An issue here however is a radiation scheme with sufficient bandband fidelity is computationally very expensive to implement within a full GCM. Also, there is no explicit representation of cloud microphysics necessary for determining the size and quantity of cloud droplets, which are central to the radiative properties of clouds. However, Abbot [2], argues these results are robust, significantly varying many parameters related to the formation of precipitation from clouds, which shows no significant decrease in cloud radiative forcing and in some cases an increase. Furthermore, if the vertical ascent had been prescribed to mimic the rising branch of the Hadley circulation, it is likely that the cloud radiative forcing would be greater.

3.3 Further Important Feedbacks for Climate Sensitivity SB Earth

Other important parameter considerations which are inherently difficult to quantify accurately without explicitly being diagnosed within a GCM include the water vapour and atmospheric lapse rate and horizontal temperature gradients as these are dependant

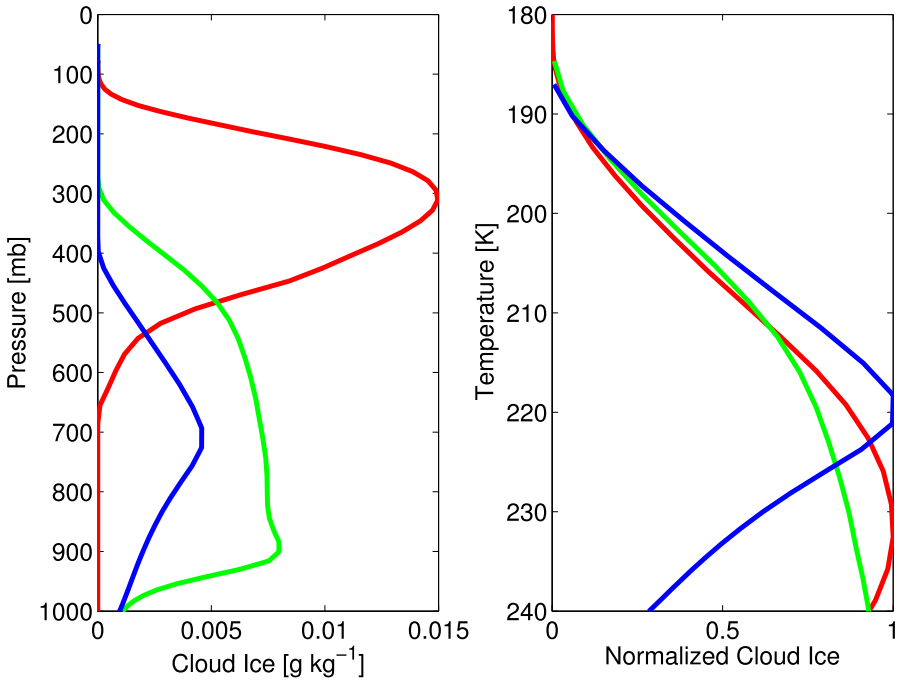

FIGURE 3.6: Vertical profiles of cloud ice as a function of pressure (left) and air temperature (right) for the reference state SAM snowball simulation with 10^{-4} vmr (blue), a SAM snowball simulation with $CO_2 = 10^{-2}$ vmr (green), and the reference SAM modern tropics simulation (red). Adopted from Abbot [2].

on the interactions between the dynamics, convection and the resulting water vapour transport through the release of latent heat.

The capacity for the atmosphere to hold water vapour is dependant on the atmospheric temperature as described by the Clausius-Clapeyron relation which suggests that the ability of the atmosphere to maintain water in a gaseous phase should grow exponentially with increased temperature. This is backed up by GCM simulations which consistently show that the relative humidity stays about constant regardless of the forcing (Bony et al. [8]), so that at warmer (colder) temperatures the specific humidity will increase (decrease). Water vapour is the strongest greenhouse gas though short-lived in the atmosphere (about 10 days), means it is not in itself a climate forcing but instead acts as a positive feedback contributing additional warming or cooling in response to other climate forcings. Water vapour therefore acts to increase climate sensitivity and in doing so influences the shape of the W and SB climate attractors. As shown in Fig. 3.7, Soden and Held [109] compare the observed mid-tropospheric cooling following the eruption of Mount Pinatubo in 1991 against GCM simulations with and without the water vapour feedback. The result here indicates that GCM's are reasonably well able to estimate the effect of the water vapour feedback and that it increases climate sensitivity by around 40%.

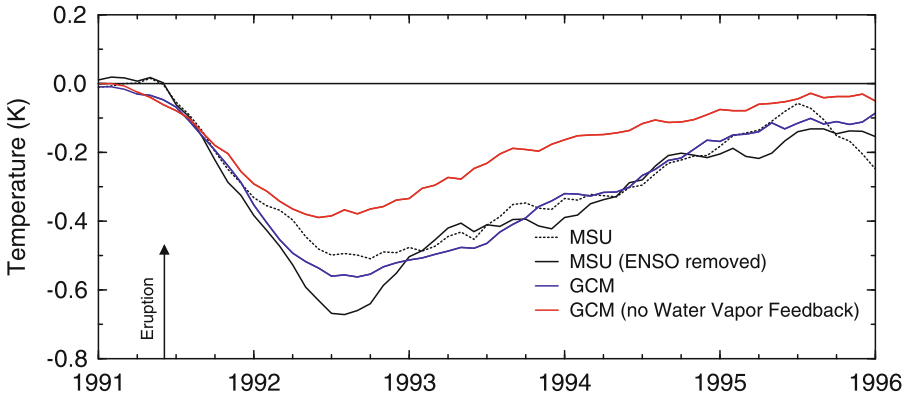

FIGURE 3.7: Global mean temperature anomaly in the mid-troposphere after the eruption of Mount Pinatubo in 1991. A global cooling of 0.7K was observed with remotely sensed radiation measurements (microwave sounding unit, MSU) after a warming effect of the 1992/1993 ENSO was subtracted. A climate model in which the water vapour feedback was turned off shows a smaller cooling inconsistent with the observations. Figure adopted from Soden and Held [109].

This study is useful as it provides a rare instance for comparison with real world data, however, it only considers a narrow temperature range within a specific scenario under transient conditions. Colman [15], Soden and Held [110], Winton [122] find the likely equilibrium climate sensitivity from GCM's due to water vapour to be around a factor of two. By contrast, the minimal moisture content in the snowball atmosphere means the water vapour was found by Pierrehumbert [97] to provide only a "slight enhancement" to the overall climate sensitivity.

The lapse rate defines the rate at which the temperature decreases with increasing altitude. In the tropics, a decrease in temperature reduces the moist convection leading to a decrease in the latent heat release in the upper atmosphere as well as the greenhouse warming due to water vapour discussed in the previous section. This in turn increases the lapse-rate which intensifies the ascending motion. In the SB state it is likely their is insufficient moisture to sufficiently warm the upper atmosphere, in part because the cloud condensation occurs at a far lower altitude, leaving dry air aloft. As a consequence, an increase in climate temperature increases the surface more so than for the upper atmosphere. The lapse rate will therefore increase as a function of temperature and so to the circulation will be intensified.

3.4 Climatic Features of an SB State

A snowball climate state represents a distinctly different mode of the climate system when compared to that of the contemporary Earth, characterised by an eminently dry atmosphere and an ice covered surface which pictorially may look similar to the depiction

shown in Fig. 3.1. The thermal inertia and low vapour content of the ice covered surface compared to one dominated by ocean means the atmosphere is able to react more quickly to local changes in solar radiation, leading to greater (temperature) seasonal variability. This is not too indifferent to Mars (Putziga et al. [101]), though the thickness of the Earth's atmosphere dampens some of the potential additional variability in the diurnal cycle which is nonetheless significantly increased when compared to the modern Earth.

Beyond the thermodynamic properties of sea-ice, as important are the dynamics of its formation. The dynamic properties depend on the Coriolis force, as well as the stresses applied to the top and bottom of the sea-ice from the atmosphere and ocean currents, respectively. Furthermore, the internal stress within the ice, and the stress due to sea surface tilt of the geoid are also parametrised in such models as used by Briegleb et al. [10, 11], Yang et al. [124]. Further crucial properties which require consideration occur below the surface and are connected with the complexity of the ice stalactite formation, pattern and development on its underside which should be of general interest as this is important not just for the development of sea-ice but also the effect on the ocean dynamics.

Snowball Hadley Cell Circulation

The Hadley cell circulation of the snowball climate is formed under rather different conditions than our well documented modern warm climate. The low thermal inertia of the snowball's icy surface means the atmosphere will respond far more quickly to seasonal variations. This makes the annual mean representation of the Hadley circulation even less meaningful than under warm climate conditions. During the NH and SH summer's there is a single Hadley cell roughly centred over the equator. For the NH (SH) summer the acending from north (south) of the equator, travelling aloft in a southward (northward) direction, descending south (north) of the equator. During the equinoxes, their is a more traditional dual cell structure which forms either side of the equator with air ascending at the equator and moving polewards aloft before descending around up to $20°-30°$ either side of the equator. Pierrehumbert [97] produced one such experiment showing the Hadley cells for January, April, July and October (Fig. 3.8). Interestingly, Pierrehumbert [97] finds that during the solstices, the circulation of the SB state has a greater intensity than of the contemporary climate. By comparison, the equinox Hadley cells are rather weak. Despite the strength of the Hadley cell the low thermal inertia coupled with minimal moisture means the tropics do not homogenize temperature either zonally nor meridionally, something which is very must a key characteristic in Tropics of the modern Earth.

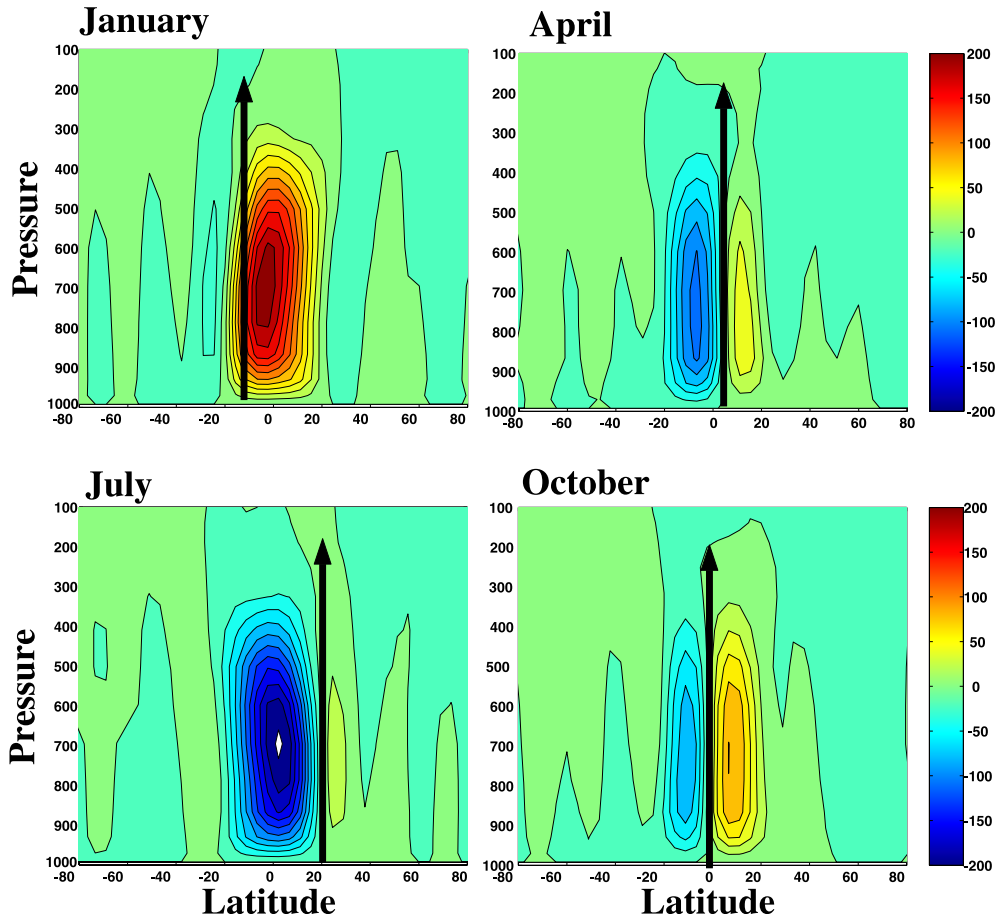

FIGURE 3.8: Seasonal cycle of the mass flux streamfunction of the Hadley circulation, for the case with 100 ppm CO2. Units are 10^9 Kgs^{-1}. The contour interval and colour scale are the same for all panels. Adopted from Pierrehumbert [97]

.

While the general state of atmospheric circulation can be well represented on seasonal time scales, the evap-precipative properties of the climate are largely reliant on the diurnal cycle.

The annual residual precipitation - evaporation pattern for the SB state tell us the regions where snowfall settles and has a similar precipitation pattern to that of the Warm climate, however Pierrehumbert [97] reports the largest accumulation rate, which occurs at roughly +-16°, is only about 1cm per year in liquid water equivalent. The individual amount of precipitation and evaporation being much larger at about 40cm liquid water equivalent per year. The main factor which makes even this relatively modest evaporation and precipitation possible is again the low thermal inertia which allows for large temperature differences across the period of the diurnal cycle, with evaporation occurring mainly in the afternoon and precipitation soon afterwards before significant transport of moisture can take place. This mostly occurs during the summer

months in either hemisphere in almost metronomic fashion and is the dominate weather feature of the summer months, highlighting the importance of resolving both the seasonal and daily time scales for gauging the SB state.

3.5 Global Thermodynamic properties of the Warm and SB Climate states

From the thermodynamic quantities considered throughout section 2.1 the most obviously relevant and easily conceptualised for the global climate are temperature and MET. It is also important to consider how these quantities are defined. In the case of temperature, ideally it would be practical to be able to talk in terms of surface or surface air temperature though as this defines the lower surface boundary, it is not trivial to assume whether or not it is the most important determinant of other properties in the system. Instead, the average temperature, T_{av} of the atmosphere or the emission temperature, T_E may be more important, however, as in the case of Earth-like planetary atmospheres, the majority of solar radiation enters the system first via differential heating of the surface. The forcing effect of the surface heating on the circulation is likely to be an important contributing factor. Conversely, in atmospheres optically thick to incoming solar radiation, the passive role of the surface is likely to be of less importance In the case of MET one must consider the importance of defining the transport from a specific latitude or use the maximum transport as the most important indicator for making a judgement on the overall change in the energy transport on the system.

A study by O'Gorman and Schneider [86] shows how increasing T_S in the warm state affects the MET. Here, MET is found to increase rather linearly/steadily with global surface air temperature up to conditions comparable to the contemporary Earth (288K), after which the rate of increase reduces significantly before plateauing at 303K and falling thereafter. O'Gorman and Schneider [86] also dissects the contributions associated with the latent and sensible heat transport. From 260K to 285K both increase, at which point the sensible heat transport reaches it's peak. The latent heat increases monotonically up to the maximum temperature of 315K as one might expect due to the increased availability of water vapour. The sensible heat fluxes decrease steadily from 285K as the increased effectiveness of latent heat energy in equilibrating the atmosphere means that the meridional temperature difference decreases so that latent heat transport has an indirect effect of inhibiting the sensible transport.

This model does however lack a parametrisation for sea-ice which through the study of EBM's as shown above, should have a strong influence on climate sensitivity. In

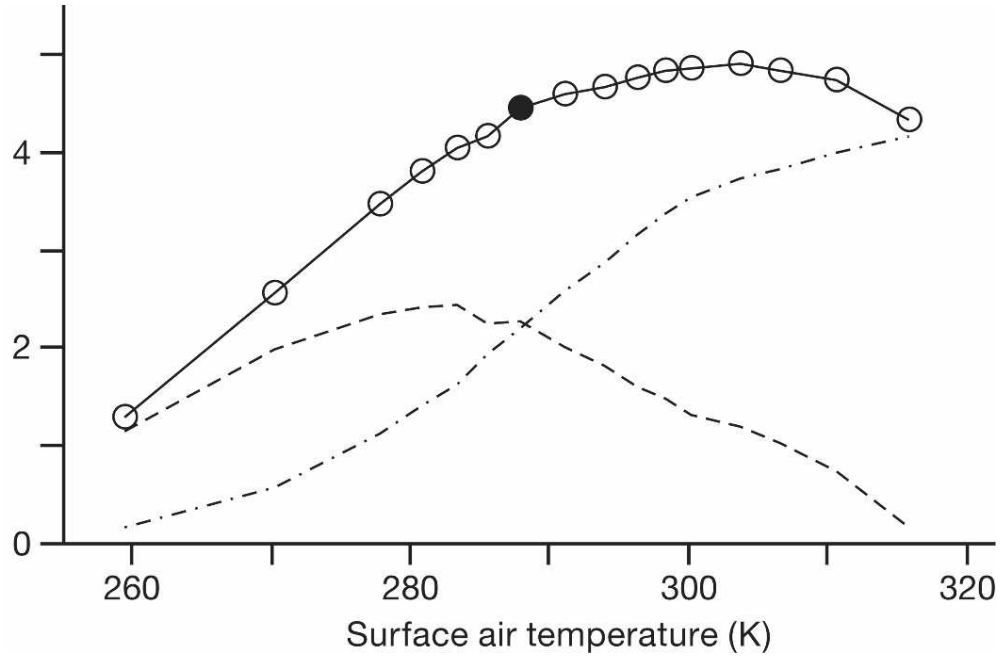

FIGURE 3.9: Meridional energy flux (solid line and circles) at 50° latitude vs global-mean surface air temperature and decomposition into dry static energy flux (dashed line) and latent heat flux (dash-dotted line). Adopted from O'Gorman and Schneider [86]

.

particular, this is likely to be realised through an increase in the change in the meridional albedo contrast with a given climate forcing and therefore also the meridional temperature gradient which influences the MET.

Lucarini et al. [76] goes another step further and performs a similar experiment to O'Gorman and Schneider [86] but with a vastly expanded thermodynamic description using the PlaSim climate model. This involves applying a set of novel diagnostic quantities from Lucarini [75] which have been previously summarised in sections 2.1.4 and 2.1.5 which provide a methodology for calculating the η, W, $\overline{\dot{S}_{mat}}$ and irreversibility, (α) within the climate system. In all cases, the climate response behaves approximately linearly with the logarithm of CO_2 concentration where T_S, $\overline{\dot{S}_{mat}}$ and α increase while W and η decrease monotonically with the logarithm of increasing CO_2 concentration while again the efficiency and Work done by the system decrease in magnitude. A summary of the main results are shown in fig. 3.10.

A thermodynamic analysis of the climate hysteresis performed using GCM's is extremely rare, however Lucarini et al. [77] performed such an experiment applying the same methodology used inLucarini et al. [76], with the main exception being that S^* was modulating instead of the CO_2 concentration. The focus of this paper is more intended to gain understanding of the non smooth response of the climate around the tipping

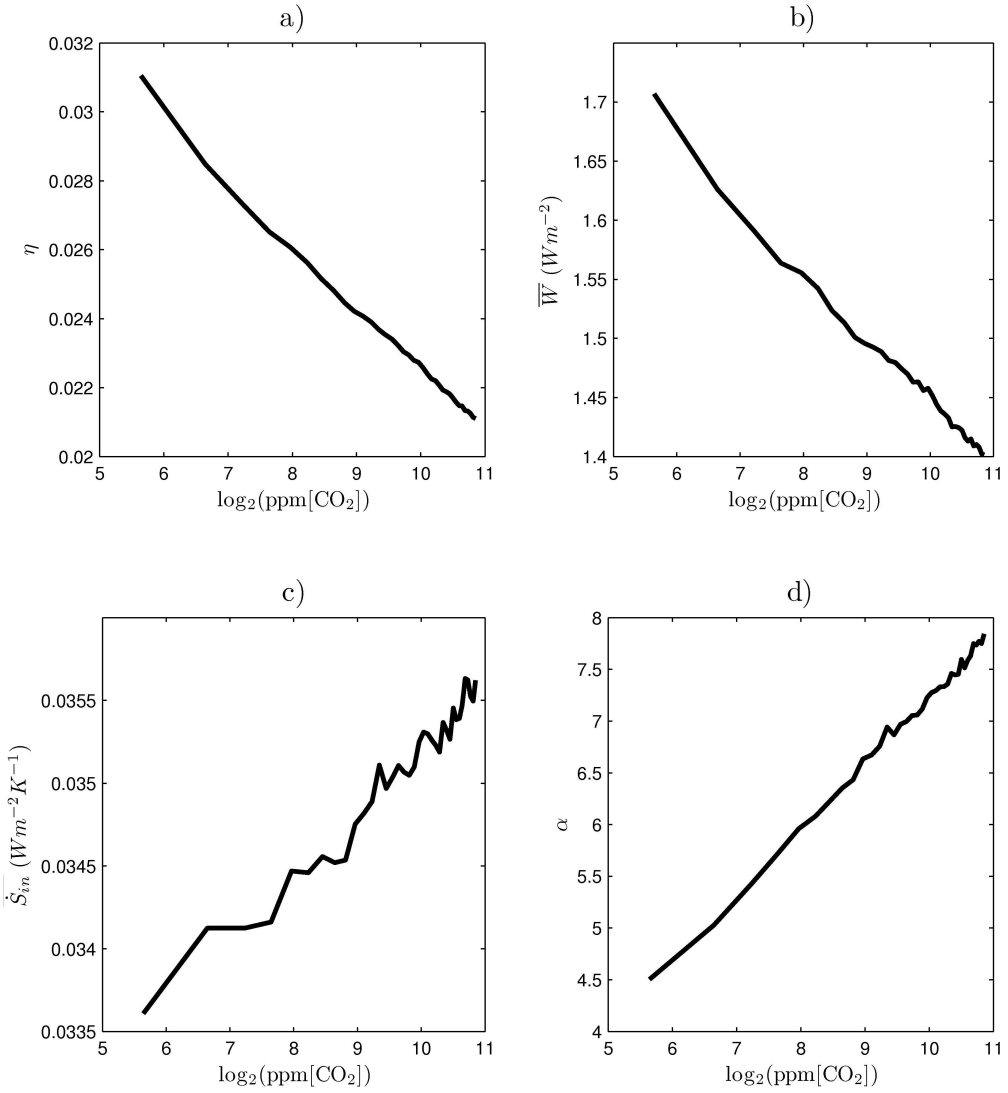

FIGURE 3.10: Generalised climate sensitivities. CO2 concentration dependence of macroscopic thermodynamic variables: (a) efficiency; (b) intensity of the Lorenz energy cycle (or, equivalently, total dissipation); (c) material entropy production; (d) degree of irreversibility. See text for details.). Adopted from Lucarini et al. [76]

points in addition to comparing the smooth response of the W and SB climate attractors to S^*, using the aforementioned thermodynamic tools.

As expected this paper shows that temperature increases with an increase to the solar forcing. In the analysis of the $\overline{\dot{S}_{mat}}$, this was found to behave similarly and also increased monotonically with solar forcing and is much greater in the warm climate state than that of the cold. Lucarini et al. [79] derives an approximation method described in session 2.1.5.1 which shows that for the warm climate states the majority of $\overline{\dot{S}_{mat}}$ occurs as a result of vertical process, most of which are associated with the transfer of latent heat energy. Thus the minimal water vapour production accounts for the significant difference between the values of $\overline{\dot{S}_{mat}}$ found for both regimes. In this sense, the $\overline{\dot{S}_{mat}}$

is fundamentally related to the effect caused by the positive albedo feedback on the climate and is therefore a trustworthy means in which to distinguish between both climate attactors. In fact, $\overline{\dot{S}_{mat}}$ was shown to more clearly separate the W and SB states than the temperature. It was also found that irreversibility is far greater in the W relative to the SB state which thus infers this is also related to the increased presence of latent heat in the warm climate states. By contrast to the aforementioned quantities, the W and η were shown to behave in an opposite manner in both climate states when modulating the solar forcing, decreasing and increase with increasing solar irradiance in the W and SB states, respectively, so that the maximum magnitude of both quantities occurs for climate states near to and proceeding the $W \rightarrow SB$ and $SB \rightarrow W$ transitons. The Work performed in the W states are greater than those of the SB states at the transition but in the case of the efficiency both are comparable. While the work appears to be more vigorous in the W states, which is consistent with the fact that the absorbed differential energy applied to the system is greater, its ability to transport sensible energy fluxes per unit energy absorbed by the system is comparable to that of the SB states near there respective attractors because the irreversibility of the warm climate is greater.

3.6 Concluding Remarks and Questions Beyond Earth's Snowball

The interwoven nature of the climate properties discussed above demonstrate some of the difficulties with accurately recreating the climate of planetary systems. While EBM's have provided useful insight, continued development of GCM's is crucial so that the properties and their feedbacks can be better understood. Ocean dynamics are a key component to the precise out come of a SB state and whether there is ice formation encompassing the tropics. Considering the orbital properties of a planet, there are additional factors which may assist planetary atmospheres in general to resist a hard snowball state. EBMs in which heat transport across the ice line is inhibited are more resistant to global glaciation because the tropics cannot export heat to higher latitudes Lindzen and Farrell [70]. This therefore leaves many open ended questions.

For instance, it may be the case that planets with much higher planetary rotation rates will behave similarly to Lindzen and Farrell [70], as the Hadley circulation is far less efficient, forming smaller cell structures (albeit more intense) leading to a weaker MET. If the MET is sufficiently weak, as well as potentially supporting far stronger meridional temperature gradients between an ice free equator and a deep frozen state in all other areas, the global bistability properties may also be rather different. If the modern Earth's planetary rotation rate was sufficiently spun up without adjustment to

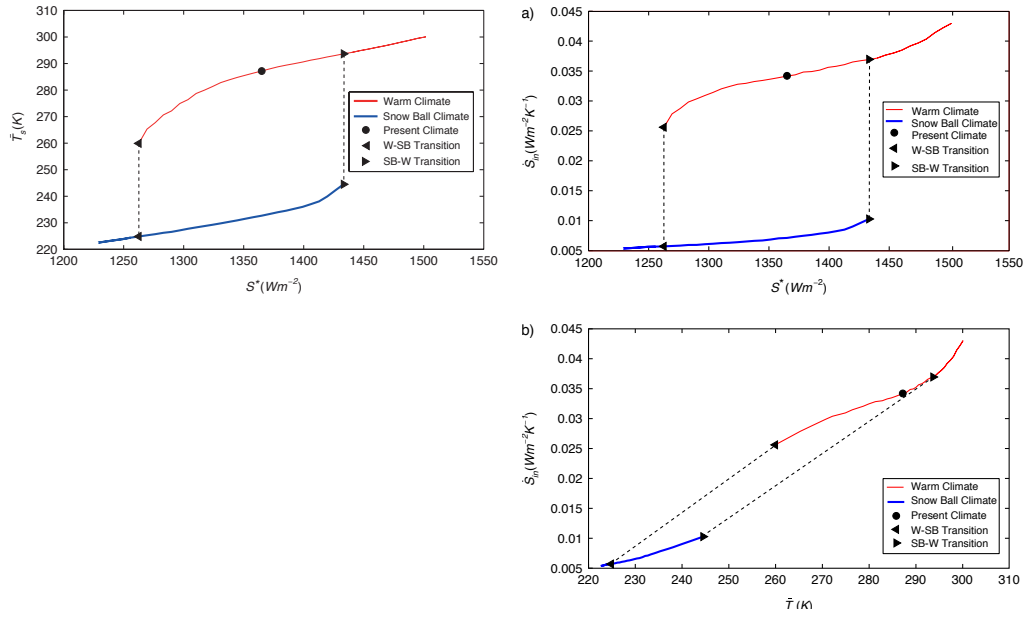

(A) (B)

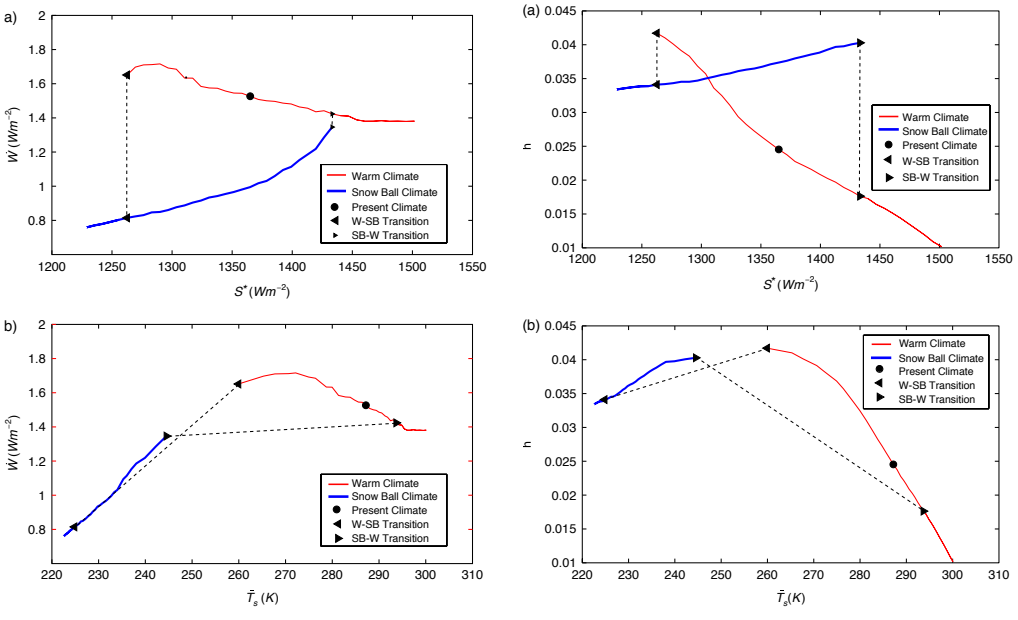

(C) (D)

FIGURE 3.11: Time average of (A) the global surface temperature (T_s), (B) the material entropy production ($\overline{\dot{S}_{mat}}$), (C) Work (W, conversion from moist static energy to kinetic energy) and (D) efficiency (η). (a) and (b) denote quantities which are plotted against the solar constant and the surface temperature, respectively. Adopted from Lucarini et al. [77].

any other parameter, it may be plausible that this alone may be a sufficient criteria to produce a soft SB state. In this case the expectation of the modern Earth's orbital parameters being multi stable may not apply to the newly produced state. Reproducing

the same experiments as Lucarini et al. [77] which involve modulating the radiative forcing but with far increased rotation rate may then shift the W→SB transition to higher levels of radiative forcing. Additionally, an upper limit for the SB→W transition must exist where direct solar irradiance is always too large, even at the poles, to maintain an icy surface. Thus, with a sufficiently large rotation rate the points of the W→SB and SB→W transitions will meet so that the bistable region disappears and the transition between warm and snowball states will occur without hysteresis.

Conversely, if the rotation rate is decreased sufficiently (while maintaining symmetry and keep the diurnal cycle short), the Hadley cell will extend to the poles leading to a far more efficient poleward heat transport, effectively cooling the equatorial region and warming the poles. The meridional temperature gradient will thus be minimal so that the development of sea-ice will occur almost uniformly across the surface. This scenario may ultimately be well represented by 0-D EBM. Such 0-D model experiments suggest that the latitudinal dependence of sea-ice growth seen in 1-D EBM's is not a necessary criteria for climate bistability. In that case, for a given planetary albedo and diurnal cycle, the W→SB transition as a function of the applied perturbation, may only be weakly dependant on Ω. If so, does this imply a constraint on the climate sensitivity to changes in Ω even where the climate response behaves in a smooth manner? Whatever the eventual result may be, analysis of the thermodynamic properties while performing such hysteresis experiments with differing orbital property values may unlock key relationships to which climate response is bound by.

Chapter 4

Thermodynamic insights into the role of solar forcing and opacity

[1][2]

4.1 Introduction

4.1.1 Habitability conditions and climatic bistability

The paleohistory of our planet provides strong evidence that the present astronomical and astrophysical parameters of the Sun-Earth system support two distinct steady states: a warm state (W) characterised by widespread liquid water and a moist atmosphere; with the other characterised by the global glaciation of water and an extremely dry atmosphere, i.e. the so-called Snowball state (SB). Proposed here is a thorough investigation of these two states in a bi-dimensional parameter space, with the goal of detailing the region of bistability for an Earth-like system in order to analyse the bifurcation points and the mechanisms of transitions between both states. This investigation deals with Earth-centric conditions because this is the only system where an extensive body of literature exists for the Snowball state and the Snowball-Snowfree transitions, be it observational, theoretical, or model-assisted, however, the scope of applicability may be much wider.

[1]Extracts from **Boschi R.**, V. Lucarini, S. Pascale, 2013. *"Bistability of the climate around the habitable zone: a thermodynamic investigation"*, Icarus 226, 1724-1742.

[2]Extracts from **Boschi R.**, V. Lucarini, S. Pascale, 2014. *"Thermodynamic insights into transitions between climate states under changes in solar and greenhouse forcing"*; Chapter in *"Beyond the Second Law: Entropy production and non-equilibrium systems"* , RC Dewer, C Lineweaver, R Niven, K Regenauer-Lieb (eds), Springer, ISBN: 978-3-642-40153.

Probably the most notable examples of climate change events on the Earth occurred during the Neoproterozoic (period spanning from 1000 million to 540 million years ago), when the Earth is believed to have suffered two of its most severe periods of glaciation (Hoffman et al. [38]) and entered into a SB climate state. This period coincided with large carbon dioxide fluctuations, while the solar constant (about 1360 Wm^{-2} under present conditions) is believed to have been 94 % of current levels, rising to 95% by the end of the Neoproterozoic era (Gough [36], Pierrehumbert et al. [99]). The two main factors effecting the concentration of atmospheric CO_2 are biotic activity and volcanism. Volcanic eruptions bring about very sudden and dramatic increases in CO_2 concentration. This process provides a potential mechanism through which the climate can exit the SB state, by increasing the opacity of the atmosphere and enhancing the greenhouse effect. The biospheric effect tends to occur more gradually as the biotic activity and atmospheric composition are coupled so that large fluctuations of the carbon pools take place over long time scales. Note that the effect of SB events on the biosphere is believed to have been disastrous. Carbon-isotope ratios characteristic of Earth's mantle (Hoffman et al. [38], Kennedy et al. [48]) rather than of biologically active terrain recorded immediately below and above the glacial deposits imply that oceanic photosynthesis was effectively non-existent during SB events. The result of this and anoxic conditions beneath the ice should have lead to the disappearance of most kinds of forms of life except bacteria. The final disappearance of SB conditions since the Neoproterozoic may have been the main contributing factor in the development of complex multi-cellular life that began around 565 million years ago.

Based on the evidence supported by [38] and [39], it is therefore expected that the Earth is potentially capable of supporting multiple steady states for the same values of some parameters such as the solar constant and the concentration of carbon dioxide, which directly affect the radiative forcing. It is important therefore to explore this hypothesis, due to its relevance for the history of our planet but also to help understand other planets capabilities for supporting life.

The presence of such catastrophic climate shifts (Arnol'd [4]) suggest the existence of a global bifurcation in the climate system for certain combinations of its descriptive parameters (Fraedrich [29]). The loss of stability realized in the W→SB and SB→W transitions is related to the catastrophic disappearance of one of the two attractors describing the two possible climatic states, as a result of a set of complex bifurcations.

Starting from present conditions, the most obvious physical parameters to modulate in order to bring about the transition to the SB state is the solar constant. Even if other model experiments (Voigt and Marotzke [119]) show that a decrease in CO_2 alone can bring about the transition to the SB state, this requires more than an 80% decrease in

CO_2 concentration, compared to a decrease of less than 10% for the solar luminosity. The Neoproterozoic however highlights the importance of considering changes in CO_2 levels as a mechanism for transition to and from the SB climate state, and the dramatic impact it can have on the overall state of the climate system. It is therefore interesting to alter both the solar luminosity and the atmospheric opacity as these are two important parameters affecting the overall properties of the system. If one wants to explore extensively a parameter space of climate steady states in terms of these two quantities, it is therefore necessary to consider a wide range of values. The originality of the work present in the following sections, comes from exploring both the solar and greenhouse forcings together but also from this analysis of the transitions between both states of the climate system from the point of view of the Carnot efficiency.

When using a complex climate model to study transitions, it is important to choose the correct physical observables to provide information about the global properties of the system. The temperature, which is the variable traditionally investigated in climate sciences, gives an overall view of the state of the system but does not give immediate information about the processes occurring within it. In addition to temperature, it is therefore important to consider diagnostic quantities that provide information on the behaviour of processes occurring within the system. Since the climate system is in a non-equilibrium state [5, 27] the best way is to approach this problem from a non-equilibrium thermodynamics point of view. This means introducing diagnostic tools which complement the more traditional diagnostics based on classical climatological fields as temperature, precipitation and winds. It will be discovered at the end of this study that the temperature is a good physical observable for the climate as it is intimately interconnected with the thermodynamical quantities.

Note, this work differs from most others done on the snowball state, in the sense that it explores the snowball state using the Earth's present land configuration as opposed to how it was during the Neoproterozoic era. It is well known that the land mass distribution is important in determining the specific details of the transitions between the SB and W states Voigt and Marotzke [120]. Nonetheless, the structural properties of the system are not expected to be significantly affected when a wide range of values of the solar constant and CO_2 concentration are considered.

Another aspect to mentioned in regard to interpreting these results for more general planetary systems, is their sensitivity to the spectral distribution of stellar irradiance and atmospheric composition. Obviously, a different spectrum of incoming stellar radiation and optical properties of the atmosphere will surely change the results. However, so long as radiation is mostly absorbed at the surface; clouds have the dual effect of scattering shortwave and trapping long wave radiation; ice, most importantly, has a much

higher albedo than land or ocean; and have a greenhouse gas that can be parametrically modulated (that is equivalent to CO_2), the basic properties described here will obviously be affected but not altered in a fundamental way.

The work presented in this chapter builds on and unifies the work done by [77] with the analysis performed in [76], where $[CO_2]$ variations alone are considered, in order to obtain a more complete picture of how radiative and dynamical processes are coupled in a vast range of climates. Specifically, a detailed thermodynamic, parametric sensitivity study of the steady state climate system is performed with respect to S^* and $[CO_2]$. Using PlaSim, a general circulation model of intermediate complexity [10], I study the climate states realised when the solar constant is modulated between 1160 Wm^{-2} and 1510 Wm^{-2} and the values of $[CO_2]$ are varied between 90 to 2880 ppm. The aim here is to produce a simulation-based reconstruction of the global structural properties of the climatic attractors. For both W and SB states I compute the surface temperature, material entropy production, meridional energy transport, Carnot efficiency [22, 37] and dissipation of kinetic energy and propose empirical relationships in the parametric plane ($[CO_2]$, S^*). An empirical relation will be formulated for the two transition lines (W→SB and SB→W) in the parametric plane between S^* and the natural logarithm of $[CO_2]$ which marks the boundaries of the hysteresis in the climate system. The aforementioned quantities will be used to explain changes in large-scale climate behaviour and the effect of climate change on features such as stratification and baroclinicity in order to understand changes in the MET across the parameter range. It will also be shown that the Carnot-like efficiency has a key role in defining the stability of the system, which is related to abrupt climatic shifts.

Note, a priori is not expected in Paleoclimatic terms, nor are the emirically derived relations expected to apply universally for all planetary systems. However, new potentially relevant methods for addressing both problems will be proposed. In doing so, it is hoped to move a small step in the direction of deriving more general properties, by showing that reducing the rotation rate of the planet by a factor of two does not significantly alter any of the properties obtained with the terrestrial value of the rotation rate, despite specific meteorological features of the planet being very different. Of course, such sensitivity analysis is not exhaustive and needs to be completed in future studies by looking at the impact of changing other astronomical and astrophysical parameters.

The chapter is structured in the following way: Section 4.2 to the experimental setup. In Section 4.3.1 the results of the simulations are examined. Note, Appendix B provides a description of the PlaSim climate model.

4.2 Experimental setup

As already discussed in Chapter 3, this model features multistability for $[CO_2]$ = 360 ppm: there is a range of values of S^* centered approximately around the present value of S^*=1360 Wm^{-2} such that for each choice of S^*, there are two attractors, and so two distinct climates, exist. One climate is characterised by extremely cold and dry conditions, and it is referred to as the Snowball (SB) state. The other climate, instead, resembles present-day conditions and it will be referred to as the Warm (W) state. For values of S^* larger than those included in the range of multistability, only the W state is present, whereas only the SB state is present for low values of S^*. The two critical values of S^* (Fig. 3.11a) determining the range of multistability are the tipping points of the system. In this chapter, this analysis is extended for different values of $[CO_2]$, in order to treat in more generality the problem of multistability of the climate system. Changing S^* over a wide range of $[CO_2]$ of 90, 180, 270, 360, 540, 720, 1080, 1440, 2160 and 2880 ppm, a reconstruction of the SB and W climate states is performed. The procedure occurs as follows for each of the considered values of $[CO_2]$:

1. the model is run to a W steady state for 100 years with S^* equal to 1510 Wm^{-2};
2. S^* is decreased by a small amount for each value of CO_2 and the model run is continued until a steady state is reached;
3. step 2 is repeated until S^* is reduced to 1165 Wm^{-2}; the point of W→SB transition is noted down;
4. the reverse operation is then performed with S^* increased step by step, up to the value of 1510 Wm^{-2}, each time allowing the system to reach a steady state; the point of SB→W transition is noted down.

Further to this, the position of the transition is identified to a higher resolution than the rest of the parameter range in the direction of S^*. For values of S^* within 10 Wm^{-2} before the transition, S^* is decreased in intervals of 1 Wm^{-2}, each time permitting 50 years for the system to reach a steady state, until after the transition is observed.

It is important to address a caveat related to the suitability of the model used in this study. The radiation scheme adopted by PLASIM has been devised to deal with Earth-like CO_2 concentrations, and in this range it is reasonably accurate. While in this study the radiation code is pushed beyond the conditions usually considered, it is still done so using CO_2 concentrations which are within one order of magnitude of those found currently and therefore, retain confidence in this model. Moreover, this study does not intend to obtain precise quantitative estimates as a result of strong perturbations to the

atmospheric opacity and/or solar irradiance, but rather at deriving the overall behaviour of the system. The effect of considering ultra-high values of CO_2 concentrations (much higher than what has been considered here) has been analysed in detail by [97], who discussed how using a radiative model designed for Earth climate conditions can be problematic. Note that for very high CO_2 concentrations additional effects may become relevant like the onset of CO_2 condensation, which is not described by the microscopic physics of climate models.

4.3 Phenomenology of the Snowball state

In order to provide some context to the thermodynamic description which shall follow, a brief description of the climatic features of the SB and W states with identical forcings is compared, using values which are akin to that of the current Earth climate i.e 360ppm CO_2 concentration and $S^* = 1360\text{Wm}^{-2}$. The general circulation structure of the SB state is found to be less intense than that of the warm state (see Fig. 4.1, especially during the equinoxes where it shares a similar dual cell structure to the Hadley cell of the W climate state. During the Northern (Southern) hemisphere summer, the atmospheric general circulation forms a single cell structure over the equator similar to [97], flowing aloft, predominantly from the North (South) toward the equator, leading to an Easterly jet within 20° north (south) and a Westerly jet around 40° south (30° north) of the equator, which are comparatively strong to one another. A weaker Westerly jet/wind also exists in the mid-to-high latitudes of the North (South) hemisphere.

Relative to the W state the mid-latitude westerly jets are far less intense and focused at around 350hPa as opposed to being at the very top of the troposphere. The latitudinal position of the jet streams are also more strongly dependant on the orographic asymmetry between the hemispheres where the average annual position is located at approximately 38N/38S and 63N/40S for the W and SB states, respectively. An additional feature observed in the SB state is the existence of an equatorial upper tropospheric easterly jet at around 250hPa. Note, while the circulation of the SB state exhibits a similar pattern to that of [97] discussed in session 3.4, due to the lower thermal inertia, here the SB circulation is weaker, while in [97] it was stronger than there respective W regime.

The orography plays a larger role in the SB states as the lower temperatures mean the height of the troposphere is considerably lower (12km compared to 16km). The hemispheric asymmetry which slows the mid-latitudinal zonal westerly flow in the northern hemisphere so that the general circulation readjusts to deposit more zonal momentum in the southern hemisphere. In accordance, an overall bias in the annual overturning circulation where the atmospheric motion favours transport in the upper troposphere

toward the equator and southern hemisphere from the Northern hemisphere with the opposite being true at the surface.

The temperature structure of the SB regime is also rather different (see Fig. 4.2). In the mid to high latitudes, vertical temperature gradient is virtually non-existent, which is indicative of the fact that the MET is significantly weaker. The exception to this is during the summer months where the largest vertical temperature gradient is located in the midlatitudes and extra-tropics in the summer and winter months, respectively.

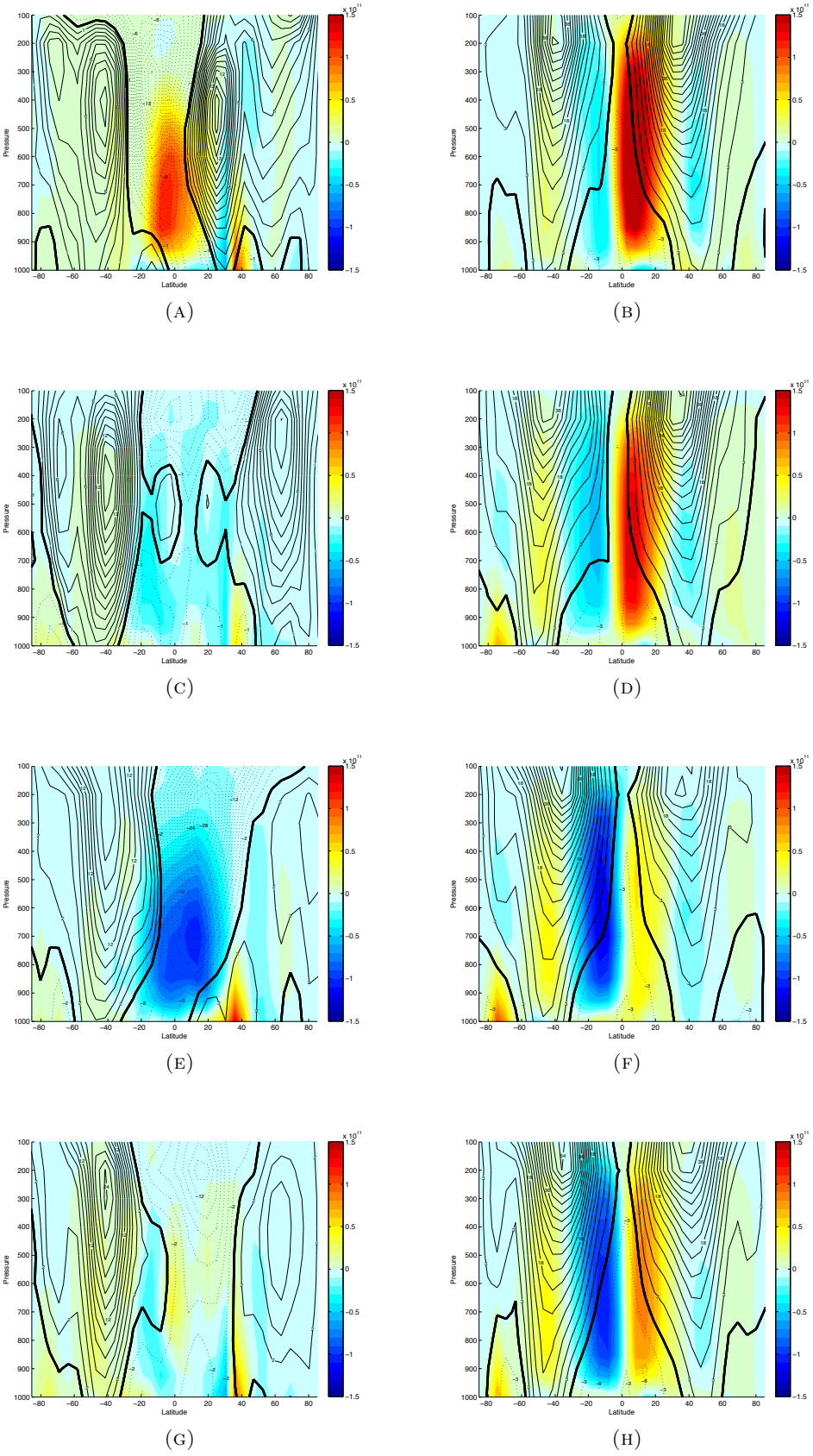

(A) (B)

(C) (D)

(E) (F)

(G) (H)

FIGURE 4.1: The figures show for winter (A), spring (B), summer (C) and Autumn (D), the general circulation for the W and SB states where the $[CO_2]$ is 360ppm and S^* is 1360Wm^{-2} thin black contours show zonal-mean zonal wind and the zero-wind contour is given by a thick black contour. The red-yellow and blue colour scales depicts the clockwise and anti-clockwise mean-meridional streamfunction, respectively. The left and right columns denote the SB and W states, respectively.

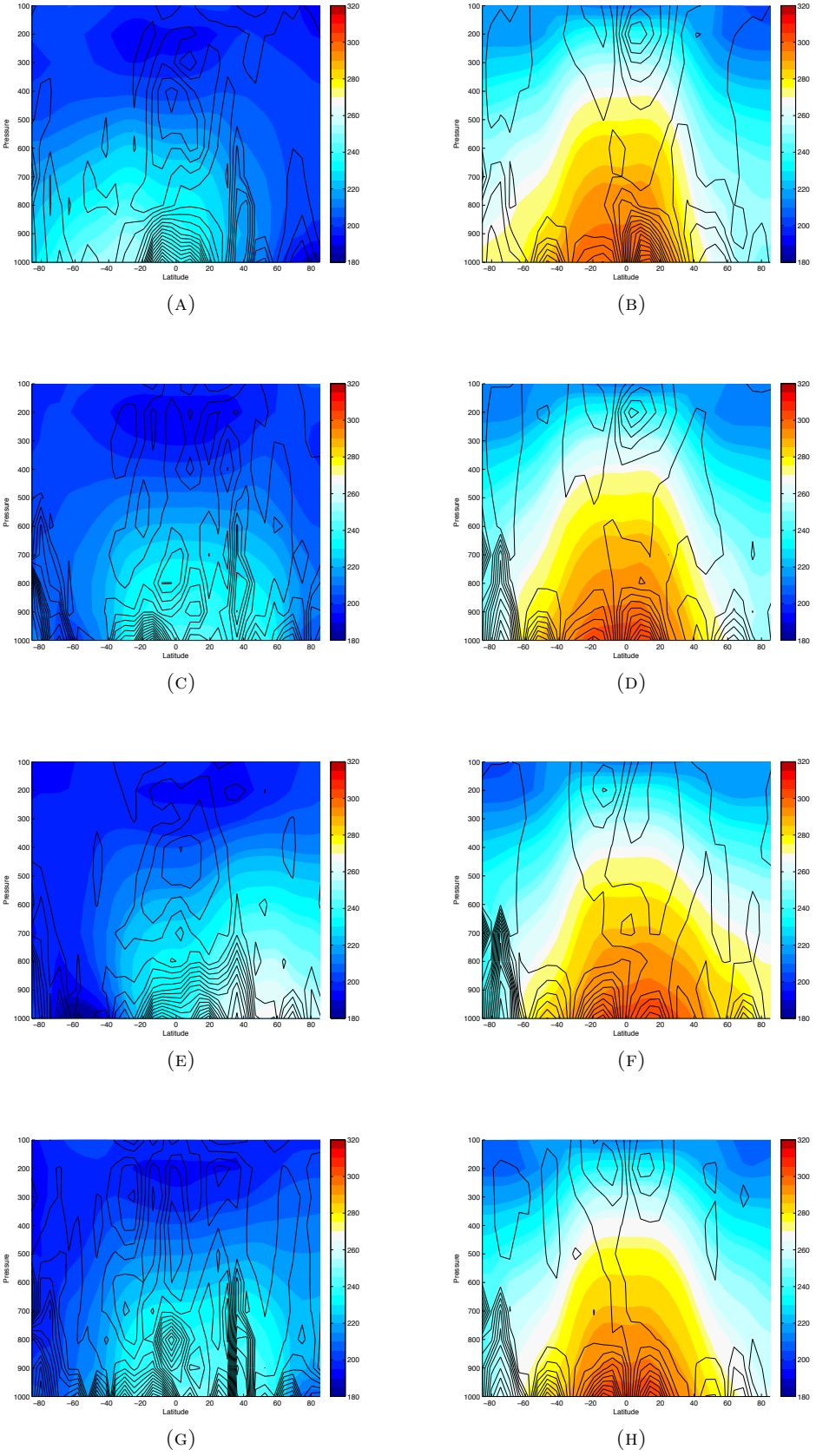

(A) (B)

(C) (D)

(E) (F)

(G) (H)

FIGURE 4.2: The figures show for winter (A), spring (B), summer (C) and Autumn (D), the zonally averaged temperature profile for the W and SB states where the $[CO_2]$ is 360ppm and S^* is 1360Wm^{-2}. The left and right columns denote the SB and W states, respectively.

4.3.1 Climate Bistability

Initially, focus is put on analysing the parametric plane ([CO_2], S^*), which shall be referred to as the CS space, as a function of global mean surface temperature, T_s. The transition zones between the climate states are clearly defined from the temperature profiles. Note, the two qualitatively distinct properties of the climate system in the CS space, namely the presence of bistability, can be reconstructed from any observable of the climate state, but it is most instructive to select first the surface temperature. The temperature profile through the CS space of both manifolds is illustrated in Fig. 4.3. In order to aid the reader in visualising the CS space correctly, Appendix A contains two figures showing 3D representations of the CS space as functions of T_s and $\overline{\dot{S}_{mat}}$, where the W and SB manifolds are presented on a single figure.

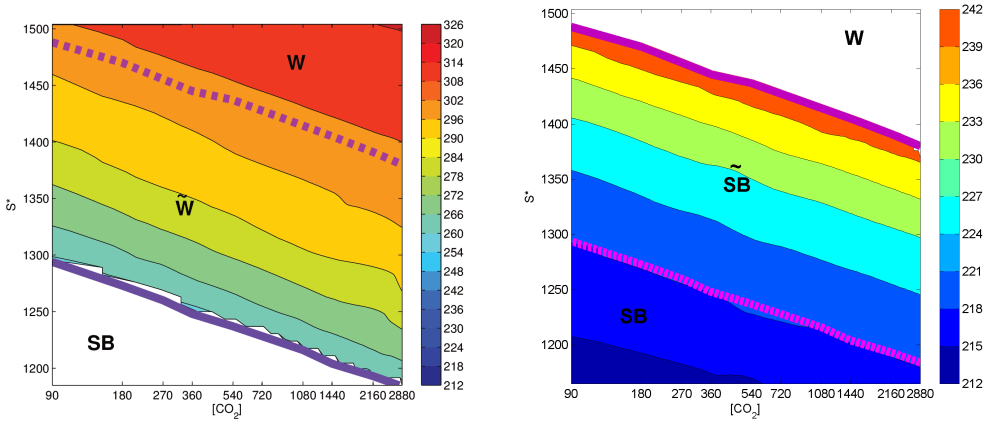

(A) (B)

FIGURE 4.3: Contour plot of surface temperature (K) as a function of S^* and the [CO_2]. The lower SB (a) and upper W (b) manifolds are shown. The transition SB→W and W→SB are shown by the upper and lower purple lines respectively. The blue dots indicate the values of (S^*,[CO_2]) for which simulations have been performed.

From 4.3a,4.3b and 4.3, two main climatic regimes are identified, observed as two distinct manifolds ([CO_2], S^*, T_s) and characterized by a sharp change in T_s when jumping from one manifold to another. These are referred to as the upper and lower manifolds, representative of the W and SB regimes respectively. As expected, there is a monotonic increase of temperature with increasing CO_2 or S^* on both manifolds (Pierrehumbert [97], Voigt and Marotzke [119]). Across the explored parametric space, the temperature range on the SB and W manifolds are 212 K-242 K, and 254 K-326 K respectively. It is found that the temperature range 242 K-254 K is not permitted by the climate system.

The temperature range of the bistable region in the SB and W regimes are 218 K-242 K and 254 K-300 K respectively, meaning that the rate of change of surface temperature over the same range of S^* and [CO_2] is approximately twice as large in the W regime

with respect to the SB regime. The climate sensitivity of the W state is much higher than that of the SB state because SB is almost entirely dry, so that the positive water vapour feedback is not active and the surface temperature difference between the two manifolds ranges between 40 K and 60 K, respectively, for identical values of S^* and $[CO_2]$. The W states (upper manifold) exists only in the region of the CS space above the W→SB transition line (the position of this line is expressed as $S^* = S^*_{sbw}$) whereas the SB states (lower manifold) only in the CS region below the SB→W transition line (the position of this line is expresses as $S = S^*_{wsb}$). Such lines, which are well separated and approximately parallel, are illustrated as solid and dashed purple dashed lines on Figs 4.3-4.9 and have been found within an accuracy of 2 Wm^{-2} of the solar constant. The solid purple lines indicate the tipping points: for the SB states they correspond to the SB→W transitions, for the W states they correspond to the W→SB transitions, respectively. Instead, when considering the W (SB) manifold, the dashed lines indicate the location of the tipping points destabilising the the SB (W) states. The bistable region is therefore located between the dashed and solid purple lines. As a result, a property of the system is that regardless of which combination of $[CO_2\ ]$ and S^* is used, the transition from one state to another always occurs at almost exactly the same temperature. This indicates that the climate system is insensitive to the mechanism of forcing. The position of the two boundaries can be parameterised in terms of S^* and CO_2 concentration as:

$$S^*_{sbw} = a_{sbw} \log_{10}[CO_2] + C_{sbw}, \quad S^*_{wsb} = a_{wsb} \log_{10}[CO_2] + C_{wsb} \tag{4.1}$$

where $a_{sbw} \approx a_{wsb} \approx -72$ Wm^{-2}, $C_{sbw} \approx 1629$ Wm^{-2} and $C_{wsb} \approx 1438$ Wm^{-2} for the transition SB→W and W→SB respectively and $[CO_2]$ is expressed in ppm. The size of the bistable region, which is defined as B, along S^* can therefore be defined by the difference between C_{sbw} and C_{wsb} :

$$B = C_{sbw} - C_{wsb}. \tag{4.2}$$

It is found that B is approximately 200 Wm^{-2}. The displacement between the position of the boundaries gives a precise measure of the hysteretic properties of the climate (Budyko [12], Lucarini et al. [77], Sellers [106], Voigt and Marotzke [119]) since it indicates the size of the overlap between the two manifolds in the CS plane. The presence of a bistable region implies that when the values of S^* and $[CO_2]$ are changed from an initial to a final value, the final steady state depends on the initial steady state and on the path of change of S^* and $[CO_2]$. Let us assume that we start from an initial point $(S^*_0, [CO_2]_0)$ in the bistable region and in the W state. Let us also assume we perform a close path of variation of S^* and $[CO_2]$ so that $S^*_0 = S^*_f$ and $[CO_2]_0 = [CO_2]_f$. If the path does not

cross S^*_{wsb} the final state will be identical to the initial one, that is, in a time-averaged sense:

$$T_s(S^*_0, [CO_2]_0) = T_s(S^*_f, [CO_2]_f). \tag{4.3}$$

On the other hand, if the closed path crosses the transition line to the second manifold, the final state will be different from the initial:

$$T_s(S^*_0, [CO_2]_0) \neq T_s(S^*_f, [CO_2]_f). \tag{4.4}$$

If, furthermore, the closed path crosses first S^*_{wsb} and then S^*_{sbw}, then again $T_S(S^*_0, [CO_2]_0) = T_S(S^*_f, [CO_2]_f)$, since the system has performed first a W→SB, and then a SB→W transition. The same applies starting from a SB state and exchanging SB with W in the previous discussion. This is true for any climate diagnostic. More specifically, in the case of T_s, for W→SB and SB→W transitions,

$$T_s(S^*_0, [CO_2]_0) > T_s(S^*_f, [CO_2]_f) \qquad \text{and} \qquad T_s(S^*_0, [CO_2]_0) < T_s(S^*_f, [CO_2]_f) \tag{4.5}$$

respectively. Note that for $S^* > 1440$ Wm^{-2}, even if CO_2 is 0 ppm, no transition to SB state can occur. Furthermore, it is important to underline that while it is reasonable to expect that some details of the characterisations of the phase portrait of the system given above may depend on this model and on its parameterisations, the qualitative features are expected to remain robust.

Fig. 4.4 show the reconstruction for the material entropy production, $\overline{\dot{S}_{mat}}$ for both manifolds in the CS space, computed directly as described in [31]. As with temperature, $\overline{\dot{S}_{mat}}$ increases monotonically with increasing S^* and $[CO_2]$ on both manifolds. In the SB state, the entropy is mostly generated by dissipation of kinetic energy and by irreversible sensible heat transport, because the planet is almost entirely dry. For the W manifold the main contribution to entropy production comes from latent heat due to large scale and convective precipitation . In the bistable region, the range of $\overline{\dot{S}_{mat}}$ is $(10, 19)$ 10^{-3}W m^{-2} K^{-1} and $(34, 62)$ 10^{-3}W m^{-2}K^{-1} for the SB and W respectively, therefore a factor of 3 larger in the W regime with respect to the SB regime. This confirms that $\overline{\dot{S}_{mat}}$ may be a better indicator than temperature for discriminating the SB and W states as already discussed in [77]. Again, there is a range of values of $\overline{\dot{S}_{mat}}$ – from 19 to 34 10^{-3}W m^{-2} K^{-1} – which is not allowed by the system.

In the bistable region, the SB and W states are quantitatively very different with respect to their physical properties. The two disjoint attractors can be thus thought of as representing two different worlds, with completely different dynamical and thermodynamical properties. For this reason in the following two sub-sections dynamical and thermodynamical properties of the manifolds will be analysed individually in terms of the vertical

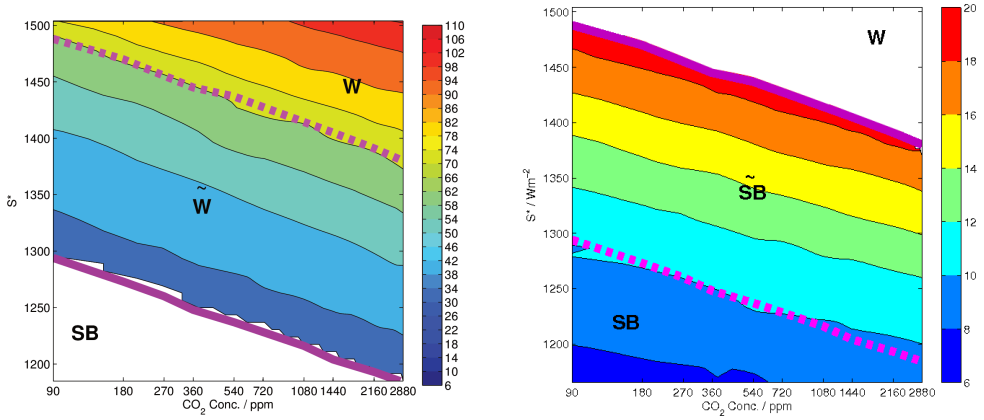

(A) (B)

FIGURE 4.4: Contour plot of $\overline{\dot{S}_{mat}}$ ($10^{-3}\mathrm{Wm}^{-2}\mathrm{K}^{-1}$) as a function of S^* and the [CO_2] for the lower SB (a) and upper W (b) manifolds.

and horizontal surface temperature differences, Carnot efficiency, MET and dissipation of kinetic energy. Furthermore, these properties shall be related to the average mean global temperature and the material entropy production. As is illustrated as solid and dashed purple lines, in the CS space figures, each manifold will be divided up in to two sub regions: W, W/Bistable, on the upper manifold and SB, SB/Bistable on the lower. Then, in a third sub-section, the transitions between the two manifolds occurring in bifurcations regions are analysed.

4.3.2 The warm state

The MET profile is calculated ([79, 94]) by integrating over latitudes, the longitudinally averaged TOA radiation budget as described in section 2.1.2. A scalar indicator of the transport is defined as half of the sum of the peak values of the poleward transport in both hemispheres, MET. In a moist atmosphere, the average global temperature and the meridional surface temperature difference, defined in this case as the difference between the mean surface temperature of the tropical (30S,30N) and the polar (90S,60S) and (60N,90N) regions (see Fig. 4.6a), are the main contributing factors for controlling the MET (see Fig. 4.5a). This is due to the fact that temperature controls the latent heat released in the atmosphere because of the Clausius-Clapeyron effect (Ambaum [3], Held and Soden [37]) and the meridional temperature gradient controls baroclinicity of the atmosphere (Stone [113]). Additionally, another modulating factor is the vertical stratification of the atmosphere, as conditions of low stratification in the midlatitudes support stronger baroclinic activity for a given meridional temperature gradient (Holton [41]). In the bistable region of the W state, the MET has a flat response to increasing S^* and $[CO_2]$ and is by and large independent of T_s, because of the two contrasting and compensating effects: With increased T_s, water vapour concentration of the atmosphere increases, thus leading to the strengthening of the poleward latent heat fluxes. In addition, the increased T_s causes sea and continental ice as well as seasonal snow cover to retreat towards the poles, thus lowering the surface albedo gradient. This contributes negatively to the changes in MET, because it leads to a decrease in the baroclinicity. This extends the results obtained by Caballero and Langen [13].

In the W regime, the boundary between the bistable and the monostable regime approximately marks the point at which the Earth surface loses its permanent sea-ice cover, thus supporting the idea that the presence of bistability is intimately linked with the powerful ice-albedo feedback. For T_s larger than approximately 300 K, the meridional temperature gradient decreases at a far slower rate with increasing T_s. This essentially means that in this region the MET is controlled only by the availability of water vapour in the atmosphere. Therefore at temperatures above 300K, the MET becomes decoupled from the surface meridional temperature difference. This analysis consequently shows how important the involvement of the hydrological cycle is in the magnitude of the MET and moreover, it indicates that when going from warm to very warm climates the hydrological cycle becomes the dominant climatic feature, leading to strong positive dependence of the MET on the surface temperature. These results agree with the findings of [13], who found in aqua planet simulations, that there is little scope for reducing the meridional temperature gradient further once the sea-ice and snow have melted. For

a constant meridional temperature gradient, an increase in the meridional latent heat fluxes with increasing global mean temperature was shown.

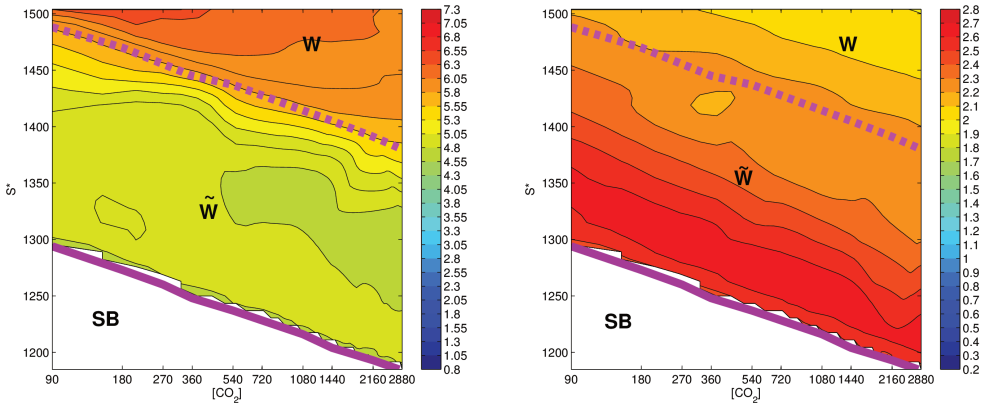

(A) (B)

FIGURE 4.5: Contour plot of: (a) meridional energy transport MET (PW, 1 PW= 10^{15} W) and (b) average rate of dissipation of kinetic energy $\overline{W}$ (W m^{-2}) as a function of S^* and the [CO_2] for the W states.

The conclusions drawn above find further support when looking at the mid-latitudes vertical temperature difference, ΔT_v, defined as the mean temperature difference between the surface and the 500 hPa level (see Fig. 4.6b) and which provides a rough measure of the stratification of the atmosphere in the baroclinically active region. The vertical temperature difference is largest along a band of the CS space centered half way through the bistable region in the direction of S^*. Our current climate conditions would appear to be positioned at the centre of the band peak where the verticle temperature difference is maximized, implying conditions of reduced vertical stratification. For climates colder than present, increasing surface temperature causes the melting of sea-ice and seasonal snow cover, so that the ensuing decrease in surface albedo (leading to increased surface absorption) accounts for the increasing vertical temperature difference. Instead, in climates colder than present, the decrease in equatorial vertical temperature difference with T_s can be understood in terms of increased moist convection from warmer surface temperatures, resulting in an increase of moisture fluxes to the upper atmosphere, which then condense and release latent heat.

In the bistable region, for the reasons discussed above, a pronounced weakening of the dynamics of the climate system with increasing surface temperature is expected to be found. This hypothesis is tested by computing the strength of the Lorenz energy cycle (Fig. 4.5b), which is equal to the average rate of dissipation of kinetic energy, and the Carnot efficiency of the system (Fig. 4.7), which measures, instead, how far from equilibrium the system is. The dissipation, similarly to the meridional temperature gradient, decreases monotonically with the surface temperature, and reaches its largest

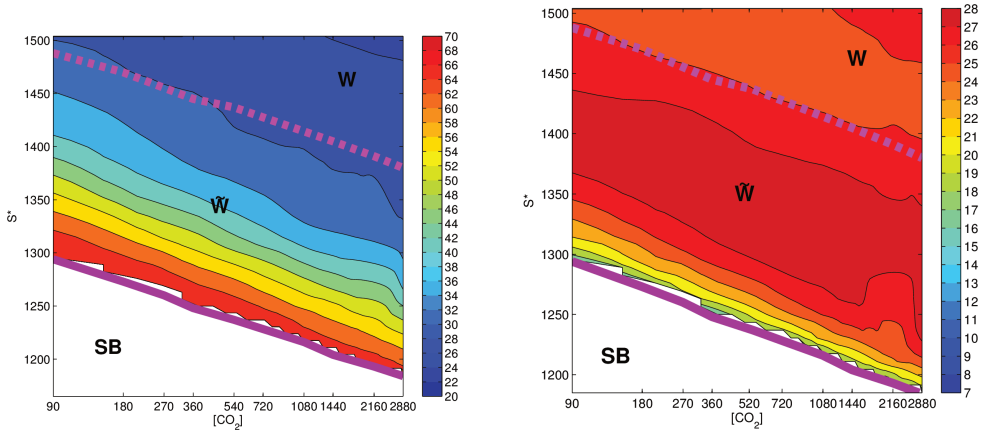

(A) (B)

FIGURE 4.6: Contour plot of: (a) meridional temperature gradient (K) and (b) mid-latitude vertical temperature difference (K) as a function of S^* and the [CO_2] for the W states.

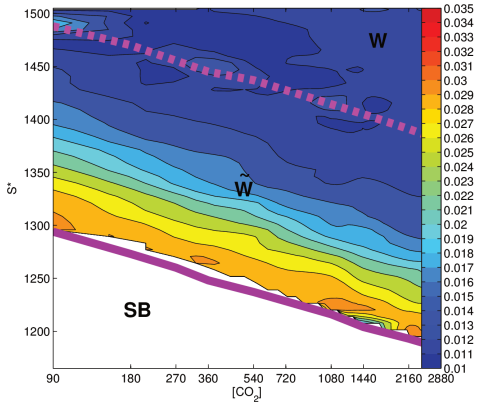

FIGURE 4.7: Contour plot of the efficiency as a function of S^* and the CO_2 concentration for the W states.

value just at the cold boundary of the W manifold. The work done by the climate is maximized along a band of climate states characterised by slightly higher temperatures. This region in the CS space lies about half way between the peak in the meridional and vertical temperature gradients, since a large value of work done by the climate, by its very definition, requires a compromise between maximizing these two gradients. The Carnot efficiency decreases monotonically with increasing CO_2 or S^*: warmer climates are characterised by smaller temperature differences, since the transport of water vapour acts as a very efficient means for homogenising the temperature across the system. The system has reduced ability to produce mechanical work and is characterised by very strong irreversible processes, as illustrated by the very large values of $\overline{\dot{S}_{mat}}$ realised in these conditions. Consequently the value of the parameter of irreversibility α increases

as conditions become warmer and warmer (not shown); see also 3.10.

4.3.3 The snowball state

The SB state is intrinsically simpler than the W state because the hydrological cycle has a negligible influence. This is due to the fact that atmospheric temperatures are so low that there is in all cases an almost dry atmosphere. As a result it is the case, e.g. that, as opposed to the W state, the parameter α is small (~ 1) and weakly dependent on the value of the parameter S^* and [CO_2] (not shown).

Moreover, in the SB state the meridional gradients (and not only the globally averaged values) of albedo are very low and depend weakly on S^* and the CO_2, because under all conditions the sea surface is frozen almost everywhere and the continents are covered by ice and snow. The MET (Figure 4.8a) is much smaller than for the corresponding W states, because in the SB state a large fraction of the radiation is reflected back to space and the meridional albedo gradients are small, so that the energy imbalance between low and high latitudes is small.

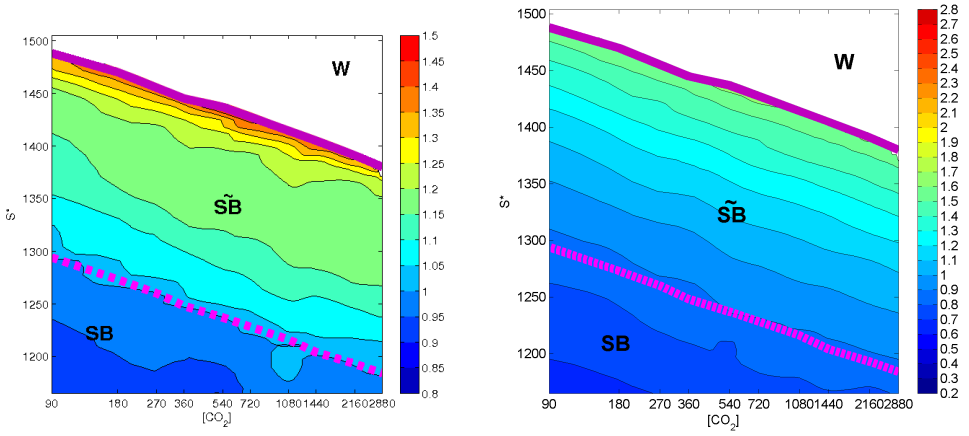

(A) (B)

FIGURE 4.8: Contour plot of: (a) meridional energy transport MET (PW) and (b) average rate of dissipation of kinetic energy (W m^{-2}) as a function of S^* and the [CO_2] for the SB states

Throughout the SB state, increases in S^* and [CO_2] , lead to an increase in T_s and $\overline{\dot{S}_{mat}}$. This is accompanied by increases in the MET and in the dissipation of kinetic energy (Fig. 4.8b), which implies that with increased MET the intensity of the circulation also increases. However it is found that the meridional temperature difference (not shown) has a very weak dependence on changing [CO_2] and S^*, as it varies by only 4 K across the explored parameter range. Therefore, the changes in the baroclinicity of the system which lead to changes in the MET and the intensity of the Lorenz energy cycle,

can not be due to changes in the meridional temperature difference. The lack of large variations in the meridional surface temperature profile are essentially due to the fact that the net input of shortwave radiation is kept almost fixed by the constant surface albedo and by the virtue of almost no cloud cover. The system therefore can be seen as rather rigid, as changes in the absorbed radiation are almost exactly compensated for by changes in the MET. The re-equilibration mechanism must then contain elements which are not present in the classic baroclinic adjustment [113]. It has been found that the vertical temperature gradient in the midlatitudes (Fig. 4.9b), increases substantially with increased value of S^* and $[CO_2]$, as an effect of the increased absorption of radiation near the surface. The reduced vertical stratification leads to more pronounced baroclinic activity even for a fixed meridional temperature gradient, thus leading to an increase in MET and in the intensity of the Lorenz energy cycle. The argument is in this case quite straightforward because the atmosphere being considered is almost dry. The efficiency has a dependence on S^* and $[CO_2]$ which, as in the W case, is intermediate between those of the meridional and vertical temperature gradient fields. In the case of the SB state, the main signature is given by the vertical gradient (Fig. 4.9b). This further reinforces the idea that the investigation of meridional temperature gradients is not enough to grasp the mechanisms through which the system generates available potential energy and material entropy production [79].

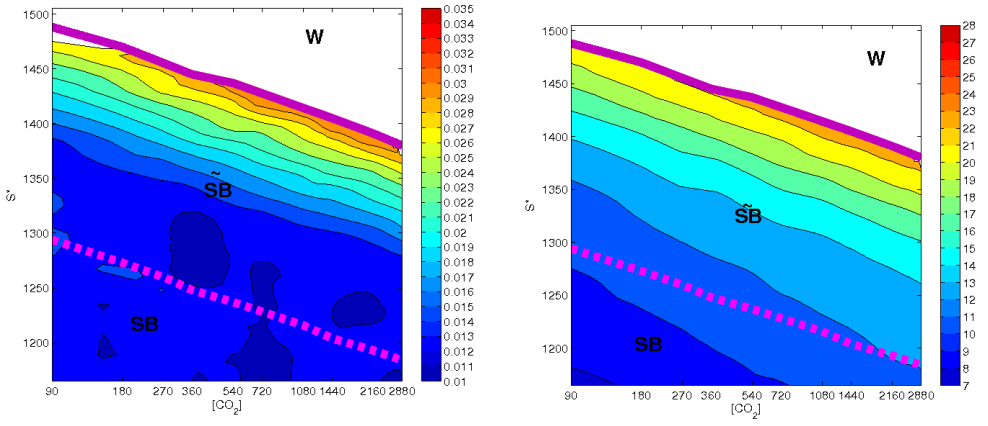

(A) (B)

FIGURE 4.9: Contour plot of (a) the Carnot efficiency η and (b) midlatitude vertical temperature difference (K) as a function of S^* and the $[CO_2]$ for the SB.

4.3.4 Transition and comparison between manifolds

Up to now, the W and SB states have been characterised as two entirely distinct climate regimes, and have underlined that the basic mechanisms of re-equilibration are rather different. Presented in this subsection, are some ideas aimed at making sense of the

transitions between the two states occurring when getting close to the boundaries of the upper and lower manifolds. As has been seen, the W→SB transition is associated with a large decrease in T_s, $\overline{\dot{S}_{mat}}$ and MET. This is intimately related to the fact that whereas in the W state the hydrological cycle plays a major role in the climate dynamics, in the SB state the hydrological cycle is almost absent. Nonetheless, this does not say much about the processes leading to the transition between the two states, or better, describing how one of the attractors disappears.

It has also been discovered here that the usual dynamical indicators of the atmospheric state, i.e. the meridional temperature gradient and the vertical stratification do not necessarily indicate whether or not the system is close to an irreversible transition of the system, e.g. by signalling something equivalent to a loss of elasticity of the system. In this regard, it is much more informative to observe how the efficiency behaves near the transitions. It is found, that as a general rule, each transition is associated to a notable decrease (more than 30%) of the efficiency of the system, and the closer the system gets to the transition in the CS space, the larger is the value of the efficiency. This can be interpreted as follows. If the system approaches a bifurcation point, its positive feedbacks become relatively strong and the negative feedbacks, which act as re-equilibrating mechanisms, become less efficient. As a result, the differential heating driving the climate is damped less effectively, and the system is further from equilibrium, since larger temperature differences are present. Therefore, the system produces more work, thus featuring an enhanced Lorenz energy cycle and a stronger circulation. At the bifurcation point, the positive feedbacks prevail and the circulation, even if rather strong, is not able to cope with the destabilising processes, and the transition to the other manifold is realised. The new state is, by definition, more stable, and thus closer to equilibrium. The decreased value of the efficiency is exactly the marker of this property. This confirms what has been proposed by [77] but in much greater generality and can be conjectured to be a rather general property of non-equilibrium systems featuring structural instabilities.

4.4 Conclusions

Motivated by the recent discoveries of extrasolar planets, a re-examination for the case of an Earth-like planet, being in the habitable zone is a sufficient condition for ensuring the presence of liquid water at the surface, has been performed. This has been done by considering the case of a planet with the same geography and topography of the present Earth and have performed an extensive parametric study by exploring the effect

of changing the solar irradiance and the atmospheric opacity (the latter modulated by the CO_2 concentration).

Within a rather wide parametric space, which includes the present conditions, the climate is multistable, i.e. there are two coexisting attractors, one characterised by warm conditions, where the presence of sea-ice and seasonal snow cover is limited (W state), and the other by a completely frozen sea surface, the so-called snowball (SB) state. These results, obtained using the climate model PlaSim, confirm and extend what has been obtained in various studies performed with models of various degrees of complexity. The reader is pointed to [99] and [77] for an extensive discussion. In this regard, the main improvement of this work is that a two dimensional parametric space is explored (whereas usually variations in the solar constant and atmospheric opacity are considered separately), which allows the gathering of more complete information on the possible states of the climate system and actual mechanisms relevant in a paleoclimaticological and planetary context. Since this exploration of the parametric space is limited and considering specific boundary conditions typical of our planet, this investigation is not fully comprehensive nor universal. Nonetheless, it is maintain that this study provides methodological hints and qualitative results of wide interest.

For all considered values of $[CO_2]$, which range from 90 to 2880 ppm, the width of the bistable region is about 200 Wm^{-2} in terms of the value of the solar constant, and its position depends linearly on the logarithm of the $[CO_2]$, being centered around smaller values of the solar constant for increasing opacity of the atmosphere, shifting by about 15 Wm^{-2} per doubling of CO_2 concentration. The W state is characterized by surface temperature being $40K - 60K$ higher than in the SB state. In terms of the material entropy production, it is larger by a factor of 4 (order of $40-60\ 10^{-3}\mathrm{Wm}^{-2}\mathrm{K}^{-1}$ vs. $10-15\ 10^{-3}\mathrm{Wm}^{-2}\mathrm{K}^{-1}$). The boundaries of the bistable region are approximately isolines of the globally averaged surface temperature, and in particular, the warm boundary, beyond which the SB state cannot be realized, is characterized by the vanishing of the permanent sea-ice cover in the W regime. This reinforces the idea that the ice-albedo feedback is the dominant mechanism necessary for obtaining the multistability properties of the climate system.

The thermodynamical and dynamical properties of the two states are largely different, as if two entirely different planets were being discussed. In the W state the climate is dominated by the hydrological cycle and latent heat fluxes are prominent in terms of redistributing energy in the system and as the main contributor to the material entropy production. The SB state is an extremely dry climate, where heat transport is realized through sensible heat fluxes and entropy is mostly generated through the dissipation

of the kinetic energy. The dryness of the SB atmospheric states also explain why the climate sensitivity is much smaller.

In the bistable region of the W states, the MET is rather constant, as the contrasting effect of the increasing latent heat fluxes driven by increasing surface temperature, coupled with the reduction in the baroclinicity due to the decrease in the meridional temperature gradient compensate almost exactly. In the W state beyond the bistable region, the MET increases quite dramatically with the surface temperature (Fig. 4.6a and 5.5) since the compensating albedo mechanisms are shut off as sea-ice is completely removed from the surface. In the SB states, increased incoming radiation or increased $[CO_2]$ leads to increases in the MET. In this case, the water vapour plays little part, and, somewhat surprisingly, the meridional temperature difference has also a rather flat response to the parametric modulation. In this case, the dominant mechanism determining the properties of the MET is the change in the vertical stratification, which becomes weaker for warmer climate conditions because the atmosphere is more strongly heated from below. This implies that the atmospheric circulation strengthens for increasing values of the solar constant and of $[CO_2]$. In fact, the Lorenz energy cycle becomes stronger for warmer climate conditions, and the Carnot-like efficiency of the climate system has an analogous behaviour. The opposite holds for the W state, where the intensity of the Lorenz energy cycle and the efficiency decreases for warmer conditions, the reason being that the water vapour becomes more and more efficient in homogenizing the system and destroying its ability to generate available potential energy.

A general property which has been found is that, in both regimes, the efficiency increases when getting close to the bifurcation point and at the bifurcation point the transition to the newly realized stationary state is accompanied by a large decrease in the efficiency. This can be framed in a rather general thermodynamical context: the efficiency gives a measure of how far from equilibrium the system is. The negative feedbacks tend to counteract the differential heating due to the sun's insolation pattern, thus leading the system closer to equilibrium. At the bifurcation point, the negative feedbacks are overcame by the positive feedbacks, so that the system makes a global transition to a new state, where, in turn, the negative feedbacks are more efficient in stabilizing the system. On a more phenomenological note, the transition from the W to SB states occurs at a critical value of the sea-ice fraction of about 0.5. This agrees with previous findings Voigt and Marotzke [119]. After the transitions, the sea-ice fraction becomes unitary. When considering the reverse tipping point, the transition is even more dramatic as the sea-ice fraction changes abruptly from unity to virtually zero.

Chapter 5

Some Empirical Laws for Planetary Thermodynamics

[1]

5.1 Introduction

5.1.1 Planetary atmospheres and extrasolar planets

A very active field of research in astrophysical sciences at the moment, is the observational, model-assisted, and theoretical investigation of extra-solar planetary objects. In less than two decades, the development of new instruments have lead to the detection of the first extra-solar planet in the mid 90s to more refined observations of the characteristic properties of several hundred planetary bodies. The properties of planets vary greatly, in terms of their compositions - gaseous or rocky -, nature of their atmosphere, and of their size - ranging in several orders of magnitude. Astronomical and astrophysical factors of great relevance include the temperature and the intensity of the radiation emitted by the parent star, the orbital parameters, and whether or not the planet is tidally locked. A great deal of effort has been directed at constraining the combinations of physical configurations potentially compatible with life (habitable zone) , that is to say with the possibility of observing water, either prominently or at least partially in liquid form at the surface. Obviously, the so-called habitable zone is the setting where we hope to find forms of extraterrestrial life, or at least life analogous to that found on Earth. Recently, ESOs HARPS planet finder estimated that just in the Milky Way

[1] **Boschi R.**, V. Lucarini, S. Pascale, 2013. *"Bistability of the climate around the habitable zone: a thermodynamic investigation"*, Icarus 226, 1724-1742.

billions of habitable Earth-like rocky planets could orbit around faint red dwarfs, with in the order of one hundred being in the immediate vicinity of our Solar system (Bonfils et al. [7]). The reader is refered to the website (http://exoplanet.eu/index.php) – which is dedicated to collecting information on all newly discovered planets and on the related bibliography – and recently published books [22, 47, 95, 103].

A great deal of interest is now being paid to the inference, study, and modeling of planetary atmospheres, i.e., in the case of rocky planets "Super-Earths"), the fluid envelope that surrounds the planet and its response to the differential heating due to the absorption of incoming solar radiation. Planetary atmospheres may feature complex chemical compositions and be characterised by the relevant presence of phase transitions of some of these components, which may have large effects on the radiative properties. The geometry describing how the planet and its parent star face each other, determines to a first approximation the horizontal inhomogeneities, whereas the atmospheric optical properties, and in particular its opacity to the incoming radiation, has an effect on the vertical structure (e.g. Earth's optically thin atmosphere is typically heated from the planets surface). The general circulation of the planetary atmosphere is powered, just like a Carnot engine by such inhomogeneities with, on average, heating occurring in regions of higher temperatures before being then removed in cooler areas. The circulation acts to reduce the temperature gradients through transport processes, and on average the generation of kinetic energy is compensated for by irreversible viscous dissipation processes. Irreversible heat transport and dissipation, as well as, processes such as radiative absorption and emission contribute to the generation of entropy. The steady state is realised by balancing energy and entropy fluxes between the planetary atmosphere and the surrounding space. Various aspects of this closed chain of interdependent processes have been described for terrestrial conditions [45, 72, 75, 79, 94], but the theoretical framework proposed in these contributions could be applied with more generality to planetary atmospheres.

The awareness of recent findings in planetary astronomy and astrophysics are gradually filtering through to the classical geophysical sciences (by definition Earth-centred). The study of, e.g. the general circulation of Jupiter, Venus and Mars has a rather old history, but with the recent and foreseeable future discoveries of exoplanets, the opportunity of facing a vast array of planetary configurations, mean moving from considering special cases of climates, to being able to study a quasi-continuous distribution in some parametric space. Following [102], one should note that it is possible to reduce the variety of climate settings by adopting the fluid-dynamical classical method of similarity, i.e. by defining a set of dimensionless numbers that fully characterise the climate state. When two climate states share the same set of dimensionless numbers, they are dynamically equivalent, so that the statistical properties of one can be mapped into those of the other

with simple algebraic operations. At this stage, there are two additional elements left to be dealt with:

- how to characterise succinctly a climatic state, conveying minimal but comprehensive physical information for planetary atmospheres which are, in general, turbulent fluids with variability on a very vast range of spatial and temporal scales?
- how to verify, or at least approximate, the validity of our simulations and of our theoretical understanding of planetary circulations that we are able to model?

The two items are closely related to the definition of robust observables. Energy conservation imposes that the incoming radiation onto a planet is instantaneously equal to the sum of the radiation that is absorbed and scattered by the planet. Assuming steady state, when averaging over a sufficiently long time interval, the radiation absorbed by the planet is equal to the radiation the planet emits out to space (assuming that the planet has no internal energy sources). These quantities allow defining the average albedo and the effective thermodynamic temperature, which constitute the most fundamental description of the properties of a planet, in terms of the first law of thermodynamics. As recorded by a telescope, observations made of a planet represented by a single pixel, provides a sufficient level of detail to gather such information. It is then possible for the overall macroscopic properties of the planets atmosphere to be found. Obviously, most observations provide much more than this, such as the emission spectrum of a planet (and that of the star in orbits). Moreover, spectral windows may prove useful for measuring its surface temperature. Nevertheless, in terms of the macroscopic thermodynamic properties of the planet, the spectrally integrated quantities are the most relevant.

Moreover, empirical functions are proposed which express the global non-equilibrium thermodynamical properties of the system in terms of either the mean surface temperature or the mean planetary emission temperature. This is indeed promising, because it suggests the possibility of expressing thermodynamic properties which are very hard to observe experimentally, as functions of quantities which can be measured.

In Section 5.2 parameterisations of the main non-equilibrium properties of the system as a function of the mean surface temperature or emission temperature are proposed. Further to this, in Section 5.3 the effect of reducing the rotation rate of the planet by a factor of 2 is discussed, and in Section 4.4 the conclusions are presented.

5.2 Results

In the previous chapter, a systematic investigation of the thermodynamical properties of the planet in the SB and W states has been presented, obtained by exploring the CS parametric space. What makes this work more general than what has preceed it, such as those discussed in Chapter 3, is the fact that here the system is forced by two distict different sources: S^*, which controls the energy entering the planetary system and the $[CO_2]$, which inhibits the release of energy from it. Despite this as mentioned above, in many cases the main quantity controlling the thermodynamic properties is only the average surface temperature, T_s. This statement can be substantiated by looking at Figs. 4.3-4.9 and observing that in most cases the isolines of the depicted thermodynamic quantities are approximately parallel, both in the W and SB state, to the isolines of T_s. This suggests the possibility of establishing approximate empirical laws of the form $\Gamma_{SB}(S^*, [CO_2]) \approx \Gamma_{SB}(T_s(S^*, [CO_2]))$ and $\Gamma_W(S^*, [CO_2]) \approx \Gamma_W(T_s(S^*, [CO_2]))$, where Γ is a thermodynamical property such as, e.g. entropy production, and the lower index refers to whether we are in the SB or W state. For a given Γ, the empirical laws will be in general different in the SB vs the W state. This result is quite interesting in a classical perspective of climate dynamics, where it is customary to parameterise large scale climate properties as a function of the surface temperature, especially when constructing simple yet meaningful models [104].

This approach is complemented by testing whether it is possible to construct empirical laws expressing the thermodynamical properties of the system as a function of its emission temperature $T_E = (LW_{TOA}/\sigma)^{1/4}$ – where LW_{TOA} is the area- and time-averaged outgoing long wave radiation at the top of the atmosphere and σ the Stefan-Boltzmann constant – , which is a quantity of more readily astrophysical interest and more fundamental physical significance. Therefore, the goal is to be able to observe well-defined functions of the form $\Gamma_{SB}(S^*, [CO_2]) \approx \Gamma_{SB}(T_E(S^*, [CO_2]))$ and $\Gamma_W(S^*, [CO_2]) \approx \Gamma_W(T_E(S^*, [CO_2]))$, which, given the observation made above, requires also the existence of an approximate relationship $T_E \approx T_E(T_s)$.

Indeed, Fig. 5.1 shows that it is possible to observe an empirical, monotonic relationship between T_s and T_E in a vast range of climate states, including both the W and SB states. Obviously, the correspondence between the two variables is not perfect, so that for each value of T_s it is possible to have climates featuring a range of values of T_E, and vice versa. The spread associated with the ensemble points is of order 10 K and 5 K for T_E, and 20 K and 10 K for T_s, in the W and SB states respectively. A range of values of T_E $(230 - 240$ K) and T_s $(240 - 260$ K) are not permitted by the system as a result of the ice-albedo instability. We can now proceed to see to which extent the quantities T_s and T_E can be used as a good predictor of the thermodynamic properties of the planet and

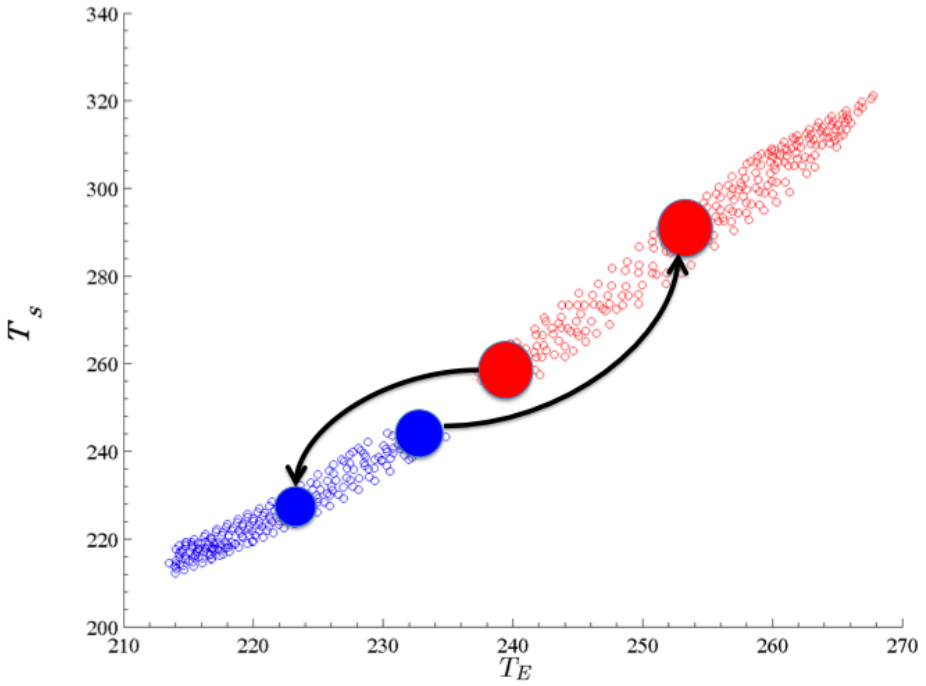

FIGURE 5.1: Surface temperature T_s (K) versus emission temperature T_E (K) for the W and SB states (each circle represents a simulation). The transitions have been marked $W \rightarrow SB$ (red dot – arrow – blue dot) and $SB \rightarrow W$ (blue dot – arrow – red dot). Same convention is used in Figs. 5.2-5.5

compare their skill with T_s. The following description is, on purpose, purely qualitative, because the goal is to show to what extent T_E and T_s can be used as predictors, rather than discussing in detail what are the appropriate transfer functions.

Fig. 5.2 shows that a clear monotonic relationship exists between T_E, T_s and the material entropy production $\overline{\dot{S}_{mat}}$, with higher values of T_E and T_s associated with larger values of $\overline{\dot{S}_{mat}}$. It is important to note that while the values of $\overline{\dot{S}_{mat}}$ and T_s are related to a high degree of accuracy, while, the functional dependence between T_E and $\overline{\dot{S}_{mat}}$ is less well defined (the spread of points is much wider than in the T_s case, and especially so in the very warm regimes). Note also that the dependences, while monotonic in both cases, are very different between the W and SB states. The consensus is that the greater the energy absorbed by the planet (larger values of T_E), the more intense is the production of material entropy. Note that this is indeed not the case when considering the intensity of the Lorenz energy cycle (Fig. 5.3): higher absorption of energy corresponds to a weaker energy cycle in the W state and to a stronger cycle in the SB state. Therefore, the increase in the entropy production with T_E is due, in the SB case, to the increased dissipation of kinetic energy, while in the W state it is due to the greatly enhanced hydrological cycle. In agreement with what has been discussed in the previous section,

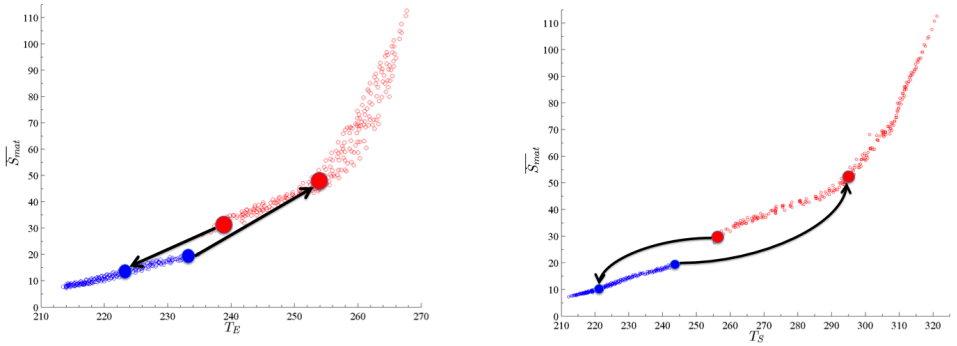

(A) (B)

FIGURE 5.2: Material entropy production $\overline{\dot{S}_{mat}}$ (10^{-3}W m^{-2} K^{-1}) *vs.* (a) emission temperature T_E (K) and (b) surface temperature T_s (K).

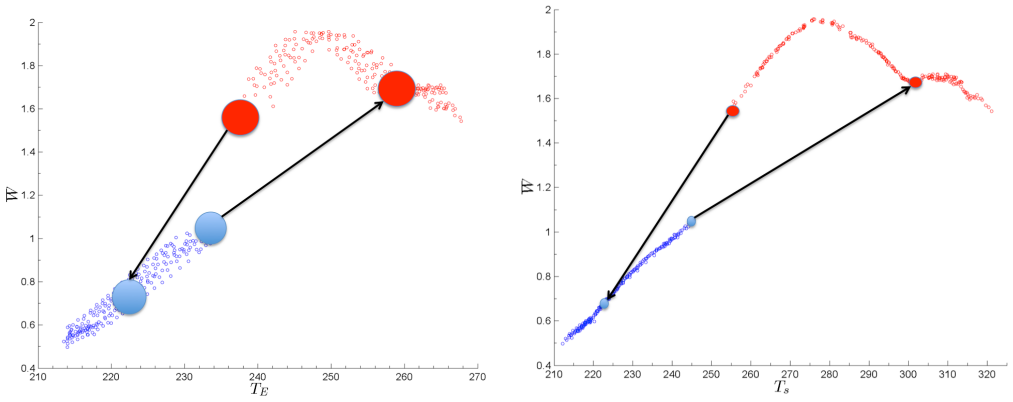

(A) (B)

FIGURE 5.3: Lorenz Energy cycle strength $\overline{W}$ (W m^{-2}) *vs.* (a) emission temperature T_E (K) and (b) surface temperature T_s (K).

one can explain the contrasting responses of the W and SB states to increases in the absorption of energy by analyzing the Carnot efficiency of the planetary fluid (Fig. 5.4).

It is interesting to note that, at the transitions, the values of the efficiency are almost equal: $\eta_{W\rightarrow SB} \approx \eta_{SB,W} \approx 0.03$. Moreover, it is observed that η saturates in the very cold regime of SB states and very warm regime of W (see Fig. 5.4) at $\eta_{sat,W} \approx \eta_{sat,SB} \approx 0.012$. Also note, that as with $\overline{\dot{S}_{mat}}$, T_s does a better job than T_E, as a predictor of the other thermodynamic quantities considered here i.e. the Lorenz energy cycle and efficiency, since the spread of points is much narrower.

Now, the link between T_E, T_s and MET (Fig. 5.5) is discussed. It is observed that in the SB regime there is a weakly positive relationship between T_E (T_s) and the transport, for the reasons described in the previous section. Instead, for a vast range of values of T_E (T_s) in the W regime, the transport is almost insensitive to T_E (T_s), as discussed

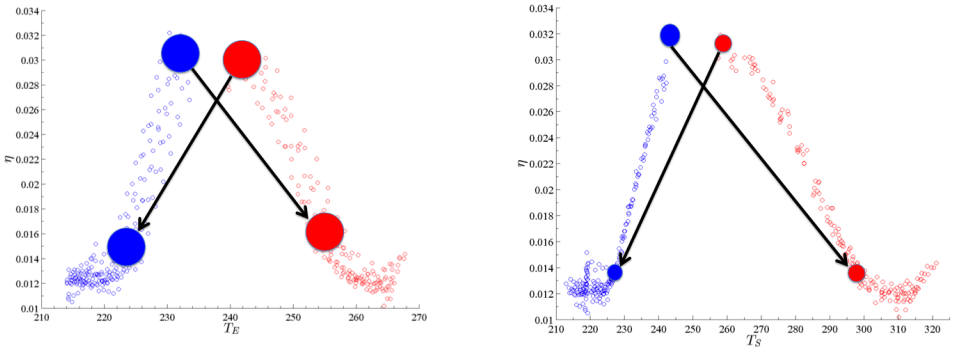

(A) (B)

FIGURE 5.4: Carnot efficiency η *vs.* (a) emission temperature T_E (K) and (b) surface temperature $T_s(K)$.

thoroughly in [13] and [20, 21]. The rigidity of the climate system has been attributed by [20, 21] to the fact that the MET is mainly determined by planetary albedo and thus atmospheric composition rather that surface albedo and sea-ice coverage. However, such a mechanism ceases to exist when the ice albedo feedback becomes ineffective because of the disappearance of sea-ice above a threshold value of $T_E \approx 255$ K ($T_s \approx 300$ K). Above this value, a steep monotonic increase of the transport with temperature is observed, because changes in the latent heat transport are mainly responsible for this behaviour. This agrees with the idea that the dynamics and sensitivity of a warm planet is, in some sense, dominated by the hydrological cycle. In this latter case, the skill of the two temperature quantities in parameterising the MET is comparable. Indeed, the details of the transfer functions will depend on various specific properties of the planetary system under investigation. The focus here is on the fact that these results suggest that it is possible to define such empirical relations. Finally, Fig. 5.6 describes how the sea-ice fraction can be parameterised as a function of the surface and emission temperature. As is seen, the surface temperature is an almost exact predictor of the sea-ice fraction, whereas the emission temperature provides a noisier signal, especially in the W states. It is interesting to note that transition from the W to SB states occurs at a critical value of the sea-ice fraction of about 0.5, in broad agreement with previous results by [120]. The freezing of the planet leads to the sea-ice fraction tending to unity, whereas the reverse SB→W transition has an even more dramatic change, because it goes from a completely frozen to a virtually ice free ocean. This elucidates even more so, the strength of the ice-albedo feedback.

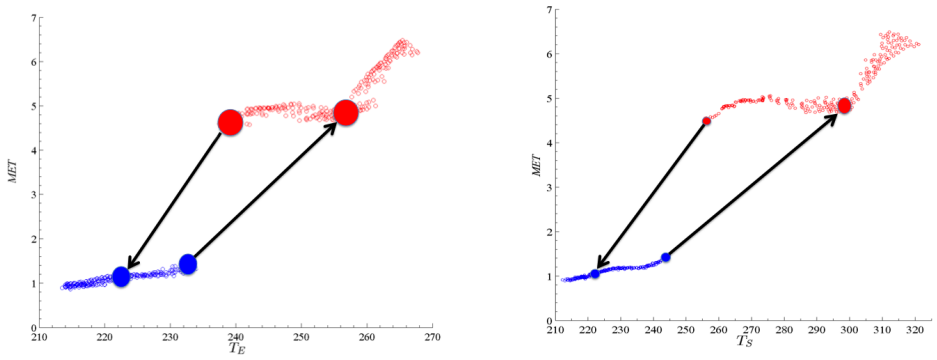

(A) (B)

FIGURE 5.5: Meridional enthalpy transport index MET (in PW) *vs.* (a) emission temperature T_E (K) and (b) surface temperature T_s (K).

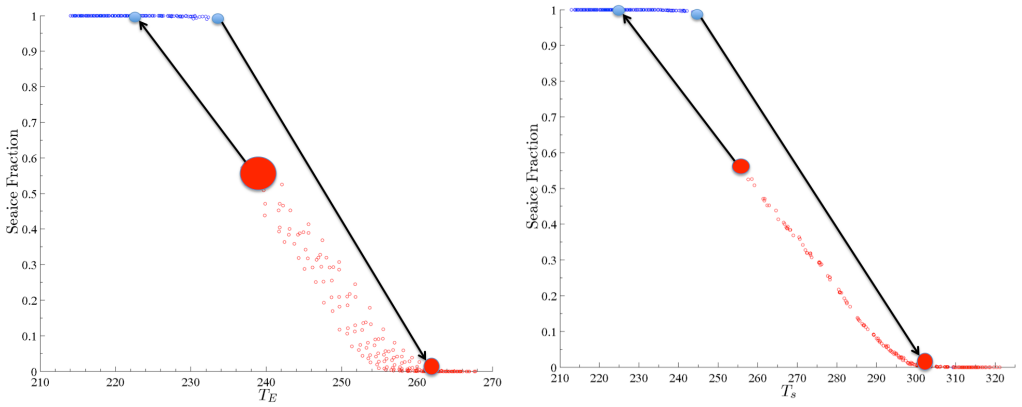

(A) (B)

FIGURE 5.6: Sea ice fraction (in %) *vs.* (a) emission temperature T_E (K) and (b) surface temperature T_s (K).

5.3 Thermodynamics of a slowly rotating planet

Figs 5.2-5.6 clearly define the transfer functions allowing to compute the thermodynamic properties of the planet from the value of T_E or T_s only. This is definitely intriguing because it paves the way for computing non-equilibrium properties from a quantity describing the zero-order radiation balance of the system at the top of the atmosphere and of the radiative-convective equilibrium at surface (in the case of T_s). Figures (5.2-5.6) leave various open questions which definitely need to be accurately addressed in future studies: i) why is it possible to use to a good degree of approximation the quantity T_E to parameterise the non-equilibrium thermodynamical properties of a system? ii) why does the surface temperature do an even better job (actually, astounding) in controlling such complex properties? iii) is the result where the efficiency is found to decrease at the bifurcation points for both W→SB and SB→W, a transition of more general relevance?

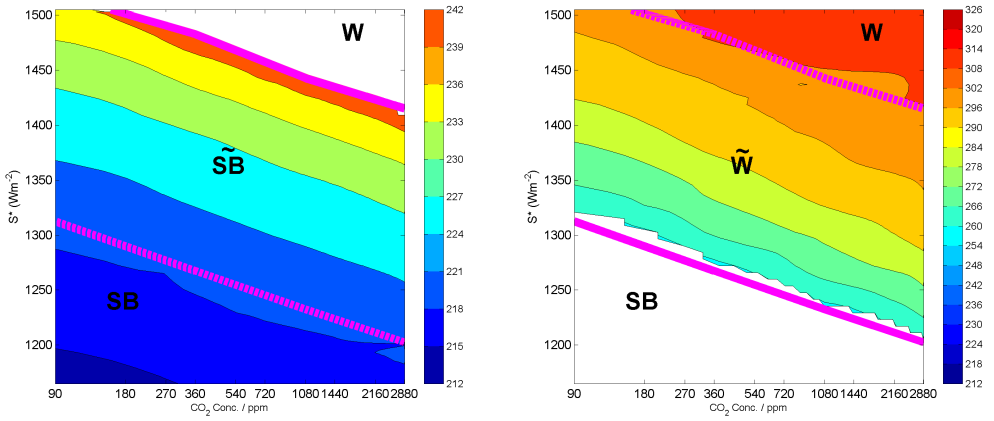

(A) (B)

FIGURE 5.7: Contour plot of $\overline{T_S}$ (K) as a function of S^* and the $[CO_2]$ for the lower SB (a) and upper W (b) manifolds for the slowly rotating planet.

The results presented in the previous sections are indeed not universal because they have been obtained making specific choices on some crucial ingredients such as the position and size of the continents, the radius of the planet, the eccentricity of its orbit, the orbital tilt and its rotation rate, among others. Obviously, it is virtually impossible to explore such a vast multidimensional parametric space, and one must come to terms with the fact that only partial explorations are possible (and future investigations will deal with different axes of such parametric space). A small step is taken in this direction by testing the sensitivity of these results with respect to changes in the planetary rotation rate Ω. In particular, investigated here is the case where Ω is reduced by a factor of 2. As well known from dynamical meteorology, reducing the rotation rate *ceteris paribus* implies that the mid-latitude flow is more weakly constrained to being in the vicinity of geostrophic equilibrium, because the Rossby number is increased. Baroclinic instability is weakened because the Rossby deformation radius is increased, and, the meridional extent of the Hadley cell increases because angular momentum conservation constraints become less stringent. This causes a dramatic readjustment between the key mechanisms of poleward atmospheric transport and of the transformation of available into kinetic energy. Therefore, some of the experiments described before have been repeated but with a lower value of the rotation rate. In particular, the $[CO_2]$ values of 90,360,1080 and 2880 have been considered, while S* has been modulated between 1510 Wm^{-2} and 1150 Wm^{-2} in steps of 30 Wm^{-2}.

First, it is also noted that for such a lower value of Ω the system features bistability, and the overall structure of the phase space is only modestly altered. The W→SB and S→BW boundaries described above are still approximately parallel straight lines in the (S*, log$[CO_2]$) plane, but both shifted to the right with respect to what was found

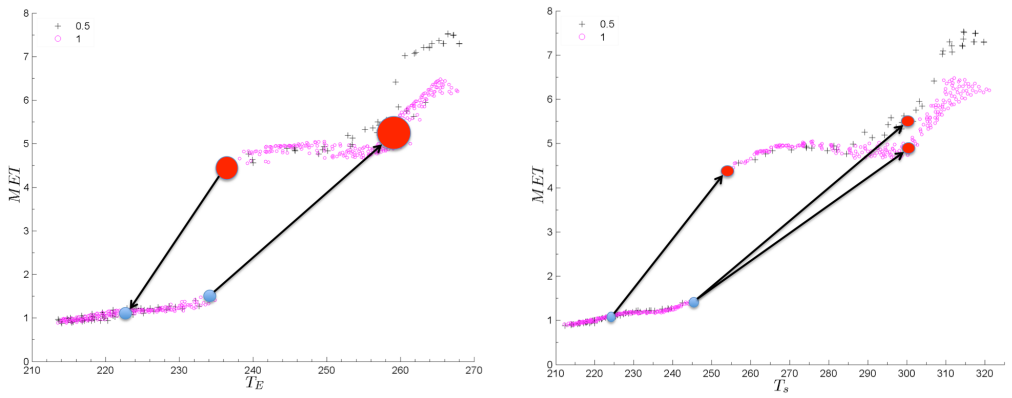

(A) (B)

FIGURE 5.8: Meridional enthalpy transport index MET (in PW) *vs.* (a) emission temperature T_E (K) and (b) surface temperature T_s (K) for $\Omega/\Omega_E = 1$ (magenta) and $\Omega/\Omega_E = 0.5$ (black).

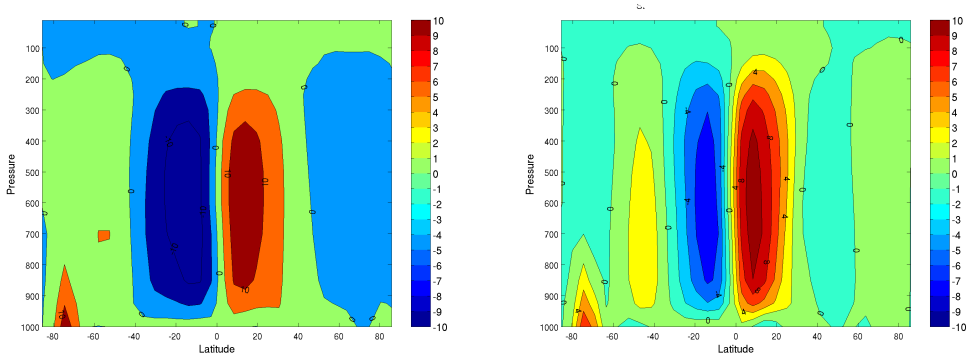

(A) (B)

FIGURE 5.9: Zonal mean streamfunction profile for: (a) $\Omega/\Omega_E = 0.5$ and (b) $\Omega/\Omega_E = 1$. Solar constant and CO_2 concentration set to present terrestrial level.

previously. More specifically, the lines are shifted towards higher values of $[CO_2]$ and S^* of 50 ppm or 5 W m^{-2} respectively. Interestingly, the S→BW and W→SB transition lines are also in this case closely aligned along isolines of the surface temperature, and with approximately the same value observed for the regular rotation rate. This is reported in Figs 5.7.

Now, the extent to which the results shown in Figs 5.2-5.6a can be replicated is explored. The first notable observation is that for a slowly rotating planet, non-equilibrium thermodynamical variables like η, $\overline{\dot{S}_{mat}}$ and MET can still be expressed to a high degree of accuracy as functions of T_S or T_E. The second aspect is that the empirical laws that are found in this case are analogous to what were found for the terrestrial value of Ω.

In particular, the reults show the empirical parameterisations of MET is virtually identical for both cases (Fig. 5.8), even if corresponding climate states for different values

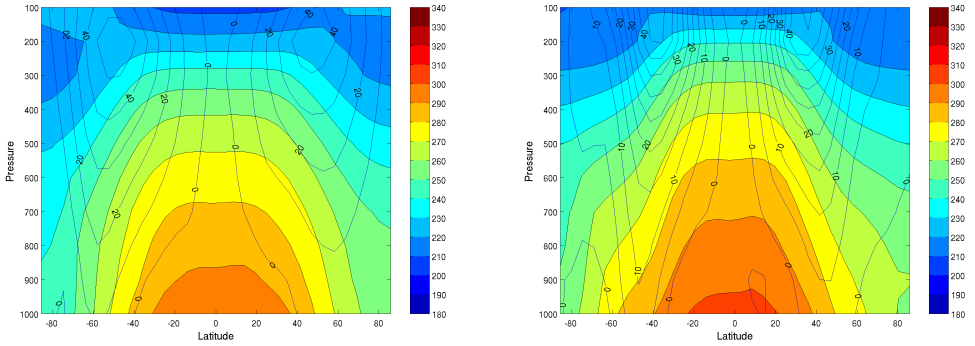

(A) (B)

FIGURE 5.10: Zonal mean distribution of westerly winds (ms^{-1}) and atmospheric temperature for: (a) $\Omega/\Omega_E = 0.5$ and (b) $\Omega/\Omega_E = 1$. Solar constant and CO_2 concentration set to present terrestrial level.

of Ω are very different. In general it is observe that in the case of weaker rotation, the meridional streamfunction extends further polewards and similarly the jet stream is shifted polewards, as expected (see Figs 5.9 and 5.10). The system with faster rotation features stronger eddy heat transports, as its mid-latitude dynamics are dominated more so by baroclinic conversion. Despite these relevant differences, within this range of rotation rates the total MET is not highly sensitive to the specific mechanisms of transport.

An even more fundamental indication of the robustness of the thermodynamic parameterisations proposed above is that the functional dependence of $\overline{\dot{S}_{mat}}$ with respect to T_s is almost unchanged when considering the slower rotation case (Fig. 5.11), both in the SB and W regimes. Therefore, the global effect of the irreversible processes, is not highly sensitive to the specific dynamical features determining mixing and dissipation throughout the domain. Moreover, the other basic measure of the non-equilibrium properties of the system, i.e. the efficiency η, has a very weak dependence on the rotation rate, as shown in Fig. 5.12. Finally, the Lorenz energy cycle (Fig. 5.13) also behaves similarly in both cases, though the intensity of the more slowly rotating planet is biased low, as the atmospheric features have in this case larger spacial scales and therefore undergo weaker viscous dissipation. Finally, it is observed that the sea-ice fraction is also weakly influenced by the slower rotation rate (Fig. 5.14).

These results are encouraging as they suggest that the empirically derived functional relations between thermodynamic quantities and averaged temperatures are reasonably robust with respect to reductions in the rotation rate. While no strong degree of universality is claimed by these results, such robustness hints at the fact that this proposed approach has some degree of generality.

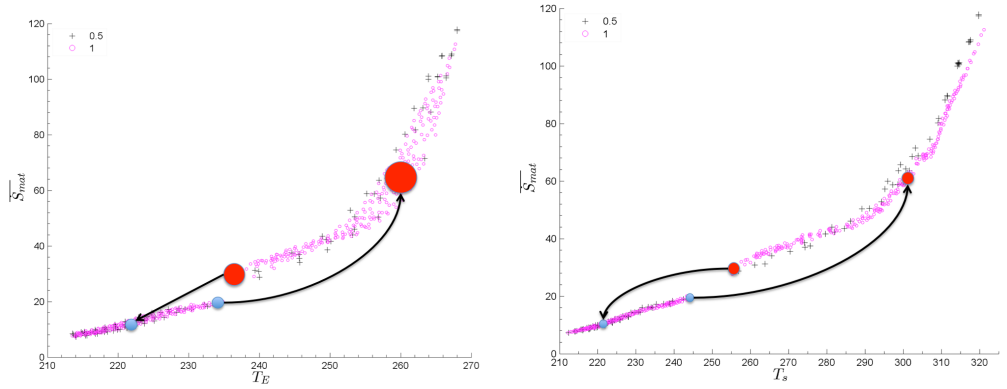

(A) (B)

FIGURE 5.11: Material entropy production $\overline{\dot{S}_{mat}}$ (10^{-3}W m^{-2} K^{-1}) *vs.* (a) emission temperature T_E (K) and (b) surface temperature T_s (K) for $\Omega/\Omega_E = 1$ (magenta) and $\Omega/\Omega_E = 0.5$ (black).

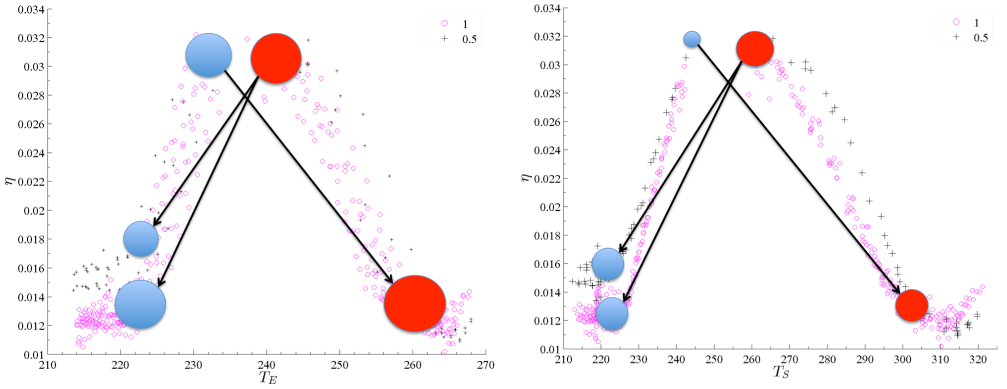

(A) (B)

FIGURE 5.12: Carnot efficiency η *vs.* (a) emission temperature T_E (K) and (b) surface temperature T_s (K) for $\Omega/\Omega_E = 1$ (magenta) and $\Omega/\Omega_E = 0.5$ (black).

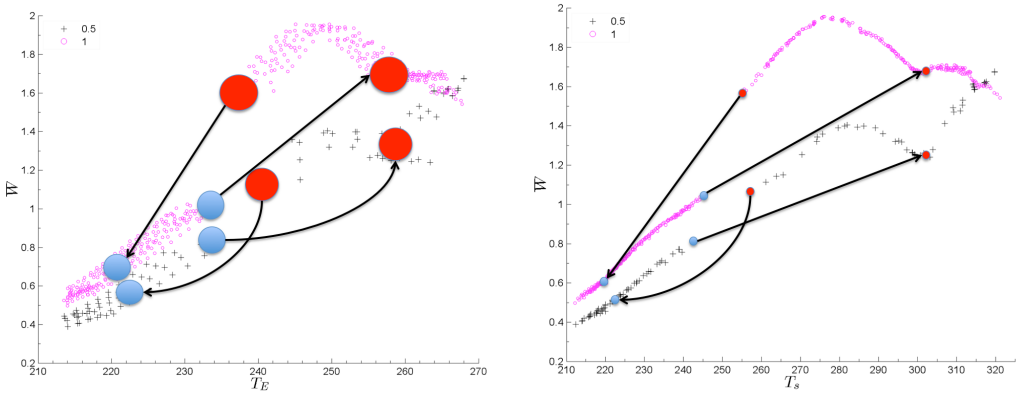

(A) (B)

FIGURE 5.13: Lorenz energy cycle strength $\overline{W}$ (W m^{-2}) *vs.* (a) emission temperature T_E (K) and (b) surface temperature T_s (K) for $\Omega/\Omega_E = 1$ (magenta) and $\Omega/\Omega_E = 0.5$ (black).

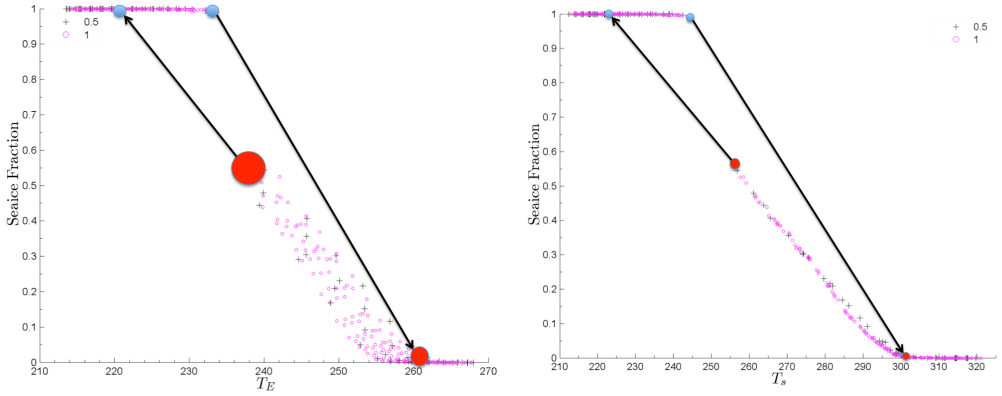

(A) (B)

FIGURE 5.14: Sea ice fraction (in %) *vs.* (a) emission temperature T_E (K) and (b) surface temperature T_s (K) for $\Omega/\Omega_E = 1$ (magenta) and $\Omega/\Omega_E = 0.5$ (black).

5.4 Conclusions

Recent theoretical results suggest that it is possible to derive up to a good degree of approximation the full thermodynamical properties of planetary atmospheres from the coarse observations of radiative fluxes at the TOA and surface [79]. This work has pursued this line of research and has been done by projecting the results obtained in exploring a 2D parametric space onto a single variable, thus constructing approximate parametrisations It has been found that the surface temperature and the emission temperature provide fairly good predictors of thermodynamic quantities representing the out-of-equilibrium characterisation of the system. In some sense, such parameterisations provide an equation of state of the system.

The results discussed in this chapter support the adoption of new diagnostic tools based on non-equilibrium thermodynamics for analysing the fundamental properties of planetary atmospheres. The results of this thesis do not claim in any sense to be universal. However, the results support the fact that such parameterisations are in principle possible. In order to modestly expand the scope of this chapter, it has been investigated how these findings change when considering a slower rotation rate. Nonetheless, all of these approximate relations are only very weakly affected by such a radical change to the system. This is far from being a conclusive proof of universality, but does indeed show a degree of robustness for these results.

The reasons why these parameterisations work so well, and why this is especially the case for globally averaged surface temperature definitely require further investigations. These results reinforce the relevance of the globally averaged surface temperature as a meaningful thermodynamical quantity of the climate system, beyond its obvious practical importance. Moreover, they pave the way for the possibility of practically deducing

fundamental properties of planets in the habitable zone from relatively simple observables. Future investigations will analyse more systematically how robust these findings are with respect to changes in relevant orbital parameters.

Chapter 6

Conclusion

The experiments performed in chapters 4 and 5 are now summarized. The overall conclusions drawn from the results of both chapters are then brought together and discussed. This is followed by further discussion on the outlook and possible outcomes of future research which could be performed to expand the scope of this work.

6.1 Summary and Discussion

Motivated by paleoclimatic evidence and the recent discoveries of a large number of exoplanets, this thesis has set out to extend our understanding of the multistability properties of the climate system in a more generalised setting than has previously been achieved. The work presented here highlights the possibility of using global thermodynamic properties, namely, the peak in the poleward meridional enthalpy transport (MET), emission temperature (T_E), material entropy production ($\overline{\dot{S}_{mat}}$), Lorenz energy cycle strength (as the work done by the system, $\overline{W}$) and the Carnot efficiency (η), as a tool to better understand multistability and sensitivity of the climate system. To this end, the general circulation model PlaSim was employed to simulate the climates for a wide array of steady states. The solar constant (S^*) was modulated at regular intervals of 15 Wm^{-2} between 1150 Wm^{-2} and 1510Wm^{-2}, for 10 different values of the CO_2 concentration, [CO_2],ranging from 90ppm to 2880ppm. Within 10 Wm^{-2} of a transition point, intervals of 1 Wm^{-2} were used. This data has been used to produce for the first time, a reconstruction of the thermodynamic climate properties within a 2-Dimensional phase space of two distinct climate forcings, (Log([CO_2]),S^*), where one controls the sink of energy to space and the other the source of energy entering the system, respectively. This experiment was then repeated but with the planetary rotation rate (Ω) decreased by a factor of 2. Altogether, over 500 climate states were simulated, each time

permitting at least 50 years of simulation time to allow the system to reach a steady state.

In chapter 4, it has been shown that the climate system is bistable, supporting two coexisting attractors. One contains a range of warm, moist states with either partial or no ice cover (W). The other is far colder and very dry with a totally ice covered surface (SB). The width of the bistable region is observed to remain constant across the entire phase space with its boundaries, approximately laying along isolines of surface temperature (T_s).

Across the entire phase space, T_s and $\overline{\dot{S}_{mat}}$ increase monotonically with increasing [CO_2] and S^*. The linear manner in which the T_s is found to increase with any combination of log([CO_2]) and S^* mean that the temperature response is approximately independent of the type of perturbation. This is also found to be the case for the other thermodynamic properties investigated here. This means the thermodynamic properties are to a good approximation dependant only on T_S. It is therefore possible to plot the thermodynamic properties as a function of T_s independent of the source used to force the system. It is also found that a similar functional dependence of the thermodynamic properties exists with T_E albeit within slightly less well defined bounds, indicating a weak dependence on the source of the forcing. A description of the thermodynamic properties as a function of T_s and T_E is given in chapter 5.

In the W regime the MET remains roughly constant up to T_s of roughly 300K. Beyond 300K is the point where the sea-ice completely disappears leading to meridional surface temperature difference remaining approximately constant with T_s. The consequence of this is that the the MET begins to increases monotonically up to the warmest states considered here of 320K. This result shows that at T_s below 300K where the surface is partially ice covered, that the sensible heat fluxes are largely controlled by the meridional temperature gradient, decreasing up to 300K despite the increase in energy to the system. Conversely, the latent heat transport is solely dependant on the temperature and increases monotonically with increasing temperature as the atmospheres capacity to hold moist improves consistent with the Clausius-Clapeyron relation. Thus, the relative increase and decreases in the respective contributions with temperature mean the overall transport remains roughly constant. Beyond 300K, the lack of sea-ice means the MET is no longer dependant on the meridional surface temperature difference and may increase without restriction up to the warmest states considered here.

In the SB state, increased incoming radiation or increased [CO_2] lead to increases in the MET. In the SB state however, the extremely dry atmosphere means the latent heat transport is negligible. The dominant mechanism by which energy is transferred to high latitudes is via sensible heat. However, the meridional temperature difference has also

a rather flat response to the modulation of forcings and can not be attributed to the increase in MET toward the SB$\rightarrow$ W transition. In this case, the dominant mechanism determining the properties of the MET is the change in the vertical stratification, which becomes weaker for warmer climate conditions. This implies that the atmospheric circulation strengthens for increasing values of the solar constant and of the [CO_2]. In fact, the strength of the Lorenz energy cycle becomes stronger for warmer climate conditions, and the Carnot efficiency of the climate system has an analogous behaviour.

In addition to adjusting parameters which directly influence the fluxes coming to and from the climate system, the final study in Chapter 5 has analysed how the climate response would be altered by a change to the large scale fluid dynamic properties of the system. This has been done by repeating the same experiment, except this time with the Earth's planetary rotation rate (Ω_E) decreased by a factor of 2, Ω_s, ($\Omega_s/\Omega_E = 0.5$). For all the aforementioned thermodynamic quantities tested with respect to the temperature, the functional form remains approximately the same. In the case of $\overline{\dot{S}_{mat}}$ the values are also almost identical. The largest difference in magnitude is observed with $\overline{W}$ which shows roughly a one third decrease in the strength of the Lorenz energy cycle. This may be attributed to the fact that the Rossby radius of deformation is significantly increased due to a factor of 2 decrease in Ω, resulting in the climatic fluid forming larger, less intense cell structures.

A general property which has been found here is that the η, in both manifolds, always increasing towards the transitions between W and SB climatic regimes. For Ω_s, the value of η is slightly higher at comparative values of T_s, relative to Ω_E, however, the value of η converges toward the transition. Thus, for a given transition, η is approximately the same, regardless of the planetary rotation rate or the transition in question, be it in the W$\rightarrow$SB or SB$\rightarrow$W direction. These findings support the idea that η maybe considered a measure of how far the system is from equilibrium. This may be understood as follows: Away from the transitions, the negative feedbacks tend to counteract the differential heating due to the solar insolation pattern. At the point of transition, the positive feedbacks overcome the negative feedbacks and the climate can therefore no longer support the current regime and thus performs an abrupt transition to a state where the negative feedbacks are more efficient in stabilising the system.

The results presented here therefore show the climate response to be rather robust to a large change in the parameters of the planetary system via the rotation rate. This is however far from being a conclusive proof of universality, however, the results of this thesis are consistent with the notion that within reasonably well defined bounds, the surface and emission temperatures may be used to estimate the climates thermodynamic properties as empirical functions.

6.2 Outlook

While the analysis presented here provides a more generalised setting in which to test the bistability properties of the climate system compared to previous work, it is nevertheless not exhaustive and depends on some specific characteristics of the Earth system. It does however highlight the possibility of using efficient parametrisations of complex non-equilibrium properties and to being able to practically deduce fundamental properties of a distant planetary system from a relatively simple observable. It is thus necessary to expand the scope of this work to see over a far wider range of parameters, for which properties of the system the response remains the same and over what range.

Just from observations of Earth's neighbouring planets, it is already known how vastly different atmospheric states of planetary systems can differ in terms of there dynamics, composition, orography and orbital parameters. In addition, external properties such as the spectra or intense gravitation forces exerted on to a planet by a parent star, can have substantial influence on its climate state and stability. All these parameters deserve investigation following a similar methodology as adopted in this thesis. Already in this study, a rather large amount of data storage and CPU time was required to complete the experiments, which pushed the significant resources available to its limit, so taking in to account all these parameters is a mammoth task and sensible choices should be made as to which best fulfil the outcome one wishes to achieve.

One of the most logical next steps to take to expand the scope of this investigation, is to examine the climate response and multistable properties of planetary systems where Ω is significantly faster (Ω_f) and slower (Ω_s) than those studied here, while maintaining the length of the diurnal cycle constant. In the case of $\Omega_s << \Omega_E$, the MET should be far more efficient than for the present Earth so that the meridional temperature gradient is far less and the development of sea-ice should occur more homogeneously across the entire surface with decreasing S^*. This may therefore prove to be not to dissimilar to the case of the 0-D energy balance model so a slowly rotating system should still exhibit global bistability properties. If so, this may imply a constraint on the overall climate sensitivity meaning the global climate response is robust to even larger decreases in Ω than considered in this thesis. For the case where $\Omega_f >> \Omega_E$, the MET will be very weak so that the meridional temperature difference will be large. In such a scenario, the W$\rightarrow$SB transition is likely to occur at high values of the solar forcing, perhaps higher than the level received by our present Earth. Furthermore, there must be an upper limit for the SB$\rightarrow$W transition where the magnitude of direct solar forcing even at the poles is large enough to maintained the planet in an ice free state regardless of the MET. Thus, if the rotation rate is high enough, there will be a point where the SB$\rightarrow$W and

W→SB transitions coincide, so that the bistable region disappears and the transition between both states occurs without hysteresis.

Another important orbital parameter which is of significant interest and should be pursued is to investigate the role played by the diurnal cycle when made significantly longer or in a tidally locked configuration with its parent star, while keeping Ω constant. A study by Edson et al. [24] shows that regardless of the rotation rate, a tidily locked Earth-like planet will not maintain a zonally symmetric temperature profile as the motions of the atmosphere are insufficient to compensate for the lack of direct solar heating. Indeed, in non tidally locked configurations where the diurnal cycle is sufficiently long, it is likely to be the case that the zonal temperature gradients will also be too large to homogenise, so that the climate will be maintained in a permanent transient state. Thus far, all simple to complex model investigations into global climate sensitivity and multistability have done so with a zonally symmetric input of energy or where the diurnal cycle is sufficiently short for thermal inertia to maintain zonal symmetry. In breaking the zonal symmetry and supplying the system with energy over a far narrower region, the global climate response is likely to be radically different. It will therefore be interesting to observe whether the multistability of such planetary systems is retained and what additional insights this may provide into our general understanding of the thermodynamic properties of the climate system.

Appendix A

CS Space Plots

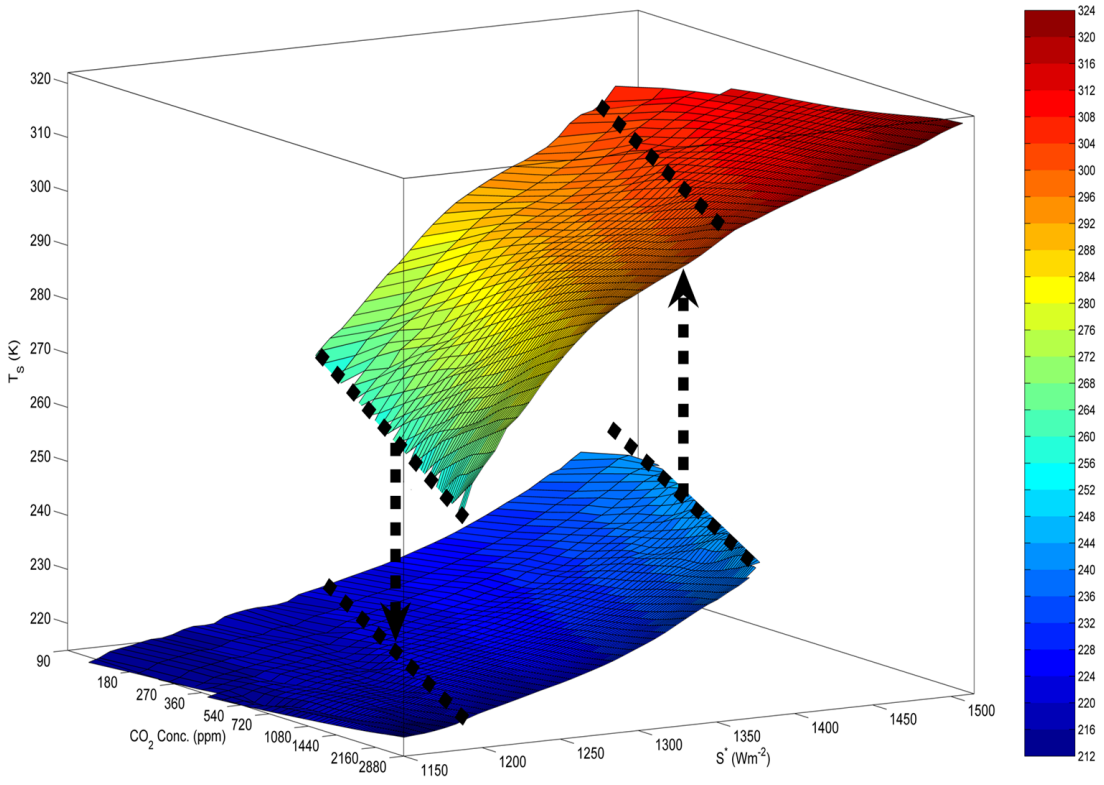

FIGURE A.1: Surface temperature, T_s, as a function of solar constant, S^*, and the CO_2 concentration. The transition SB→W and W→SB are marked with dashed arrows starting from the tipping point regions.

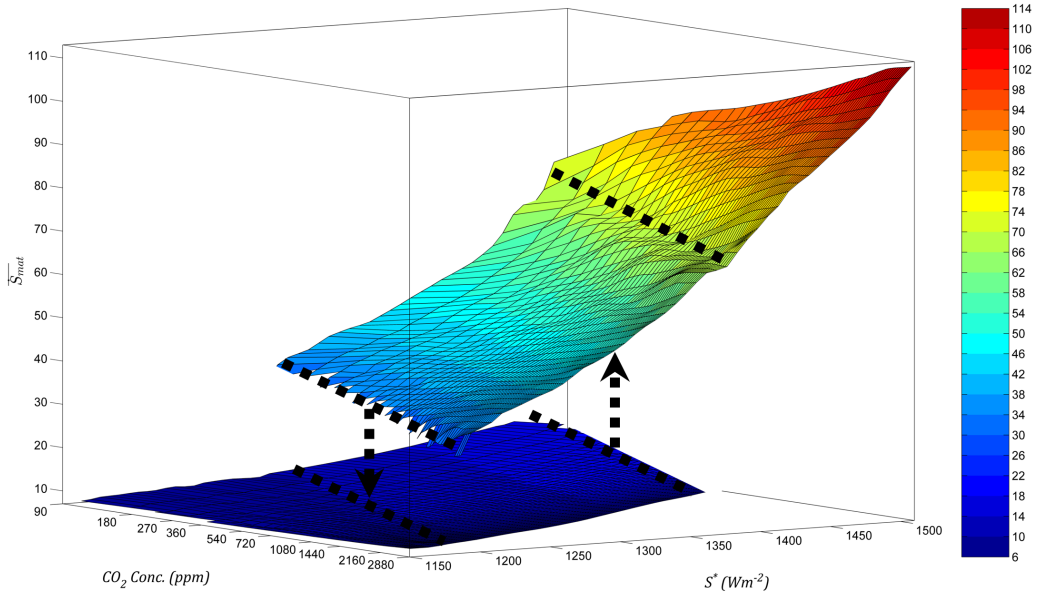

FIGURE A.2: Material entropy production, (mWm^2K^{-1}) as a function of solar constant, S^*, and the CO_2 concentration. The transition SB→W and W→SB are marked with dashed arrows starting from the tipping point regions.

Appendix B

PlaSim

B.1 The Planet Simulator

The Planet Simulator (PlaSim) is an open source atmospheric general circulation model developed at the University of Hamburg, which is freely available at http://www.mi.uni-hamburg.de/plasim. In this section a brief description of the the model is provided, based of the PlaSim manual Lunkeit et al. [80], including the dynamical core, parametrizations and coupled slab ocean.

The tool being used here to study the dynamical and thermodynamical properties of the Earth's climate system is the GCM named PlaSim. This is motivated by the fact that this study requires altering very extensively some parameters of the climate system and producing many simulations. Therefore, a model is needed which is flexible and fast to run rather then a state-of-the-art model encompassing as many processes occurring in the Earth as possible.

PlaSim [30] is a climate model of intermediate complexity. Its dynamical core is formulated using the primitive equations for vorticity, divergence, temperature, specific humidity, and the logarithm of surface pressure, solved using the spectral transform method [25, 88] with semi-Lagrangian advection. Unresolved processes for long [105] and short [57] wave radiation, shallow, moist [55, 56] and dry convection, cloud formation [108, 111, 112] and large scale precipitation, latent and sensible heat boundary layer fluxes, horizontal and vertical diffusion [59, 73, 74] are parameterized. The model is coupled to a 50-m deep mixed layer ocean which contains a thermodynamic sea-ice model. The advantage of using a slab ocean as opposed to a full ocean is that it allows for the climate system to reach a steady state in less than 35 years after a change in e.g. the solar constant. With full ocean coupling, the integration time of the model and the

time needed to reach a steady state would be an order of magnitude larger [119]. Fig. B.1 illustrates the coupling between of the main modules in PlaSim.

It is important to emphasize that whereas most state-of-the-art general circulation models feature an imperfect closure of the global energy budget in the order of 1 Wm^{-2} for standard climate conditions, due to inaccuracies in the treatment of the dissipation of kinetic energy and the hydrological cycle [65, 78]. In these simulations, which cover very extreme climate conditions, the energy bias is always smaller than 0.5 Wm^{-2}. Therefore, this model should be thermodynamically consistency. Moreover a tested entropy diagnostic is available Fraedrich and Lunkeit [31], thus making it well suited for this work.

The model is run at T21 resolution (approximately $5.6° \times 5.6°$) with 10 vertical levels. While this resolution is relatively low, it is expected to be sufficient for obtaining a reasonable description of the large scale properties of the atmospheric dynamics, which are most relevant for the global features of interest in this thesis. Note, previous analyses has shown that using a spatial resolution approximately equivalent to T21 allows for obtaining an accurate representation of the major large scale features of the climate system and of its global thermodynamical properties [46, 91]. Moreover, since an extensive parametric investigation is being performed here, a parsimonious climate model is required. The PlaSim manual by Lunkeit et al. [80] which provides a more detailed decription of the individual modules and the coupling is summarised in Fig. B.1.

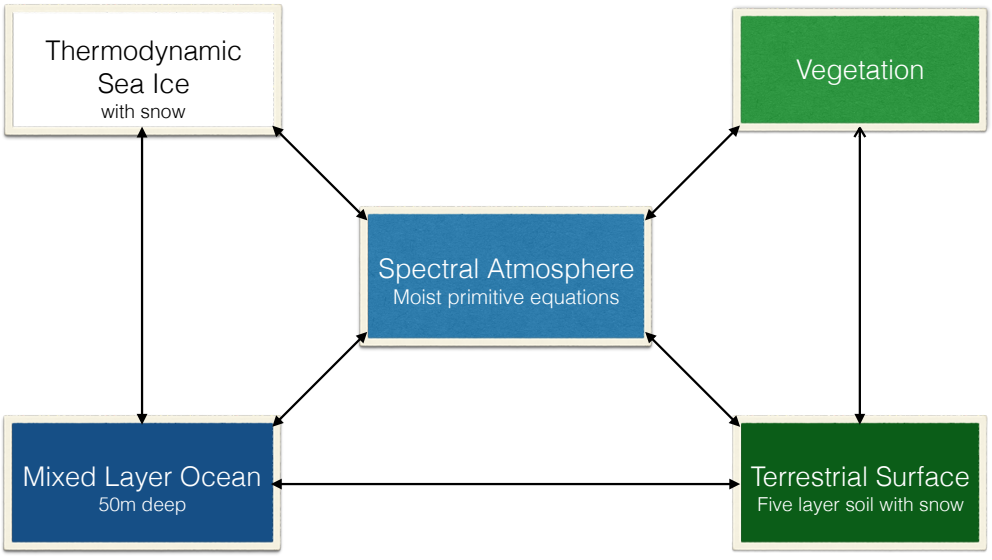

FIGURE B.1: Schematic overview illustrating the coupling between of the main modules in PlaSim.

Bibliography

[1] Abbot, D., A. Voigt, M. Branson, R. T. Pierrehumbert, D. Pollard, G. Le Hir, and D. D. Koll, (2012). *Clouds and snowball Earth deglaciation.* Geophys. Res. Lett., 39, L20711, doi:10.1029/ 2012GL052861.

[2] Abbot, D., (2014). *Resolved Snowball Earth Clouds.* Geophys. Res. Lett., 39, DOI: 10.1175/JCLI-D-13-00738.1.

[3] Ambaum, M. H. P., (2010). *Thermal Physics of the Atmosphere.* Wiley-Blackwell, DOI: 10.1002/9780470710364

[4] Arnol'd, (1992). *Catastrophy theory, III edition.* Springer, Berlin.

[5] Becker, E., (2003). *Frictional heating in global climate models.* Mon. Wea. Rev., 131, 508–520.

[6] Bódai T., V. Lucarini, F. Lunkeit and R. Boschi, (2015). *Global instability in the Ghil–Sellers model.* Clim. Dyn., 44:3361–3381, DOI 10.1007/s00382-014-2206-5.

[7] Bonfils, X. and Coauthors, (2013). *The HARPS search for souther extra-solar planets XXXI. the m-dwarf sample.* Astronomy and Astrophysics, AA 549, A109.

[8] Bony, S. and Coauthors, (2012). *How Well Do We Understand and Evaluate Climate Change Feedback Processes?.* American Meteorological Society, 19, 3445–3482.

[9] Brandt, R. E., S. G. Warren, and A. D. Clarke (2011). A controlled snowmaking experiment testing the relation between black carbon content and reduction of snow albedo, J. Geophys. Res., 116, D08109, doi:10.1029/2010JD015330.

[10] Briegleb, B. P., E. C. Hunke, C. M. Bitz, W. H. Lipscomb, M. M. Holland, J. L. Schramm, and R. E. Moritz, (2004). *The sea ice simulation of the Community Climate System Model, version two.* NCAR Tech. Note NCAR/TN-45+STR, 34 pp.

[11] Briegleb, B. P. and B. Light, (2007). *A Delta-Eddington multiple scattering parameterization for solar radiation in the sea ice component of the Community Climate System Model.* NCAR Tech. Note 472+STR, 100 pp.

[12] Budyko, M. I., (1969). *The effect of solar radiation variations on the climate of the earth.* Tellus 21, 611–619.

[13] Caballero, R. and P. L. Langen, (2005). *The dynamic range of poleward energy transport in an atmospheric general circulation model.* Geophys. Res. Lett. 32, L02705, doi:10.1029/2004GL021581.

[14] Cartier., K. M. S., R. L. Gilliland, J. T. Wright, and D. R. Ciardi, (2015). *Revision of Earth-sized kepler Planet Candidate Properties with High-Resolution Imaging by the Hubble Space Telescope.* The Astrophysical Journal, Volume 804, Number 2.

[15] Colman, R., (2003). *A comparison of climate feedbacks in general circulation models.* Climate Dyn., 20, 865–873.

[16] Coustenis, A., (2005). *"Formation and evolution of Titan's atmosphere".* Space Science Reviews 116 (1-2): 171–184. Bibcode:2005SSRv..116..171C. doi:10.1007/s11214-005-1954-2.

[17] Dadic, R., B. Light, and S. G. Warren (2010). Migration of air bubbles in ice under a temperature gradient, with application to "Snowball Earth", J. Geophys. Res., 115, D18125, doi:10.1029/2010JD014148.

[18] Dadic, R., P. C. Mullen, M. Schneebeli, R. E. Brandt, and S. G. Warren, (2013). *Effects of bubbles, cracks, and volcanic tephra on the spectral albedo of bare ice near the Transantarctic Mountains: Implications for sea glaciers on Snowball Earth.* J. Geophys. Res. Earth Surf., 118, 1658–1676, doi:10.1002/jgrf.20098.

[19] DeGroot, S. and P. Mazur, (1984). *Non-equilibrium thermodynamics.* Dover.

[20] Donohoe, A. and D. Battisti, (2011). *Atmospheric and surface contributions to planetary albedo.* J. Clim. 24, 4402–4418.

[21] Donohoe, A. and D. Battisti, (2012). *What determines meridional heat transport in climate models?* J. Clim. 25, 3832–3850.

[22] Dvorak, R., (2008). *Extrasolar Planets.* Wiley-VHC.

[23] Dwyer H. A. and Pettersen, (1973). *Time-dependent global energy modeling.* J Appl Meteor 12:36–42

[24] Edson A., S. Lee, P. Bannon, J. F. Kasting and D. Pollard, (2011). *Atmospheric circulations of terrestrial planets orbiting low-mass stars.* Icarus 212, 1-13.

[25] Eliasen, E., B. Machenhauer and E. Rasmussen, (1970). *On a numerical method for integration of the hydrodynamical equations with a spectral representation of the horizontal fields.* Report no. 2, Inst. of Theor. Met., University of Copenhagen. ;

[26] Fasullo, J., and K. Trenberth (2008). *The annual cycle of the energy budget. Part II: Meridional structures and poleward transports.* J. Clim., 21, 2313–2325.

[27] Fermi, E. (1956). *Thermodynamics.* Dover, New York.

[28] Flasar, F.M. and coauthors (2005). *"Titan's atmospheric temperatures, winds, and composition".* Science 308 (5724): 975–978. Bibcode:2005Sci...308..975F. doi:10.1126/science.1111150.

[29] Fraedrich, K., (1979). *Catastrophes and resilience of a zero-dimensional climate system with ice-albedo and greenhouse feedback.* Q J R Meteorolog Soc 105, 147–167.

[30] Fraedrich, K., H. Jansen, U. Luksch, E. Kirk and F. Lunkeit, (2005). *The planet simulator: towards a user friendly model.* Meteorologische Zeitschrift 14, 299–304.

[31] Fraedrich, K. and F. Lunkeit, (2008). *Diagnosing the entropy budget of a climate model.* Tellus A 60 (5), 921–931.

[32] Gallavotti, G., (2006). *Encyclopedia of mathematical physics. Elsevier, Ch. Nonequilibrium statistical mechanics (stationary): overview.* pp. 530–539.

[33] Gassmann, A., (2013). *A global hexagonal C-grid non-hydrostatic dynamical core (ICON-IAP) designed for energetic consistency.* Q.J.R. Meteorol. Soc., 139: 152–175. doi: 10.1002/qj.1960

[34] Ghil, M., (1976). *Climate stability for a sellers-type model.* J Atmos Science 33, 3–20.

[35] Goosse H., (2015) *Climate System Dynamics and Modelling.* Cambridge University Press.

[36] Gough, D., (1981). *Solar interior structure and luminosity variations.* Solar Physics 74, 21–34.

[37] Held, I. M. and B. J. Soden, (2006). *Robust responses of the hydrological cycle to global warming.* Journal of Climate 19, 5686–5699.

[38] Hoffman, P., J., A. J. K. A., G. P. Halverson, D. P. Schrag, (1998). *A neoproterozoic snowball earth.* Science 281, 1342–1346.

[39] Hoffman, P. and D. P. Schrag, (2002). *The snowball earth hypothesis: testing the limits of global change.* Terra Nova 14, 129–155.

[40] Holloway, C. E., S. J. Woolnough1 and G. M. S. Lister, (2012). *Precipitation distributions for explicit versus parametrized convection in a large-domain high-resolution tropical case study.* Q.J.R. Meteorol. Soc., 138: 1692–1708. doi: 10.1002/qj.1903

[41] Holton, J., (2004). *An introduction to dynamic meteorology.* Elsevier.

[42] Huang, J. and M. B. McElroy, (2014). *Contributions of the Hadley and Ferrel Circulations to the Energetics of the Atmosphere over the Past 32 Years.* Journal of Climate 27 (7): 2656–2666. doi:10.1175/jcli-d-13-00538.1.

[43] Hudson, S. R., S. G. Warren, R. E. Brandt, T. C. Grenfell, and D. Six (2006), Spectral bidirectional reflectance of Antarctic snow: Measurements and parameterization, J. Geophys. Res., 111, D18106, doi:10.1029/2006JD007290.

[44] Johnson, D., (1997). *"General coldness of climate" and the second law: Implications for modelling the earth system.* Journal of Climate 10, 2826–2846.

[45] Johnson, D., (2000). *Entropy, the Lorenz energy cycle, and climate. General circulation model development: Past, present and future,* Randall DA (ed). Internation Geophysics Series Vol 70. Academic Press, New York, 659–720.

[46] Jones C., Gregory J., Thorpe R., Cox P., Murphy J., Sexton D., and Valdes P., (2005). *Systematic optimization and climate simulation of FAMOUS, a fast version of HadCM3.* Climate Dynamics 25, 189–204.

[47] Kasting, J., (2009). *How to find a habitable planet.* Princeton University Press.

[48] Kennedy, M. J., Runnegar, B., Prave, A. R., Hoffman, K. H., Arthur, M. A., (1998). *Two or four neoproterozoic glaciations?* Geology 26, 1059–1063.

[49] Kindel, B. C., Z. Qu, and A. F. H. Goetz (2001). Direct solar spectral irradiance and transmittance measurements from 350–2500 nm, Appl. Optics., 40, 3483–3494, doi:10.1364/AO.40.003483.

[50] Kirschivink, J., (1992). *Late Proterozoic Low-Latitude Global Glaciation: the Snowball Earth.* Cambridge University Press, 2.3, 51-52.

[51] Kleidon, A., (2009). *Nonequilibrium thermodynamics and maximum entropy production in the Earth system.* Naturwissenschaften, 96:653–677, DOI 10.1007/s00114-009-0509-x.

[52] Kolmogorov, A. N., (1941). *Dissipation of Energy in the Locally Isotropic Turbulence.* Proceedings: Mathematical and Physical Sciences, 434(1890), 15—17.

[53] Kondepudi, D. and I. Prigogine, (1998). *MODERN THERMODYNAMICS: From Heat Engines to Dissipative Structures.* John Wiley Sons.

[54] Kuhlbrodt, T., A. Griesel, M. Montoya, A. Levermann, M. Hofmann, and S. Rahmstorf (2007). *On the driving processes of the Atlantic meridional overturning circulation.* Rev. Geophys., 45, RG2001, doi:10.1029/2004RG000166.

[55] Kuo, H., (1965). *On formation and intensification of tropical cyclones through latent heat release by cumulus convection.* J. Atmos. Sci. 22, 40–63.

[56] Kuo, H., (1974). *Further studies of the parametrisation of the influence of cumulus convection on large-scale flow.* J. Atmos. Sci. 31, 1232–1240.

[57] Lacis, A., Hansen, K., (1974). *A parmetrisation for the absorption of solar radiation in the earth's atmosphere.* J. Atmos. Sci. 31, 118–133.

[58] Landau, L., Lifshitz, E., (1980). *Statistical Physics.* Part 1. Pergamon: Oxford.

[59] Laursen, L., Eliasen, E., (1989). *On the effect of the damping mehanisms in an atmospheric general circulation model.* Tellus 41A, 385–400.

[60] Lebonnois, S., F. Hourdin, V. Eymet, A. Crespin, R. Fournier, and F. Forget, (2010), *Superrotation of Venus' atmosphere analyzed with a full general circulation model.* J. Geophys. Res., 115, E06006, doi:10.1029/2009JE003458.

[61] Leconte, J., F. Forget, B. Charnay, R. Wordsworth and A. Pottier, (2014). *Increased insolation threshold for runaway greenhouse processes on Earth-like planets. Nature 504, 268–271.* doi:10.1038/nature12827

[62] Leovy, C. B., (1973), *Rotation of the upper atmosphere of Venus.* J. Atmos. Sci., 30, 1218 – 1220

[63] Li, J. and P. Chylek, (2012). *Atmospheric entropy. Part I: Climate dissipation structure.* Journal of Climate 25, 3173–3190.

[64] Liang, M-C., H. Hartman, R. E. Kopp, J. L. Kirschvink, and Y. L. Yung, (2006). *Production of hydrogen peroxide in the atmosphere of a Snowball Earth and the origin of oxygenic photosynthesis.* Proc Natl Acad Sci USA 103:18896-18899.

[65] Liepert, G. and M. Previdi, (2012). *Inter-model variability and biases of the global water cycle in CMIP3 coupled climate models.* Environ. Res. Lett. 7 014006 doi:10.1088/1748-9326/7/1/014006

[66] Liepert, G. and F. Lo, (2013). *CMIP5 update of 'Inter-model variability and biases of the global water cycle in CMIP3 coupled climate models'.* Environ. Res. Lett. 8 029401.

[67] Limaye, S. S., (2007). *Venus atmospheric circulation: Known and unknown.* J. Geophys. Res., 112, E04S09, doi:10.1029/2006JE002814.

[68] Li, L., A. P. Ingersoll, X. Jiang, D. Feldman, and Y. L. Yung (2007). *Lorenz energy cycle of the global atmosphere based on reanalysis datasets.* Geophys. Res. Lett., 34, L16813, doi:10.1029/2007GL029985.

[69] Lindzen, R. S. and B. Farrell, (1977). *Some Realistic modifications of Simple Climate Models.* J. Atmos. Sci., 34, 1487–1501.

[70] Lindzen, R. S. and B. Farrell, (1981). *The Role of Polar Regions in Global Climate, and a New Parameterization of Global Heat Transport.* Mon. Wea. Rev., 108, 2064–2079.

[71] Lorenz, E. (1955). *Available potential energy and the maintenance of the general circulation.* Tellus, 7, 157–167.

[72] Lorenz, E., (1967). *The nature and theory of the general circulation of the atmosphere.* Vol. 218.TP.115. World Meteorological Organization.

[73] Louis, J., (1979). *A parametric model of vertical eddy fluxes in the atmosphere. Bound. Layer Meteorol.* 17, 187–202.

[74] Louis, J., M. Tiedke, J. Geleyn, 25-27 Nov. (1981). *A short history of the PBL parametrisation at ECMWF. Proceedings of the ECMWF Workshop on Planetary Boundary Layer Parametrization.* 59–80.

[75] Lucarini, V., (2009). *Thermodynamic efficiency and entropy production in the climate system.* Physical Review E 80, 021118.

[76] Lucarini, V., K. Fraedrich, and F. Lunkeit, (2010). *Thermodynamics of climate change: generalized sensitivities.* Atmospheric Chemistry and Physics 10, 9729-9737.

[77] Lucarini, V., K. Fraedrich and F. Lunkeit, (2010). *Thermodynamic analysis of snowball earth hysteresis experiment: efficiency, entropy production and irreversibility.* Quarterly Journal of Royal Meteorological Society 136, 1–11.

[78] Lucarini, V. and F. Ragone, (2011). *Energetics of climate models: net energy balance and meridional enthalpy transport.* Reviews of Geophysics 49, 2009RG000323.

[79] Lucarini, V., K. Fraedrich and F. Ragone, (2011). *New results on the thermodynamic properties of the climate.* Journal of the Atmospheric Sciences 68, 2438–2458.

[80] Lunkeit F., H. Borth, M. Bottinger, K. Fraedrich, H. Jansen, E. Kirk, A. Kleidon, U. Luksch, P. Paiewonsky, S. Schubert, S. Sielmann and H. Wan, 2011. Planet Simulator Reference Manual Version 16. https://www.mi.uni-hamburg.de/en/arbeitsgruppen/theoretische-meteorologie/modelle/sources/psreferencemanual.pdf

[81] Margules, M. (1905). *On the energy of storms, transl. from german by c. abbe,* in Smithson. Misc. Collect., edited by D. A. Randall, pp. 533–595.

[82] Marotzke, J. and M. Botztet, (2007). *Present-day and ice-covered equilibrium states in a comprehensive climate model.* Geophys. Res. Lett. 34, L16704, doi: 10.1029/2006GL028880.

[83] Mayer, M., and L. Haimberger (2012). *Poleward atmospheric energy transports and their variability as evaluated from ECMWF reanalysis data.* J. Clim., 25, 734–752.

[84] Mitchell, J. and G. Vallis, (2010). *The transition to superrotation in terrestrial atmospheres.* J. Geophys. Res. (Planets), v115, E12008, DOI: 10.1029/2010JE003587.

[85] Niemann, H. B. and Coauthors et al. (2005). *"The abundances of constituents of Titan's atmosphere from the GCMS instrument on the Huygens probe".* Nature 438 (7069): 779–784.

[86] O'Gorman, P. and T. Schneider, (2008). *The hydrological cycle over a wide range of climates simulated with an idealized GCM.* J. Climate, 21, 3815–3832.

[87] Öpik, E. Y. (1953). *On the causes of paleoclimatic variations and of ice ages in particular.* Journ. of Glaciology, 2, No. 13.

[88] Orszag, S., (1970). *Transform method for calculation of vector coupled sums.* J. Atmos. Sci., 890–895.

[89] Ozawa, H., A. Ohmura, R. D. Lorenz, and T. Pujol, (2003). *The second law of thermodynamics and the global climate system: A review of the maximum entropy production principle.* Rev. Geophys., 41, 1018, doi:10.1029/2002RG000113, 4.

[90] Paoletti, S., F. Rispoli and E. Sciubba, (1989). *Calculation of exergetic losses in compact heat exchanger passager.* ASME AES 10 (2), 21–29.

[91] Pascale, S., J. Gregory and M. Ambaum, R. Tailleux, (2011). *Climate entropy budget of the HadCM3 atmosphere-ocean general circulation model and FAMOUS, its low-resolution version.* Climate Dynamics 36 (5-6), 1189–1206.

[92] Pascale, S., J. Gregory, M. Ambaum and R. Tailleux, (2011). *A parametric sensitivity study of entropy production and kinetic energy dissipation using the FAMOUS AOGCM.* Climate Dynamics, doi:10.1007/s00382–011–0996–2.

[93] Peixoto, J., A. Oort, M. de Almeida and A. Tomé, (1991). *Entropy budget of the atmosphere.* Journal of Geophysical Research 96, 10981–10988.

[94] Peixoto, J. P. and A. Oort, (1992). *Physics of the Climate.* Springer-Verlag, New York.

[95] Perryman, M., (2011). *The Exoplanets Handbook.* Cambridge University Press.

[96] Pidwirny, M. (2006). *"Global Heat Balance: Introduction to Heat Fluxes".* Fundamentals of Physical Geography, 2nd Edition. http://www.physicalgeography.net/fundamentals/7j.html

[97] Pierrehumbert, R., (2005). *Climate dynamics of a hard snowball earth.* J. Geophys. Res. 110, D01111, DOI:10.1029/2004JD005162.

[98] Pollard, D., and J. F. Kasting (2005). *Snowball Earth: A thin-ice solution with flowing sea glaciers.* J. Geophys. Res., 110, C07010, doi:10.1029/2004JC002525.

[99] Pierrehumbert, R.T., D.S. Abbot, A. Voigt, and D. Koll, (2011). *Climate of the Neoproterozoic.* Earth and Planetary Sciences. DOI: 10.1146/annurev-earth-040809-152447.

[100] Pujol, T., (2003). *Eddy heat diffusivity at maximum dissipation in a radiative-convective one-dimensional climate model.* Journal of the Meteorological Society of Japan 81 (2), 305–315.

[101] Putziga, N. E., M. T. Mellon, K. A. Kretke and R. E. Arvidson, (2004). *Global thermal inertia and surface properties of Mars from the MGS mapping mission.* Icarus173, 325-341. doi:10.1016/j.icarus.2004.08.017.

[102] Read, P., (2011). *Dynamics and circulation regimes of terrestrial planets.* Planetary and space sciences 59, 900–914.

[103] Seager, S., (2010). *Exoplanets.* University of Arizona.

[104] Saltzman, B., (2002). *Dynamic Paleoclimatology.* Academic Press: New York.

[105] Sasamori, T., (1968). *The radiative cooling calculation for application to general circulation experiments.* J. Appl. Meteorol. 7, 721–729.

[106] Sellers, W. D., (1969). *A global climate model based on the energy balance of the earth-atmosphere system.* J. Appl. Meteorol. 8, 392–400.

[107] Showman, A. and M. Polvani, (2011). *Equatorial superrotation on tidally locked exoplanets.* Astrophys J 738:71.

[108] Slingo, A. and J. Slingo, (1991). *Response of the national center for atmospheric research community climate model to improvements in the representation of clouds.* J. Geophys. Res. 96, 341–357.

[109] Soden B.J., R.T. Wetherald, G.L. Stenchikov and A. Robock, (2002). *"Global Cooling After the Eruption of Mount Pinatubo: A Test of Climate Feedback by Water Vapor."* Science 296:727

[110] Soden, B.J. and I.M. Held, (2006). *An assessment of climate feedbacks in coupled ocean–atmosphere models.* J. Climate, 19, 3354–3360.

[111] Stephens, G., (1978). *Radiation profiles in extended water clouds. II: parametrization schemes.* J. Atmos. Sci. 35, 2123–2132.

[112] Stephens, G., S. Ackermann and E. Smith, (1982). *A shortwave parametrization scheme.* J. Atmos. Sci. 41, 687–690.

[113] Stone, P., (1978). *Baroclinic adjustmnets.* J. Atmos. Sci. 35, 561–571.

[114] Tailleux, R., (2012). *Available Potential Energy and Exergy in Stratified Fluids.* Annu. Rev. Fluid Mech. 2013. 45:35–58.

[115] Tobie, G., Lunine, J. I. Lunine and C. Sotin (2006). *"Episodic outgassing as the origin of atmospheric methane on Titan".* Nature 440 (7080): 61–64. Bibcode:2006, Natur.440...61T. doi:10.1038/nature04497.

[116] Tokano, T., F. M. Neubauer, M. Laube and C. P. McKay (1999). *Seasonal variation of Titan's atmospheric structure simulated by a general circulation model.* Planet. Space Sci., 47, 493-520, 1999.

[117] Trenberth, K. E., and J. M. Caron (2001). *Estimates of meridional atmosphere and ocean heat transports.* J. Clim., 14, 3433–3443.

[118] Trenberth, K. E., and J. T. Fasullo (2010). *Simulation of present-day and twenty-first-century energy budgets of the Southern Oceans.* J. Clim., 23, 440–454.

[119] Voigt, A. and J. Marotzke, (2010). *The transition from the present-day climate to a modern snowball earth.* Climate Dynamics 35, 887–905.

[120] Voigt, A., D. S. Abbot, R. T. Pierrehumbert, and J. Marotzke, (2011). *Initiation of a Marinoan Snowball in a state-of-the-art atmosphere ocean general circulation model.* Climate of the Past 7, 249–263.

[121] Warren, S. G., R. E. Brandt, and T. C. Grenfell (2006). Visible and near-ultraviolet absorption spectrum of ice from transmission of solar radiation into snow, Appl. Optics., 45, 5320–5334.

[122] Winton, M., (2006). *Surface albedo feedback estimates for the AR4 climate models.* J. Climate, 19, 359-365.

[123] Yamamoto, M. and M. Takahashi, (2003). *The Fully Developed Superrotation Simulated by a General Circulation Model of a Venus-like Atmosphere.* J. Atmos. Sci., 60, 561–574.

[124] Yang, J., W. R. Peltier, and Y. Y. Hu, (2012). *The initiation of modern "soft Snowball" and "hard Snowball" climates in CCSM3. Part I: The influence of solar luminosity, CO2 concentration, and the sea ice/snow albedo parameterization.* J. Climate, 25, 2711–2736.

[125] Yang, J., W. R. Peltier, and Y. Y. Hu, (2012). *The Initiation of Modern "Soft Snowball" and "Hard Snowball" Climates in CCSM3. Part II: Climate Dynamic Feedbacks.* J. Climate, 25, 2737–2754.

Publication List

The following are my publications which feature work in this thesis:

Boschi R., V. Lucarini, S. Pascale, (2013). *Bistability of the climate around the habitable zone: a thermodynamic investigation*, Icarus 226, 1724-1742.

Boschi R., V. Lucarini, S. Pascale, (2014). *Thermodynamic insights into transitions between climate states under changes in solar and greenhouse forcing"*; Chapter in *"Beyond the Second Law: Entropy production and non-equilibrium systems*, RC Dewer, C Lineweaver, R Niven, K Regenauer-Lieb (eds), Springer, ISBN: 978-3-642-40153.

Lucarini, V., S. Pascale, **R. Boschi**, Kirk, E., and Iro, N. (2013). *Habitability and multistability in earth-like planets.* Astron. Nachr., 334, 576-588.

Acknowledgements

First and foremost, I would like to express my sincere and deep gratitude to my supervisor Prof. Dr. Valerio Lucarini for the opportunity to conduct research at the Research Unit of Theoretical Meteorology as well as his patient guidance, invaluable suggestions and encouragement. I am very grateful to Dr. Salvatore Pascale for our discussions, guidance and his support during my PhD. I would also like to thank Prof. Peter Hauschildt for the helpful discussions during my advisory panel meetings and for taking the time to serve as a referee for this work. I am very grateful to Dr. Edilbert Kirk and Dr. Frank Lunkeit for very helpful discussions and technical advice using PlaSim. I would also like to thank Prof. Maarten Ambaum, Dr. Richard Blender, Prof. Johanna Baehr and Prof. Peter Hauschildt for agreeing to be part of my defence examination committee. Many thanks go also to my colleagues and friends of the work group of Theoretical Meteorology for a nice and friendly working atmosphere. Thanks go to Sebastian Schubert for translating my abstract to German. I would also like to acknowledge the financial, academic and technical support of Clisap, the University of Hamburg, NAMASTE and the Central IT Services CIS.

I would like to thank my family, Natalie and Tom for their support over many years. In particular I owe special thanks to my mother, Agnieszka Boschi, who passed away before the completion of this thesis. Thank you so much for your tireless sacrifice and encouragment, you are forever in my heart.

List of Figures

Abbreviations

APE	**A**vailiable **P**otential **E**nergy
ASR	**A**bsorbed **S**hort Wave **R**adiation
CS Space	[**C**O_2]−**S**olar Constant Phase Space
EBM	**E**nergy **B**alance **M**odel
GCM	**G**eneral **C**irulation **M**odel
IR	**I**nfra**r**ed
LAH	**L**ist **A**bbreviations **H**ere
LW	**L**ong **W**ave radiation
RHS	**L**eft **h**and **s**ide
MET	**M**eridional **E**nthalpy **T**ransport
NH	**N**orthern **H**emisphire
OLR	**O**utgoing **L**ong Wave **R**adiation
RHS	**R**ight **h**and **s**ide
SAM	**S**ystem for **A**tmospheric **M**odelling
SB	**S**now**b**all (climate regime)
SH	**S**outhern **H**emisphire
SW	**S**hort **W**ave radiation
TOA	**T**op **o**f **A**tmosphere
W	**W**arm (climate regime)
n	

Physical Constants

g	acceleration due to gravity	9.81 ms^{-2}
L	latent heat of vapourisation of water	2.26476×10^{6} Jkg^{-1}
T_{sun}	solar emission temperature	5800 K
Ω_E	Earth's planetary rotation rate	7.2921150×10^{5} rads^{-1}
σ	Stefan-Boltzmann constant	$5.670367(13)\times10^{8}$ Wm^2K^4

Symbols

a	distance	m
A	avaliable potential energy	J
D	dissipation	J
c_p	specific heat capacity at constant pressure	$\mathrm{Jkg}^{-1}K^{-1}$
c_v	specific heat capacity at constant volume	$\mathrm{Jkg}^{-1}K^{-1}$
$\dot{E}$	global energy budget per meter	Wm^{-2} ($\mathrm{Jm}^{-2}\mathrm{s}^{-1}$)
$\dot{E}_S$	surface energy budget per meter	Wm^{-2}
F_{LH}	latent heat flux	Wm^{-2}
F_{SH}	sensible heat flux	Wm^{-2}
$F_{R,S}$	net radiation flux at the surface	Wm^{-2}
F_R^{TOA}	net radiation flux	Wm^{-2}
$F_{LW,S}^{\uparrow}$	upward LW radiation from surface	Wm^{-2}
$F_{LW,A,DOWN}$	downward LW radiation from atmosphere	Wm^{-2}
$F_{SW,S}^{\downarrow}$	solar radation absorbed at surface	Wm^{-2}
F_{turb}	sensible heat flux	Wm^{-2}
$F_{SW,S}$	surface absorbed short wave radiation	Wm^{-2}
$F_{SW,A}$	atmosphere absorbed short wave radiation	Wm^{-2}
F_{LW}	net long wave radiation between surf and atm	Wm^{-2}
G	generation of avaliable potential energy	Js^{-1}
h	enthalpy	J
K	kinetic energy	J
p	pressure	Pa (Nm^{-2})
P	power	W (Js^{-1})
$\dot{Q}$	total heating rate	Wm^{-2} ($\mathrm{Jm}^{-2}\mathrm{s}^{-1}$)
S^*	solar constant	Wm^{-2}

$\dot{S}_i$	internal entropy production	$\mathrm{Wm^{-2}K^{-1}}$
$\dot{S}_i$	external entropy production	$\mathrm{Wm^{-2}K^{-1}}$
$\dot{S}$	total rate of change of entropy in the system	$\mathrm{Wm^{-2}K^{-1}}$
$\dot{S}_{mat}$	material entropy production	$\mathrm{Wm^{-2}K^{-1}}$
S_{mat}^{vert}	vertical material entropy production	$\mathrm{Wm^{-2}K^{-1}}$
S_{mat}^{hor}	horizontal material entropy production	$\mathrm{Wm^{-2}K^{-1}}$
T_{atm}	atmospheric energy transport	W
T_{oc}	oceanic energy transport	W
T_{surf}	energy transport below surface	W
T_A	atmospheric temperature	K
T_E	emission temperature	K
T_S	surface temperature	K
Θ	mean temperature of the atmosphere	K
$\overline{T_T}(\sigma)$	total average MET	W
u	zonal velocity	$\mathrm{ms^{-1}}$
U	internal energy	J
v	meridional velocity	$\mathrm{ms^{-1}}$
w	vertical velocity	$\mathrm{ms^{-1}}$
W	Work	J
x	zonal distance	m
y	meridional distance	m
z	vertical height	m
$[CO_2]$	CO_2 concentration	ppm
η	Carnot efficiency	
Ω	planetary rotation rate	rad $\mathrm{s^{-1}}$
ω	angular frequency	rad $\mathrm{s^{-1}}$
ρ	specific volume	$\mathrm{kgm^{-3}}$
$\dot{\Phi}$	total non-frictional diabatic heating heating	